Abstract

Title of Dissertation: Growing Intermediate-Mass Black Holes with Gravitational Waves

Kayhan Gültekin, Doctor of Philosophy, 2006

Dissertation directed by: Professor M. Coleman Miller
Department of Astronomy

We present results of numerical simulations of sequences of binary-single scattering events of black holes in dense stellar environments. The simulations cover a wide range of mass ratios from equal mass objects to 1000:10:10 $M_\odot$ and compare purely Newtonian simulations with a relativistic endpoint, simulations in which Newtonian encounters are interspersed with gravitational wave emission from the binary, and simulations that include the effects of gravitational radiation reaction by using equations of motion that include the 2.5-order post-Newtonian force terms, which are the leading-order terms of energy loss from gravitational waves. In all cases, the sequence is terminated when the binary's merger time due to gravitational radiation is less than the arrival time of the next interloper. We also examine the role of gravitational waves during an encounter and show that close approach cross-sections for three 1 $M_\odot$ objects are unchanged from the purely Newtonian dynamics except for close approaches smaller than 10^{-5} times the initial semimajor axis of the binary. We also present cross-sections for mergers resulting from gravitational radiation during three-body encounters for a range of binary semimajor axes and mass ratios including those of interest for intermediate-mass black holes (IMBHs). We find that black hole binaries typically merge with a very high eccentricity — extremely high when gravitational waves are included during the encounter such that when the gravitational waves are detectable by *LISA*, most of the binaries will

have eccentricities $e > 0.9$ though all will have circularized by the time they are detectable by LIGO. We also investigate the implications for the formation and growth of IMBHs and find that the inclusion of gravitational waves during the encounter results in roughly half as many black holes ejected from the host cluster for each black hole accreted onto the growing IMBH. The simulations show that the Miller & Hamilton (2002b) model of IMBH formation is a viable method if it is modified to start with a larger seed mass.

Growing Intermediate-Mass Black Holes with Gravitational Waves

by

Kayhan Gültekin

Dissertation submitted to the Faculty of the Graduate School of the
University of Maryland at College Park in partial fulfillment
of the requirements for the degree of
Doctor of Philosophy
2006

Advisory Committee:

Professor M. Coleman Miller, chair
Professor Alessandra Buonanno
Professor Douglas P. Hamilton
Professor Richard F. Mushotzky
Professor Chris S. Reynolds
Professor Derek C. Richardson

Preface

Much of the material contained in this dissertation has been published. The work for Chapter 2 was published in the *Astrophysical Journal* as "Growth of Intermediate-Mass Black Holes in Globular Clusters" (Gültekin et al. 2004), and the work for Chapter 3 was published in the *Astrophysical Journal* as "Three-Body Dynamics with Gravitational Wave Emission" (Gültekin et al. 2006). Both works were parts of a single study into the dynamics of black holes in dense stellar clusters. This dissertation brings together those two works with other material for a coherent yet ongoing study of three-body dynamics with gravitational waves. It examines the influence of dynamics on gravitational waves, the influence of gravitational waves on dynamics and their influence on the formation of intermediate-mass black holes.

For Laura and our children.

Acknowledgements

I am grateful to Cole for being my advisor. Cole has been a model mentor, advisor, and research supervisor throughout my work with him. He has pushed me intellectually and professionally through his incisive Socratic questioning, his willingness to pursue a myriad of cerebral curiosities, and his consistent promotion of my work in the astronomical community. I cannot imagine a better advisor for me.

I am also grateful to Doug for being my collaborator. His advice and guidance has been helpful and much appreciated.

My time at the University at Maryland has been enriched by all of the astronomy department faculty, students, and staff.

Finally, I thank Laura for her kind patience and wonderful help throughout this long ordeal, and I thank my parents for their support and encouragement throughout my entire education. I have been lucky to have had the freedom to follow my heart's content as a career.

Contents

List of Tables

List of Figures

Chapter 1

Introduction

1.1 Scientific Motivation

1.1.1 Ultraluminous X-ray Sources

The scientific motivation for this dissertation is the evinced existence of intermediate-mass black holes (IMBHs): black holes too massive to be stellar-mass black holes and not massive enough to be super-massive black holes ($20\ M_\odot \lesssim M \lesssim 10^5\ M_\odot$). The evidence for IMBHs begins with X-ray observations of so-called ultraluminous X-ray sources (ULXs). ULXs are typically defined as point sources that are not known to be quasars, galactic nuclei, or supernovae and that have an X-ray luminosity in the $2-10$ keV band of $L_X > 10^{39}$ erg s^{-1}. Others have restricted the definition essentially to encompass intermediate-mass black hole candidates by requiring a bolometric luminosity $L_B > 2\times10^{39}$ erg s^{-1}, an irregular variability in the X-ray flux, and a resolvable separation from the host galaxy's nucleus (Kaaret et al. 2004). Here luminosities are equivalent isotropic luminosities, that is, the luminosity assuming that the observed flux is emitted isotropically, and the values given in the definition of ULXs indicate a mass larger than a stellar-mass black hole by the

Eddington argument described below. X-ray observations of galaxies in the early 1980s with the Einstein X-ray satellite revealed X-ray emission not only from active galactic nuclei (AGNs) but also, unexpectedly, from the centers of otherwise normal spiral galaxies. With a spatial resolution of $1'$ on its Imaging Proportional Counter, Einstein was not able to determine whether the ULXs were nuclear sources in their host galaxies or even if they were actually multiple objects (at a distance of 5 Mpc $1'$ is 1.5 kpc). In the early 1990s, the successful launch of the ROSAT satellite with a spatial resolution of $10''$ on its High Resolution Imager enabled astronomers to place some of the ULXs outside of the galaxy's nucleus. With the high resolution available on the current generation of X-ray telescopes ($4''$ on XMM-Newton and $1''$ on Chandra), the positions of many more ULXs have narrowed to exclude the galactic nuclei, and variability observed in multiple observations for some ULXs precludes the possibility of multiple objects within a single beam since multiple objects should not be able to coordinate their variability. In addition, these instruments can provide high spectral resolution observations while excluding contaminating sources.

There are now more than 200 known ULXs with fluxes measured to correspond to luminosities up to 10^{41} erg s^{-1}. That these sources are so bright in X-rays and are variable indicates that the sources are powered by accretion onto a black hole. The small size of a black hole allows matter to flow deep into its potential well where friction and tidal forces heat up the material enough to emit X-rays. The small size also allows for variability on short timescales. The inferred luminosity at which the source is emitting, however, cannot come from an ordinarily emitting, ordinarily accreting, ordinary-sized black hole. Assuming isotropic emission, isotropic accretion, and an opacity dominated by scattering off free electrons in a completely ionized medium, it is possible to calculate a given mass's Eddington luminosity L_E, the maximum luminosity possible without blowing the accreting medium away with

radiation pressure. Equating the force due to radiation pressure from Thomson scattering

$$F_{\rm rad} = \frac{\sigma_T F}{c} = \frac{\sigma_T L}{4\pi c r^2} \tag{1.1}$$

(where $F_{\rm rad}$ is the force from radiation pressure, σ_T is the Thomson scattering cross-section, F is the radiation flux on the medium at a distance r, and L is the intrinsic radiation luminosity) with the gravitational force on the medium

$$F_{\rm grav} = \frac{GMm_H}{r^2} \tag{1.2}$$

(where $F_{\rm grav}$ is the gravitational force of the accreting body of mass M on a hydrogen atom of mass m_H to get

$$L_E = \frac{4\pi GcMm_H}{\sigma_T} = 1.26 \times 10^{38} \left(\frac{M}{M_\odot}\right) \text{ erg s}^{-1}. \tag{1.3}$$

Taking into consideration that the X-ray luminosity is only a fraction (0.1 - 0.5) of the bolometric luminosity and given the assumptions, the ULXs are powered by black holes with masses greater than $20M_\odot$ — greater than $500M_\odot$ for the brightest sources. This is surprising because the maximum mass of black holes that form from the core collapse of an evolved star of solar metallicity is thought to be about 20 $M_\odot$ (Fryer & Kalogera 2001). The spatial separation of the ULXs from the centers of their host galaxies indicates that these objects are not supermassive black holes (SMBHs) that are in a low spectral state. SMBHs, with masses greater than 10^5 $M_\odot$ and less than 10^{10} $M_\odot$, are massive enough to sink to the center of the galaxy from the effects of dynamical friction on timescales much shorter than the age of the host galaxies. For example, the brightest ULX in M82, X1, is at a distance of 200 pc from the kinematical center of the galaxy in which the velocity dispersion is $v_{\rm disp} = 100$ km s^{-1} (Gaffney et al. 1993; Kaaret et al. 2001; Matsumoto et al. 2001). Assuming that the density is an isothermal sphere, the time for a mass M to sink

from a distance r to the center through dynamical friction is

$$t_{\rm df} = \frac{1.65}{\ln \Lambda} \frac{r^2 v_{\rm disp}}{GM} \tag{1.4}$$

where $\ln \Lambda \approx 10$ is the Coulomb logarithm (Binney & Tremaine 1987). So a modest SMBH with $M \sim 10^5\ M_\odot$ orbiting at 500 pc from the nucleus would have sunk to the center of the galaxy in less than 10^{10} yr. A SMBH with $M \sim 10^6\ M_\odot$ would sink in less than 10^9 yr. Colbert & Mushotzky (1999) found that in spiral galaxies ULXs are typically separated from the galactic nucleus with an average separation of 390 pc. ULXs, then, are less massive than SMBHs, and, by the Eddington argument, they are more massive than stellar-mass black holes. This represents a new category of black holes: IMBHs. Although there is little doubt left that stellar mass black holes and SMBHs exist and although the evidence in favor of some IMBHs is strong, the existence of this new type of black hole is not universally accepted. Universal acceptance will probably only follow dynamical measurements of the mass of the black hole that powers a ULX. The fear of writing a dissertation on a possibly non-existent object notwithstanding, alternative explanations for ULXs must be examined.

Beaming

The most commonly mentioned alternative to IMBHs as the mechanism to produce ULXs is the beaming hypothesis of King et al. (2001, see also Reynolds et al. 1997). In this model, accretion onto stellar mass black holes powers a narrow cone of emission that is pointed toward us. Because the emission is highly anisotropic, the inferred luminosities are overestimates of the ULXs' intrinsic luminosities. Thus the Eddington argument for the lower limit on the mass of the accreting black hole does not apply to these beamed sources. King et al. (2001) propose that beaming can be achieved, for example, with a medium with small scattering opacity near the

rotational poles of a compact object with a thick disk surrounding it. The beaming may also be augmented by super-Eddington emission, described below.

Although it would be reckless to say that none of the ULXs is a beamed source, there are three strong lines of observational evidence against beaming for some individual ULXs: He II emission from gas surrounding the ULXs, low temperatures of accretion disks, and observed quasi-periodic oscillations (QPO) in the X-ray fluxes in two ULXs. He II emission has been found in the nebula surrounding several ULXs. The most extensively studied such source is the bright ULX in the Holmberg II dwarf irregular galaxy with inferred X-ray luminosity $L_X = 5$ to 16×10^{39} erg s^{-1} (Kaaret et al. 2004; Pakull & Mirioni 2002). A nebula at the location of the ULX was detected with emission at $\lambda = 468.6$ nm, which comes from the recombination of fully ionized helium (Pakull & Mirioni 2002). Since the He II emission should be isotropic, the measurement of the He II flux is a measure of the X-ray luminosity required to ionize it. The observed $\lambda = 468.6$ nm luminosity of 2.5×10^{36} erg s^{-1} is calculated to come from an emitted X-ray luminosity of $L_X = 3$ to 13×10^{39} erg s^{-1} (Pakull & Mirioni 2002). This is completely consistent with a roughly isotropic emission of the observed X-ray flux. Later observations with the *Hubble Space Telescope* (HST) were able to resolve the morphology of the optical emission from this source including He II, [O I], and Hβ emission (Kaaret et al. 2004). The morphology shows that the central region of the nebula contains the He II emission, and the outer regions to the west, where the He II emission ends, contain the [O I] emission. Both of these regions also show Hβ emission. This is as expected for an X-ray photoionized nebula (Kaaret et al. 2004).

The second line of evidence against beamed emission from accreting stellar-mass black holes is the inference of cool accretion disks. X-ray spectra are typically modeled with either a power-law, a multi-color disk (MCD), or both. The hard power-law

component is thought to come from a Comptonized disk or corona. The MCD model consists of a disk with a temperature profile (for a thin disk $T(r) \propto r^{-3/4}$) so that each annulus of disk emits as a blackbody. Since the flux emitted from the disk scales as $F \propto T^4$, the bolometric luminosity from the innermost part of the disk scales as $L \propto R_{\rm in}^2 F \propto M^2 T_{\rm in}^4$ for a characteristic radius $R_{\rm in}$, which scales with the Schwarzschild radius and therefore the mass. Then for a black hole that is accreting at a fixed rate with respect to Eddington, $L \propto \dot{M} \propto M$, and the temperature of the inner disk scales as $T_{\rm in} \propto M^{-1/4}$. If the accretion rate is allowed to vary for a fixed M, the temperature scales as $T_{\rm in} \propto \dot{M}^{1/4}$. A typical disk temperature for a $\sim 10\ M_\odot$ stellar-mass black hole binary is $\sim 10^7$ K. Early spectra of ULXs from ASCA, which were modeled only with a MCD, revealed disk temperatures that were too hot to be explained by IMBHs. *Chandra* and *XMM Newton* with their higher spatial resolution, however, were able to eliminate contaminating sources, and with their higher spectral resolution, they allowed modeling of spectra with combined power-law and MCD models. With these improvements the models revealed typical temperatures of $T \sim 10^6$ K for inferred luminosities of $\sim 10^{40}$ erg s^{-1}(Miller et al. 2004). The combination of such high luminosities with low disk temperatures is indicative of higher masses. Although this measure of the mass is model-dependent and simple scalings of commonly accepted properties of X-ray binaries may not apply, it is difficult to imagine a scenario in which a beamed cone of emission could produce a spectrum that would look like a disk with a high luminosity and low temperature. One such imagined scenario would be if the beamed emission is optically thick so that it will cool along the cone of emission to a point in the cone with a large effective area. In addition, recent work by Winter et al. (2005) shows that ULXs powered by IMBHs appear to produce X-ray spectra similar to those of Galactic, stellar-mass black hole systems with high/soft and low/hard states. They also find

that some ULXs appear to be very high state stellar-mass black hole systems. So it appears that some ULXs are consistent with an accreting IMBH, and some are bright, ordinary X-ray binary systems.

The third line of evidence against beamed emission comes from the detection of QPOs in two ULXs. The first is an 8.5% rms amplitude oscillation in the X-ray flux between 2 and 10.0 keV with a centroid frequency of 54 mHz in M82 X-1 (Strohmayer & Mushotzky 2003). Although the QPOs are not completely understood, they are generally thought to be disk phenomena. This means that the disk, which will be emitting roughly isotropically, is producing a minimum of 8.5% of the total inferred luminosity $L_{\rm QPO} = 0.085 \times 4 \times 10^{40} = 3.4 \times 10^{39}$ erg s^{-1}. That is, if the disk is emitting only X-rays in the QPO, it is still above the Eddington luminosity of a 20 $M_{\odot}$ object. In addition, the observations show a broad 6.55 keV Fe K line that is required for all fits to the spectrum. Since this broad line results from the X-ray continuum illumination of cold, high-density material, it is difficult to understand how a narrow beam of emission, which would emerge perpendicular to the disk, could interact with the cold, dense matter. The second report of a QPO is a 9.3% rms amplitude QPO in the 0.2 to 10 keV band with a centroid frequency of 203 mHz in the bright ULX in Holmberg IX (Ho IX X-1 Dewangan et al. 2006). Although not as strong a case as that of M82 X1, combined with the low inferred disk temperature of $T \sim 1 - 4 \times 10^6$ K (Miller et al. 2004), it is difficult to explain how the spectrum could be created from a beamed source.

Super-Eddington Accretion

Another objection to invoking IMBHs to power ULXs is that the Eddington limit may not apply because of effects from rapidly rotating, thick disks or because of inhomogeneities in a thin accretion disk's density. For thin, radiation-pressure-dominated accretion disks, the so-called "photon-bubble instability" can form (Arons 1992; Gammie 1998). Pockets of low density within a surrounding, higher density medium effectively trap photons by way of radiative diffusion. These photon bubbles will grow due to radiation pressure, and the denser regions will grow denser as radiation leaves them and as magnetic tension prevents the gas from expanding. If the low-density regions are dynamically coupled to the high-density regions, the disk may remain in an overall state of dynamical equilibrium (Begelman 2002). This allows the photons to travel along low-density escape routes in the disk without blowing the disk apart, and thus the system may radiate above the Eddington limit. Begelman (2006) finds that the maximum luminosity is

$$L_{\max} \sim 20 \left(\frac{\alpha}{0.03}\right) \left(\frac{M}{M_\odot}\right)^{1/9} L_{\rm Edd} \tag{1.5}$$

where $\alpha = p_m/p_r$ is the ratio between the magnetic pressure and radiation pressure. For stellar-mass black holes with $M = 20\ M_\odot$, luminosities may reach up to $L_{\max} \sim 30 L_{\rm Edd} \approx 7 \times 10^{40}$ erg s^{-1}. Thus, super-Eddington accretion by means of photon bubbles alone is just enough to explain the brightest ULXs. One would, however, still expect disks accreting at super-Eddington to be hotter than is seen in some ULXs. In addition, these studies are speculative in nature, and it is possible that photon bubbles may not form at all because of the incoherence and time-dependence of the magnetic field (Begelman 2006).

Frequency of ULXs

The number of identified ULXs is currently around 200 (Colbert & Ptak 2002; Ptak & Colbert 2004; Swartz et al. 2004). Colbert & Ptak (2002) found 87 ULXs from ROSAT HRI data, and Swartz et al. (2004) used Chandra data to find 154, of which they conservatively estimate $\sim 25\%$ to be background sources. Based on ROSAT HRI observations, at least 12% of all galaxies contain a ULX with $L_X > 10^{39}$ erg s^{-1}, and at least 1% of all galaxies contain a ULX with $L_X > 10^{40}$ erg s^{-1} (Ptak & Colbert 2004). These frequencies are lower limits because the $10''$ angular resolution of HRI limits the number of ULXs found near but not in the nuclei of the galaxies and because its comparatively soft bandpass of $0.1 - 2.2$ keV will miss absorbed ULXs behind a column density greater than 10^{21} cm^{-2}. Consistent with these results is the possibility that the frequency of ULXs with $L_X > 2 \times 10^{39}$ erg s^{-1} has been evolving from $\sim 36\%$ at a redshift of $z \sim 0.1$ to $\sim 8\%$ in the nearby universe (Hornschemeier et al. 2003). ULXs also tend to be found in star-forming galaxies, but of galaxies with ULXs, ellipticals have the largest number per galaxy, perhaps because of their larger masses (Colbert & Ptak 2002; Ptak & Colbert 2004). When a spiral galaxy is the host, the ULXs tend to be found near the nucleus with an average projected separation of 390 pc (Colbert & Mushotzky 1999). When in ellipticals, however, ULXs are found in the halo (Irwin et al. 2003).

Luminosity Function of ULXs

The X-ray luminosity function of ULXs shows that ULXs in ellipticals may be of a different nature than those in spirals. In ellipticals the cumulative luminosity function is best explained by a single power-law with slope -1.7 while the luminosity function in spirals is best explained by a broken power-law with a slope -0.6 below $L_X = 10^{40}$ erg s^{-1} and -1.9 above (Swartz et al. 2004). The fact that the population

of ULXs in ellipticals can be fit by a single power law suggests that they may be high-luminosity, stellar-mass X-ray binaries, but with only 7 ULXs with $L_X > 3 \times 10^{39}$ erg s^{-1} this claim cannot be made with high statistical certainty. The absence of a break in the luminosity function does not necessarily mean that there is only a single population of sources. After all, although both accreting neutron stars and stellar-mass black holes contribute to the X-ray luminosity function, there is no break at $\sim 2 \times 10^{38}$ erg s^{-1}, the Eddington luminosity for $M = 1.4\ M_\odot$. Much has been made about the presence of a "knee" in the luminosity function of the population of ULXs in spirals, but there are only ~ 15 sources brighter than the break point, and a power-law with an exponential cutoff also produces a satisfactory fit (Swartz et al. 2004).

Cluster Associations and Companions

Observations of ULXs and their environments at other wavelengths show an association between ULXs and stellar clusters. For example, M82 X-1 is spatially coincident with the young stellar cluster MGG 11 as determined by near infrared observations (McCrady et al. 2003). Fabbiano et al. (2001) found a spatial correlation of ULXs with stellar clusters in the merging Antennae system in excess of that expected from a uniform distribution of ULXs. A comparison of Chandra and HST images of the CD galaxy NGC 1399 at the center of the Fornax cluster shows a spatial correlation between many of its X-ray point sources and its globular clusters (Angelini et al. 2001). These X-ray point sources include two of the three sources with $L_X \gtrsim 2 \times 10^{39}$ erg s^{-1}, and the globular cluster and X-ray positions agree to within the combined astrometric uncertainties.

In addition to an association with stellar clusters, individual stellar companions to ULXs have been found in several cases. These companions are thought to be the

donor stars in the accreting system. Many of these observations reveal O- or B-giant or -supergiant stars as companions such as NGC 5204 X-1 (Goad et al. 2002; Roberts et al. 2001), M81 X-11 (Liu et al. 2002), and M101 ULX1 (Kuntz et al. 2005; Mukai et al. 2005). In these cases, the ULXs appear to be very luminous X-ray binaries with black holes that are not significantly more massive than 20 $M_{\odot}$. Intriguingly, one of the best IMBH candidates, HoII X-1 also contains a hot stellar companion of spectral type between O4 and B3, but it cannot be determined whether the star is a dwarf or supergiant. Such searches for companions are of special importance because the measurement of the period and velocity of the star's orbit around the black hole would yield a lower limit to the mass of the system. Knowledge of the inclination angle gives the mass of the system. The inclination may be found from evidence of eclipses, which indicate nearly edge-on systems, and from modeling the light curve of the distorted stellar companion as the orientation of its non-spherical shape changes with time.

1.1.2 Kinematical and Dynamical Evidence for IMBHs

The presence of non-luminous matter can be inferred from the dynamical and kinematical fingerprint it leaves on the luminous matter in the area. While a bound stellar companion to a black hole is the best way to measure the black hole's mass, stars in a dense stellar environment may interact sufficiently to measure the mass of the system. In this way, evidence from radial velocities of individual stars in M15 as well as velocity and velocity dispersion measurements in G1, a large stellar cluster in the Andromeda Galaxy (M31), indicate that these globular clusters may harbor large dark masses in their cores ($\sim 3.9\ [\pm 2.2] \times 10^3\ M_{\odot}$ and $1.7\ [\pm 0.3] \times 10^4\ M_{\odot}$, respectively, Gebhardt et al. 2000, 2002, 2005; Gerssen et al. 2002). For M15 the data cannot rule out the presence of many compact remnants that contribute to

the high mass-to-light ratio, but the most recent observations of G1 can rule out the absence of dark mass at the 97% confidence level (Gebhardt et al. 2005). One caveat that should be mentioned is that at least the core of G1 is likely to be relaxed, which violates the assumption of a collisionless system in the Vlasov equations used to model the mass distribution of the cluster. In both cases, the observations are of special interest because they are the only direct dynamical measurements of the mass of possible IMBHs.

Additionally, the Galactic globular cluster NGC 6752 contains two millisecond pulsars with high, negative spin derivatives in its core as well as two other millisecond pulsars well into the halo of the cluster at 3.3 and 1.4 times the half mass radius of the globular cluster (Colpi et al. 2003, 2002). The pulsars in the cluster core can be explained by a line-of-sight acceleration by 10^3 $M_\odot$ of dark mass in the central 0.08 pc (Ferraro et al. 2003). While the pulsars in the outskirts of the cluster can be explained by exchange interactions with binary stars, the most likely explanation is that they were kicked from the core in a close interaction with an IMBH, either a single IMBH or a binary that contains an IMBH (Colpi et al. 2003, 2002).

Finally, high spatial resolution observations of an infrared source known as IRS 13E near the galactic center reveal that it is a collection of seven stars, six of which have similar proper motions (Maillard et al. 2004). The similar proper motion suggests that these stars may be the remaining core of a cluster that is in the process of becoming tidally disrupted. If one assumes that the two stars with radial velocity measurements are gravitationally bound to each other, then one infers the presence of 1300 $M_\odot$ of unseen mass. Without further observations of radial velocities of other members of this possible cluster, the IMBH interpretation remains speculative.

1.2 IMBH Formation Models

So there is strong evidence in a number of cases for the existence of IMBHs. One of the most intriguing questions regarding IMBHs is the method of their formation. They must form differently than stellar-mass black holes, and they are distinct from supermassive black holes, whose formation is still not completely understood and may require an IMBH as a seed. A stellar-mass black hole cannot become an IMBH through Bondi-Hoyle accretion alone since the accretion rate from the ISM is

$$\dot{M}_{\rm BH} \approx 4 \times 10^{-15} \left(\frac{M}{50\ M_\odot}\right)^2 \left(\frac{n_{\rm ISM}}{\rm cm^{-3}}\right) \left(\frac{T}{10^6\ \rm K}\right)^{-3/2}\ M_\odot\ \rm yr^{-1} \tag{1.6}$$

where M is the mass of the accreting black hole, $n_{\rm ISM}$ is the number density of the interstellar medium (ISM), and T is the temperature, assuming thermal velocities dominate the relative speed between the gas and the black hole. Thus a 50 $M_\odot$ black hole accreting from the hot ISM with $T = 10^6$ K and $n_{\rm ISM} = 10^{-2}$ cm^{-3} would accrete at a rate $\dot{M}_{\rm BH} = 4{\times}10^{-17}\ M_\odot$ yr^{-1}, with growth timescale $M/\dot{M}_{\rm BH} \sim 10^{18}$ yr much longer than a Hubble time. A molecular cloud can have $n_{\rm ISM} = 10^3$ cm^{-3} and $T = 100$ K, but radiation from the accretion will heat the gas to $T = 10^4$ K (see Miller & Colbert 2004). A 50 $M_\odot$ black hole accreting from such a molecular cloud has growth timescale $M/\dot{M}_{\rm BH} \approx 1.3 \times 10^{10}$ yr, which is roughly the age of the Universe but is much longer than the lifetime of a molecular cloud and the crossing time of the black hole through the cloud. Thus an IMBH requires a more exotic method of formation. The three most favored models of IMBH formation are (1) formation from Population III (Pop III) stars, (2) runaway mergers of stars during the core collapse of a young stellar cluster, and (3) repeated mergers of stellar-mass black holes.

1.2.1 Population III Stars

Madau & Rees (2001) and Schneider et al. (2002) suggest that IMBHs are the remnants of the massive ($M \gtrsim 200\ M_{\odot}$), first generation of stars. The low metallicity of these Pop III stars precludes cooling through metal line emission, and since the Jeans mass scales as $M_J \propto T^{3/2}$, Pop III stars may start their main sequence lives much more massive than solar-metallicity stars thus giving rise to an extremely top-heavy initial mass function. These large stars avoid the significant mass loss from stellar winds, which are driven by metal lines, and nuclear-powered radial pulsations, which are the result of the hotter core temperatures (Baraffe et al. 2001; Fryer et al. 2001; Kudritzki 2000). Thus a large Pop III star may retain almost all of its mass through its main sequence life. If the star is greater than $\sim 250\ M_{\odot}$, it can avoid the electron-positron pair instability that results in a completely destructive supernova and instead collapses directly to a black hole (Madau & Rees 2001).

Although Pop III stars have not been directly observed, there is little doubt that a first generation of stars with primordial abundance existed. The high-mass end of any theoretical initial mass function, however, tends to be the most uncertain, and this is especially true for zero-metallicity stars. In addition, Pop III stellar remnants would not be associated with either the globular or young stellar clusters that are associated with ULXs and other IMBH candidates.

1.2.2 Dynamics of Stellar Clusters

Core-Collapse of Young Stellar Cluster

Many studies have found that IMBHs may form in young stellar clusters where a core collapse leads to direct collisions of stars (Ebisuzaki et al. 2001; Freitag et al. 2006a,b; Gürkan et al. 2006, 2004; Lee 1993; Portegies Zwart & McMillan 2002).

Soon after the first stars in a stellar cluster form, the heaviest stars sink to the center in a process known as mass segregation (e.g., Fregeau et al. 2002; Sigurdsson & Hernquist 1993). As two objects undergo an encounter, they tend towards energy equipartition so that more massive objects tend towards lower velocity and thus sink in the potential well of the cluster. This central concentration of massive stars can lead to number densities high enough that direct stellar collisions can occur. The merger remnant of the first collision has a radius much larger than any other star and therefore the largest cross-section. Thus it is the most likely to suffer another collision before any other object. This merger remnant will have again a much larger cross-section, and the collision process becomes a runaway. The collisions continue until the massive stars explode in supernovae after which the black hole remnants will be too small for direct stellar collisions to occur, or the runaway stops when the supply of stars available for collisions is reduced. Numerical simulations show that masses up to a few 10^3 $M_\odot$ ($\sim 10^{-3}$ of the original cluster mass) can be accumulated through runaway collisions (Freitag et al. 2006b; Gürkan et al. 2004; Portegies Zwart & McMillan 2002). This merger remnant would then presumably evolve into an IMBH.

This model successfully explains the connection between IMBHs and young stellar clusters, as well as globular clusters, assuming that the IMBH produced in a young super star cluster would remain in it until it became a globular. In particular, this model has been shown to successfully describe why there is a ULX (M82 X-1) associated with the MGG 11 super star cluster and not MGG 9, which, unlike MGG 11, has a dynamical friction timescale longer than the ~ 3 Myr lifetime of the most massive stars. The long dynamical friction timescale prevents the central density of the cluster from getting high enough to promote collisions before the stars have evolved. This model, however, does not fully address the evolution

of the merger remnant, which is likely to be nontrivial. For example, the merger remnant may not fully relax from the effects of a collision before the next. The merger remnant may remain puffy and allow grazing encounters to have the impacting star's atmosphere tidally stripped while the star's core escapes. Another possibility is that during the collisional period, stellar winds drive significant mass loss perhaps augmented by metal enrichment from high-energy collisions that mix material into the merger remnant's atmosphere. If such things hamper growth, this process may not be able to create a $\sim 3000\ M_{\odot}$ black hole but, perhaps, a more modest $100 - 200\ M_{\odot}$.

Repeated Mergers of Stellar-Mass Black Holes

Miller & Hamilton (2002b) proposed that over a Hubble time stellar-mass black holes in dense globular clusters may grow by mergers to the inferred IMBH masses. In their model, the heaviest objects in a globular cluster, the black holes (including those in binaries), sink to the center of the cluster. If the total mass of black holes in a cluster is large enough that mass segregation is a runaway process, known as the "mass stratification instability," the black holes dynamically decouple from the rest of the cluster and interact almost entirely with themselves (e.g., O'Leary et al. 2006). In a typical dense globular cluster with reasonable initial mass function, there will be roughly one $50\ M_{\odot}$ black hole that will act as a seed mass for IMBH growth. Although a $50\ M_{\odot}$ is more massive than is thought to be able to form by evolution of an isolated star of solar metallicity, if a star is more massive than $\sim 40\ M_{\odot}$ after mass loss, the supernova will fail to eject the atmosphere of the star (Fryer & Kalogera 2001). This may be possible with the reduced stellar winds in the lower metallicity environment of a globular cluster. This would not apply to young stellar clusters with roughly solar metallicity, but in these clusters, non-runaway collisions

of stars could be enough to offset mass loss. Because of the large cross-section of binaries, this seed black hole will interact with binaries most frequently. Through an exchange bias in which the most massive objects tend to end up with a companion after a binary-single encounter, the seed black hole will swap into a binary. By virtue of being in a binary, the seed mass then interacts mainly with individual black holes. Heggie's Law (Heggie 1975) states that encounters with hard (tight) binaries tend to harden (shrink) the binary further. Thus, these encounters tend to take energy away from the binary and drive the two black holes in the binary toward each other until gravitational radiation, which takes energy away from the system, is strong enough to cause the two black holes to merge. The initial seed black hole has then increased its mass and may repeat the process of acquiring companions, hardening, and merging until it runs out of black holes with which to merge.

This method of IMBH formation has a clear connection to globular clusters but not to very young stellar clusters since it will take a longer time than is available in the youngest stellar clusters suspected to harbor an IMBH. There are three specific concerns regarding this model: (1) Is this process fast enough to create IMBHs? (2) Is this process efficient enough to reach 500 $M_\odot$ or 1000 $M_\odot$ with the available supply of stellar-mass black holes in a globular cluster? (3) Can this mechanism proceed without ejecting the IMBH progenitor? Additionally, one may ask (see § 1.3.2 for more): (4) What predictions does this model make about the observable gravitational wave signals from this process? These four questions are the proximal scientific motivation for this dissertation.

1.3 Background

1.3.1 *N*-body Simulations

The heart of this work is a series of N-body simulations to test the Miller & Hamilton (2002b) model of IMBH formation. While there are many unique aspects to these simulations, the basic idea has not changed since the first published computational N-body experiments by von Hoerner (1960, see also Aarseth & Lecar 1975), which stand in stark contrast to the light-bulb-and-photodetector experiments of Holmberg (1941). In its simplest form, the gravitational N-body problem is merely the solution to the equations

$$\frac{d^2}{dt^2}\boldsymbol{x}_i = G\sum_{j\neq i}^{N} m_j \frac{\boldsymbol{x}_j - \boldsymbol{x}_i}{|\boldsymbol{x}_j - \boldsymbol{x}_i|^3} \tag{1.7}$$

where $\boldsymbol{x}_i$ are the position vectors of the system's N particles with mass m_i. Though the problem is simply stated, there is no closed-form analytical solution for $N > 2$ (Bruns 1887; Poincaré 1892, see also Whittaker 1989 and Julliard-Tosel 2000). Therefore, numerical solutions are required. Much work has gone into ingenious improvements in the efficiency of the calculations as well as the stability of these techniques, especially for large N.

This work concentrates on binary-single scattering experiments. The three-body problem has been studied extensively, but with every new generation of computing power, our understanding of this rich but conceptually simple problem advances with a wider range of numerical simulations and a changing perspective. Previous studies of the three-body problem have tended to focus on the case of equal or nearly equal masses (e.g., Heggie 1975; Hut & Bahcall 1983) though other mass ratios have been studied (e.g., Fullerton & Hills 1982; Heggie et al. 1996; Sigurdsson & Phinney 1993). The nearly equal mass case does not apply to the case of an IMBH in the

core of a stellar cluster. In addition the vast majority of previous work has studied the effect of a single encounter on a binary though Cruz-González & Poveda (1971) and Cruz-González & Poveda (1972) studied the dissolution of Oort cloud comets by simulating the effects of a background of field stars on the Sun and a massless companion. To determine the ultimate fate of an IMBH, simulations of sequences of encounters are needed. Furthermore, to our knowledge no previous work has considered the effects of orbital decay due to gravitational radiation between encounters, which we expect to be important for very tight or highly eccentric binaries.

1.3.2 Gravitational Waves

Although they would occur in any theory of gravity that obeys special relativity (Einstein 1905, because information about changes in the gravitational field propotate at or below the speed of light), one of the most fascinating fallouts of general relativity (Einstein 1915) is the prediction of gravitational waves (Einstein 1916). Gravitational waves, which carry energy, are ripples of curvature in spacetime. Their generation consistent with general relativity is known to exist from period measurements of the Hulse-Taylor pulsar (Hulse & Taylor 1975; Taylor et al. 1979). Although the detection of gravitational waves (and thus their propagation) has not been achieved, the first generation of ground-based gravitational wave observatories is already operational; the next generation of ground-based observatories is in development; and the first generation of space-based observatories is being planned. The latter two are expected to detect gravitational waves from astrophysical sources.

The detection of gravitational waves is difficult because they are so weak, and they are so weak, in part, because gravitational radiation is quadrupolar. This may be seen by following Misner et al. (1973, see also Goldstein et al. 2002) in looking at

the gravitational equivalent of electric dipole radiation (e.g., Jackson 1999), which has luminosity

$$L_{\text{elec dipole}} = \frac{2}{3c^3} e^2 \ddot{\boldsymbol{x}}^2 = \frac{2}{3c^3} \ddot{\boldsymbol{d}}^2_{\text{elec}} \tag{1.8}$$

where $\boldsymbol{d}_{\text{elec}} = e\boldsymbol{x}$ is the electric dipole moment of a charge e with position vector $\boldsymbol{x}$. For the gravitational equivalent, start by writing the mass dipole moment

$$\boldsymbol{d} = \sum_A m_A \boldsymbol{x}_A \tag{1.9}$$

where the sum is carried out over all particles in the system. Since the time rate change of the mass dipole is the total momentum

$$\dot{\boldsymbol{d}} = \sum_A m_A \dot{\boldsymbol{x}}_A = \boldsymbol{p}, \tag{1.10}$$

then there is no dipole gravitational radiation by dint of conversation of momentum, $\ddot{\boldsymbol{d}} = \dot{\boldsymbol{p}} = 0$. In electrodynamics there is also magnetic dipole radiation, which comes from the second time derivative of the magnetic moment. The gravitational equivalent of the magnetic moment is

$$\boldsymbol{\mu} = \sum_A \boldsymbol{x} \times m_A \boldsymbol{v}_A = \boldsymbol{J}, \tag{1.11}$$

the total angular momentum of the system, which is, of course, also conserved. The next leading term, quadrupole radiation, has luminosity (or power)

$$L_{\text{GW quadrupole}} = \frac{1}{5} \frac{G}{c^5} \left\langle \dddot{\mathbf{I}}^2 \right\rangle \tag{1.12}$$

where $\mathbf{I}$ is the trace-free part of the second moment of the mass distribution. It has elements

$$I_{jk} = \sum_A m_A \left(x_{Aj} x_{Ak} - \frac{1}{3} \delta_{jk} x_A^2 \right) \tag{1.13}$$

where δ_{jk} is the Kronecker delta. The third time derivative of $\mathbf{I}$ does not generally vanish, and thus quadrupole radiation is the leading order of gravitational radiation.

The most obvious example of a system that generates gravitational waves is an orbiting binary pair. Dynamically, gravitational waves carry energy away from a two-body system: causing bound bodies' orbits to shrink, and causing unbound bodies to become bound or at least "less unbound." In this dissertation, the dynamical effects of gravitational radiation are the same as a dissipative drag force.

With increasing evidence in support of the existence of intermediate-mass black holes (IMBHs), interest in these objects as gravitational wave sources is also growing (Hopman & Portegies Zwart 2005; Matsubayashi et al. 2004; Miller 2002; Will 2004). Orbiting black holes are exciting candidates for detectable gravitational waves. At a distance d a mass m on a circular orbit of size r around a mass $M \gg m$ generates a gravitational wave amplitude of

$$\begin{aligned} h &\sim \frac{Gm}{rc^2}\frac{v^2}{c^2} = \frac{G^2}{c^4}\frac{Mm}{rd} \\ &= 4.7 \times 10^{-25} \left(\frac{M}{M_\odot}\right) \left(\frac{m}{M_\odot}\right) \left(\frac{r}{\mathrm{AU}}\right)^{-1} \left(\frac{d}{\mathrm{kpc}}\right)^{-1}, \end{aligned} \tag{1.14}$$

where G is the gravitational constant and c is the speed of light. For comparison, with one-year integrations both the *Laser Interferometer Space Antenna* (*LISA*) and Advanced LIGO are expected to reach down to sensitivities of 10^{-23} at frequencies of 10 mHz and 100 Hz, respectively. Thus binaries containing IMBHs with $M \gtrsim 100\ M_\odot$ with small separations at favorable distances are strong individual sources. During inspiral, the frequency of gravitational waves increases as the orbit shrinks until it reaches the innermost stable circular orbit (ISCO) where the orbit plunges nearly radially towards coalescence. Because of the quadrupolar nature of gravitational waves, the gravitational wave frequency for circular binaries is twice the orbital frequency. At the ISCO for a non-spinning black hole with $M \gg m$, where $r_{\mathrm{ISCO}} = 6GM/c^2$ and $h \sim Gm/6c^2d$ is independent of the mass of the pri-

mary, the gravitational wave frequency is

$$f_{\rm GW} = 2f_{\rm orb} = 2\left(\frac{GM}{4\pi^2 r_{\rm ISCO}^3}\right)^{1/2} \approx 4400 \text{ Hz}\left(\frac{M_\odot}{M}\right). \tag{1.15}$$

Thus a binary with a 100 $M_\odot$ black hole will pass through the *LISA* band (10^{-4} to 10^0 Hz, Danzmann 2000) and into the bands of ground-based detectors such as LIGO, VIRGO, GEO-600, and TAMA (10^1 to 10^3 Hz, Ando & the TAMA collaboration 2002; Barish 2000; Fidecaro & VIRGO Collaboration 1997; Schilling 1998) whereas a 1000 $M_\odot$ black hole will be detectable by *LISA* during inspiral but will not reach high enough frequencies to be detectable by currently planned ground-based detectors. After the final inspiral phase, the gravitational wave signal goes through a merger phase, in which the horizons cross, and a ringdown phase, in which the spacetime relaxes to a Kerr spacetime (Cutler & Thorne 2002; Flanagan & Hughes 1998a,b). The merger and ringdown phases emit gravitational waves at a higher frequency with a characteristic ringdown frequency of $f \sim 10^4(M/M_\odot)^{-1}$ Hz so that mergers with more massive IMBHs will still be detectable with ground-based detectors.

If stellar clusters frequently host IMBHs, then currently planned gravitational wave detectors may detect mergers within a reasonable amount of time. Optimistic estimates put the upper limit to the Advanced LIGO detection rate of all black holes in dense stellar clusters at ~ 10 yr^{-1} (O'Leary et al. 2006). The *LISA* detection rate for a 1-yr integration and signal-to-noise ratio of S/N = 10 is (Will 2004)

$$\begin{aligned}\nu_{\rm det} &\approx 10^{-6}\left(\frac{H_0}{70 \text{ km s}^{-1}\text{Mpc}^{-1}}\right)^3\left(\frac{f_{\rm tot}}{0.1}\right) \\ &\quad\times\left(\frac{\mu}{10\ M_\odot}\right)^{19/8}\left(\frac{M_{\rm max}}{100\ M_\odot}\right)^{13/4}\left(\ln\frac{M_{\rm max}}{M_{\rm min}}\right)^{-1} \text{ yr}^{-1},\end{aligned} \tag{1.16}$$

where H_0 is the Hubble constant, $f_{\rm tot}$ is the total fraction of globular clusters that contain IMBHs, μ is the reduced mass of the merging binary, and $M_{\rm min}$

and $M_{\rm max}$ denote the range in masses of IMBHs in clusters. If we assume that $M_{\rm min} = 10^2\ M_\odot$, $M_{\rm max} = 10^3\ M_\odot$, $\mu = 10\ M_\odot$, $f_{\rm tot} = 0.8$ (O'Leary et al. 2006), and $H_0 = 70$ km s^{-1}Mpc^{-1}, then we get a rate of 0.006 yr^{-1}. This, however, implies that $10^3\ M_\odot$ black holes are continuously accreting $10\ M_\odot$ black holes, which is unlikely to be the case. Since the distance out to which *LISA* can detect a given gravitational wave luminosity D_L scales as the square root of the integration time T, the volume probed scales as $V \sim D_L^3 \sim T^{3/2}$. This means that a 10-yr integration could yield a rate of 0.2 yr^{-1}, and if IMBHs with mass $M = 10^4\ M_\odot$ are common, the rate could be much higher. These rates, however, are optimistic and should be considered as upper limits. A gravitational wave detection of an IMBH with high signal-to-noise could also yield the spin parameter and thus shed light on the formation mechanism of the IMBH (Miller 2002). Because detection of inspiral requires the comparison of the signal to a pre-computed waveform template that depends on the orbital properties of the binary, knowing the eccentricity distribution is useful. For $e \lesssim 0.2$, circular templates are accurate enough to detect the gravitational wave signal with LIGO (Martel & Poisson 1999), and this is likely to be the case for *LISA* as well. A full understanding of the gravitational wave signals from IMBHs requires a more detailed study of the complicated dynamics and gravitational radiation of these systems.

1.4 Overview of This Dissertation

This dissertation was designed to answer the following questions.

1. Is the Miller & Hamilton (2002b) model of IMBH formation fast enough to make an IMBH before the globular cluster's supply of stellar-mass black holes eject themselves from the cluster through dynamical interactions ($\sim$ 0.4 to

1 Gyr)?

2. Can repeated mergers of stellar-mass black holes in a globular cluster produce an IMBH without ejecting too many stellar-mass black holes via the encounters that harden the IMBH-progenitor binary?

3. Will a globular cluster retain an IMBH progenitor over the course of its merger history, or will the binary-single scattering events eject the IMBH progenitor with great regularity?

4. What is the observable gravitational-wave signature of these merging and inspiraling systems?

In the process of answering these questions, several more arose and are also addressed in this dissertation.

5. What is the reason for the apparent broken power-law in the cross-section for close approach?

6. How does the cross-section for close approach change when gravitational waves are included?

7. What is the likelihood of merger because of gravitational radiation during a binary-single encounter when the leading-order terms of energy loss from gravitational waves are included?

We investigate these questions with simulations of sequences of binary-single encounters as they would occur for black holes in dense stellar clusters. In Chapter 2 we introduce the code (§ 2.2) used to integrate the sequences of three-body interactions as well as the major assumptions involved. We then present results of purely Newtonian simulations and simulations that include gravitational waves between encounters, and discuss the implications for IMBH formation and gravitational wave

detection. In Chapter 3 we describe the changes to the code necessary to include gravitational waves during the encounter. We look into close-approach and merger cross sections in § 3.3, and present results of simulations that include gravitational waves as well as their implications for IMBH formation and gravitational wave detection. In Chapter 4 we summarize our main results and conclusions.

Chapter 2

Growth of Intermediate-Mass Black Holes in Globular Clusters

2.1 Overview

In this chapter we present numerical simulations of sequences of high-mass ratio binary-single encounters. We describe the code used to simulate the encounters in § 2.2. Next, we present results of the simulations of sequences of encounters on a range of mass ratios with Newtonian gravity (§ 2.3.1) and with gravitational radiation between encounters (§ 2.3.2) and show that including gravitational radiation decreases the duration of the sequence by $\sim$ 30% to 40%. In § 2.4 and § 2.5 we discuss the implications of these results for IMBH formation and gravitational wave detection.

2.2 Numerical Method

We perform numerical simulations of the interactions of a massive binary in a stellar cluster. Simulating the full cluster is beyond current N-body techniques, so we focus instead on a sequence of three-body encounters. Massive cluster objects, such as IMBHs and tight binary systems, tend to sink to the centers of clusters so that a single IMBH is very likely to meet a binary (Sigurdsson & Phinney 1995). Exchanges in which the IMBH acquires a close companion are common. Such a binary in a stellar cluster core will experience repeated interactions with additional objects as long as the recoils from these interactions do not eject the binary. Therefore, we simulate a *sequence* of encounters between a hard binary and an interloper. We perform one interaction and then use the resulting binary for the next encounter. This is repeated multiple times until the binary finally merges because of gravitational radiation. Because typical velocities involved are non-relativistic and the black holes are tiny compared to their separations, they are treated as Newtonian point masses. In Chapter 3 we see how this changes when gravitational radiation is included throughout. In order to test the influence of the binary's mass, we use a range of binary mass ratios. To simplify the problem we study a binary with mass ratio of N:10 $M_\odot$ and a 10 $M_\odot$ interloper, designated as N:10:10, and vary N between 10 $M_\odot$ and 10^3 $M_\odot$.

The simulations were done using a binary-single scattering code that was written to be as general purpose as possible. See Appendix D for examples of other applications. Because of the vast parameter space that needs to be covered, the code uses a Monte Carlo initial condition generator. The orbits are integrated using HNBody, a hierarchical, direct N-body integrator, with the adaptive fourth-order

Runge Kutta integrator option (K. Rauch & D. Hamilton, in preparation)[1]. Because we focus on close approaches where a wide range of timescales are important, an adaptive scheme is often better than symplectic methods, which are time-reversible and bound the error in energy conservation for a fixed timestep.

In wide hierarchical triples, direct integration can consume a large amount of computational time. To reduce this, we employ a two-body approximation scheme that tracks the phase of the inner binary. For a sufficiently large outer orbit, the orbit is approximately that of an object about the center of mass of the binary. If both the distance from the outer object to the inner binary's center of mass and the semimajor axis of the outer binary are greater than 30 times the inner binary's semimajor axis, $a_{\rm ib}$, we calculate this approximate two-body orbit analytically and keep track of the inner binary's phase. When the outer object nears the binary again, we revert to direct numerical integration.

The orbit is integrated until one of three conditions is met: (1) one mass is at a distance of least $30a_{\rm ib}$ and is departing along a hyperbolic path, (2) the system forms a hierarchical triple with outer semimajor axis greater than 2000 AU, an orbit so large that it would likely be perturbed in the high density of a cluster core and not return, (3) an ionization[2] or merger is detected, or (4) the integration is prohibitively long, in which case the encounter is discarded and restarted with new randomly generated initial conditions. Roughly 10^{-4} of all encounters had to be restarted with most occurring for higher mass ratios where resonant encounters (encounters that have more than one close approach and are not simple fly-bys) are more common.

[1]See http://janus.astro.umd.edu/HNBody/.

[2]The total energy of the binary-single encounters simulated in this dissertation is negative, which precludes ionization as a possibility, but for the sake of generality this test is included. For an example in which ionization of the binary is both possible and significant, see § D.2.

It is an unfortunate reality of simulations such as ours that the integration of some small sample of encounters will require a longer time than is practical. We tested the effect of our arbitrary limit by extending the allowed integration time by a factor of 10^2 for one hundred sequences for $m_0 = 100$ and $1000 M_\odot$. There were no statistically significant differences. In particular, the average time per sequence, average final semimajor axis, and average final eccentricity all differed by less than 2%. In half of the simulations presented in this chapter, we evolve the binary's orbit due to gravitational wave emission after each encounter. Since a binary in a cluster spends most of its time and emits most of its gravitational radiation while waiting for an encounter rather than during an interaction, we only include gravitational radiation between encounters. The effects of adding gravitational waves during the encounter are discussed in Chapter 3. To isolate this effect, we run simulations both with and without gravitational radiation between encounters. We include gravitational radiation by utilizing orbit-averaged expressions for the change in semimajor axis a and eccentricity e with respect to time (Peters 1964):

$$\frac{da}{dt} = -\frac{64}{5} \frac{G^3 m_0 m_1 (m_0 + m_1)}{c^5 a^3 (1 - e^2)^{7/2}} \left(1 + \frac{73}{24} e^2 + \frac{37}{96} e^4\right) \tag{2.1}$$

and

$$\frac{de}{dt} = -\frac{304}{15} \frac{G^3 m_0 m_1 (m_0 + m_1)}{c^5 a^4 (1 - e^2)^{5/2}} \left(e + \frac{121}{304} e^3\right), \tag{2.2}$$

where m_0 and m_1 ($m_0 \geq m_1$) are the gravitational masses of the binary pair. Here G is the gravitational constant, and c is the speed of light. The orbital elements are evolved until the next encounter takes place, at a time that we choose randomly from an exponential distribution with a mean encounter time, $\langle \tau_{\rm enc} \rangle = 1/\langle n v_\infty \sigma \rangle$, where n is the number density of objects in the cluster's core, v_∞ is the relative velocity, and σ is the cross-section of the binary. If we assume the mass of the

binary $m_0 + m_1 \gg m_2$, then

$$\sigma \approx \pi r_p^2 + 2\pi r_p G\left(m_0 + m_1\right)/v_\infty^2, \tag{2.3}$$

where r_p is the maximum considered close approach of m_2 to the binary's center of mass. For a thermal distribution of stellar speeds, $v_\infty = \left(m_{\rm avg}/m_2\right)^{1/2} v_{\rm ms}$, where $m_{\rm avg} = 0.4\ M_\odot$ is the average mass of the main sequence star and $v_{\rm ms}$ is the main sequence velocity dispersion. In our simulations, the second term of Equation 2.3, gravitational focusing, dominates over the first. Averaging over velocity (assumed to be Maxwellian) we find

$$\langle \tau_{\rm enc} \rangle = 2 \times 10^7 \left(\frac{v_{\rm ms}}{10\ {\rm km\ s^{-1}}}\right)\left(\frac{10^6\ {\rm pc^{-3}}}{n}\right)\left(\frac{1\ {\rm AU}}{r_p}\right)\left(\frac{1\ M_\odot}{m_0+m_1}\right)\left(\frac{1\ M_\odot}{m_2}\right)^{1/2} {\rm yr}. \tag{2.4}$$

We then subject the binary to another encounter using orbital parameters adjusted by both the previous encounter and the gravitational radiation emitted between the encounters. This sequence of encounters continues until the binary merges due to gravitational wave emission. If orbital decay is not being calculated, then we determine that the binary has merged when the randomly drawn encounter time is longer than the timescale to merger, which is approximately

$$\tau_{\rm merge} \approx 6 \times 10^{17} \frac{\left(1\ M_\odot\right)^3}{m_0 m_1 \left(m_0 + m_1\right)} \left(\frac{a}{1\ {\rm AU}}\right)^4 \left(1 - e^2\right)^{7/2} {\rm yr} \tag{2.5}$$

for the high eccentricities of importance in this dissertation.

For binaries with unequal masses, gravitational wave emission before coalescence imparts a recoil velocity on the binary (Favata et al. 2004). As two objects with unequal masses or with misaligned spins spiral in towards each other, asymmetric emission of gravitational radiation produces a recoil velocity on the center of mass of the binary. Most of the recoil comes from contributions after the masses are inside

of the ISCO, where post-Newtonian analysis becomes difficult (Favata et al. 2004). For non-spinning black holes, the velocity kick from the recoil up to the ISCO is (Favata et al. 2004)

$$v_r = 15.6 \text{ km s}^{-1} \frac{f(q)}{f_{\max}} \tag{2.6}$$

where $q = m_1/m_0 < 1$, $f(q) = q^2(1-q)/(1+q)^5$, and $f_{\max} \approx f(0.38) = 0.018$. Favata et al. (2004) bounded the total recoil to between 20 km s^{-1} $\leq v_r \leq$ 200 km s^{-1} for non-spinning black holes with $q = 0.127$. Since the recoil velocity scales as q^2 for $q \ll 1$, this may be scaled to other mass ratios. More recently, Blanchet et al. (2005) argued from high order post-Newtonian expansions that the kick speed for very small mass ratios $q \ll 1$ was $v_r/c = 0.043q^2$, with an uncertainty of roughly 20%. This is consistent with the results of Favata et al. (2004), but as most of the recoil originates well inside the ISCO, Blanchet et al. (2005) caution that numerical results are probably required for definitive answers. Using the effective one-body approach, Damour & Gopakumar (2006) find a maximum recoil velocity of $v_r = 74$ km s^{-1}. Most recently, Baker et al. (2006) presented the first accurate, numerical relativity simulations of the merger of two non-spinning black holes, and for $q = 2/3$ found an estimated recoil velocity of $v_r = 105$ km s^{-1} with an error of less than 10%. All calculations are consistent with the wide range first reported by Favata et al. (2004). Because of the disparity among the several calculations, we chose not to include this effect in our simulations, but we comment on the possible effects it could have in § 2.4 and § 3.4.1.

Global energy and angular momentum are monitored to ensure accurate integration. The code also keeps track of the duration of encounters, the time between encounters, changes in semimajor axis and eccentricity, and exchanges (events in which the interloping mass replaces one of the original members of the binary and the replaced member escapes).

As a test of our code, we compared simulations of several individual three-body encounters with the work of Heggie et al. (1996). As part of a series of works examining binary-single star scattering events, Heggie et al. (1996) performed numerical simulations of very hard binaries with a wide range of mass ratios and calculated their cross-sections for exchange. We ran simulations of one encounter each of a sample of mass ratios for comparison. To facilitate comparison of encounters with differing masses, semimajor axes, and relative velocities of hard binaries, Heggie et al. (1996) use a dimensionless cross-section,

$$\bar{\sigma}_{\rm ex} = \frac{2v_\infty^2 \Sigma}{\pi G \left(m_0 + m_1 + m_2\right) a}, \tag{2.7}$$

where v_∞ is the relative velocity of the interloper and the binary's center of mass at infinity and Σ is the physical cross-section for exchanges. We calculate Σ as the product of the fraction of encounters that result in an exchange ($f_{\rm ex}$) and the total cross-section of encounters considered: $f_{\rm ex}\pi b_{\rm max}^2$, where $b_{\rm max}$ is an impact parameter large enough to encompass all exchange reactions. Our cross-sections are in agreement with those of Heggie et al. (1996) within the combined statistical uncertainty as seen in Table 2.1.

2.3 Simulations and Results

We used our code to run numerical experiments of three-body encounter sequences with a variety of mass ratios. The binaries consisted of a dominant body with mass $m_0 = 10$, 20, 30, 50, 100, 200, 300, 500, or 1000 $M_\odot$ and a secondary of mass $m_1 = 10\ M_\odot$. Because of mass segregation, the objects that the binary encounters will be the heaviest objects in the cluster. In order to simplify the problem, we consider only interactions with interlopers of mass $m_2 = 10\ M_\odot$. The binary starts with a circular $a = 10$ AU orbit, and the interloper has a relative speed at infinity of $v_\infty =$

Table 2.1. Single Encounter Cross-sections for Exchange.

m_0:m_1:m_2	Ejected Mass	HHM96	This Work
10 : 1 : 1	1	1.086 ± .105	1.054 ± .023
	10	—	—
10 : 1 : 10	1	7.741 ± .360	7.825 ± .255
	10	0.513 ± .087	0.520 ± .043
3 : 1 : 1	1	2.465 ± .170	2.311 ± .073
	3	0.072 ± .025	0.059 ± .007

Note. — This table compares dimensionless cross-sections for exchange $\bar{\sigma}_{\rm ex}$ (see text for details) calculated by Heggie et al. 1996 and by us. The first column lists the masses, with binary components m_0 and m_1. Column two shows the mass of the ejected object. The ejection of the smaller mass is energetically favored so it always has a larger cross-section. There is general agreement between the two calculations to within the statistical uncertainty, which we calculate as $\bar{\sigma}/N_{\rm ex}^{1/2}$, where $N_{\rm ex}$ is the total number of exchanges.

10 km s^{-1} and an impact parameter, b, relative to the center of mass of the binary such that the pericenter distance of the hyperbolic encounter would range from $r_p = 0$ to $5a$. In order to represent an isotropic distribution of encounters, the distribution of impact parameters is $P(b) \propto b$. For all binaries, $v_{\rm circ} = \left[G\left(m_0 + m_1\right)/a\right]^{1/2} \geq 40$ km s^{-1} $\gg v_\infty$, and thus all are considered hard. The Monte Carlo initial condition generator distributes the orientations and directions of encounters isotropically in space, and the initial phase of the binary is randomized such that it is distributed equally in time. In a multi-mass King model for a stellar cluster, the scale height of bodies with mass m scales as $(m_{avg}/m)^{1/2}$ (Sigurdsson & Phinney 1995). Thus black holes with mass $m = 10M_\odot$ have a scale height 1/5 of the scale height of the average-mass main sequence star, $m_{\rm avg} \approx 0.4\ M_\odot$. The volume occupied by black holes, then, is more than 100 times smaller than the volume occupied by average-mass main sequence stars, and if black holes are at least 10^{-2} times as numerous, which would be expected for a Salpeter mass function, then their core number

density is at least comparable to that of visible stars (Miller & Hamilton 2002b). Thus we assume the cluster core has a density of $n = 10^5$ pc^{-3} and an escape velocity of $v_{\rm esc} = 50$ km s^{-1} for the duration of the simulation. We discuss the consequences of changing the escape velocity in § 2.4. For each mass ratio, we simulate 1000 sequences with and without gravitational radiation between encounters.

2.3.1 Pure Newtonian Sequences

Figure 2.1a shows the change of semimajor axis and pericenter distance as a function of time over the course of a typical Newtonian sequence. The encounters themselves take much less time then the period between encounters, so a binary spends virtually all its time waiting for an interloper. Most of the time in this example is spent hardening the orbit from 1 AU to 0.4 AU because as the binary shrinks, its cross-section decreases and the timescale to the next encounter increases. Figure 2.1b shows the same sequence plotted as a function of number of encounters. The semimajor axis decreases by a roughly constant factor with each encounter. This is expected for a hard binary, which, according to Heggie's Law (Heggie 1975), tends to harden with each encounter at a rate independent of its hardness. The eccentricity and therefore the pericenter distance, $r_p = a\,(1-e)$, however, can change dramatically in a single encounter (for a discussion on eccentricity change of a binary in a cluster, see Heggie & Rasio 1996). This sequence ends with a very high eccentricity ($e = 0.968$), which reduces the merger time given by Equation 2.5 to less than $\tau_{\rm enc}$.

Table 2.2 summarizes our main results and shows a number of interesting trends. The average number of encounters per sequence, $\langle n_{\rm enc} \rangle$, increases with increasing mass ratio since the energy that the interloper can carry away scales as $\Delta E/E \sim m_1/\left(m_0 + m_1\right)$ and since $n_{\rm enc} \sim E/\Delta E$ for a constant eccentricity (Quinlan 1996). Energy conservation assures that every hardening event results in an increased rel-

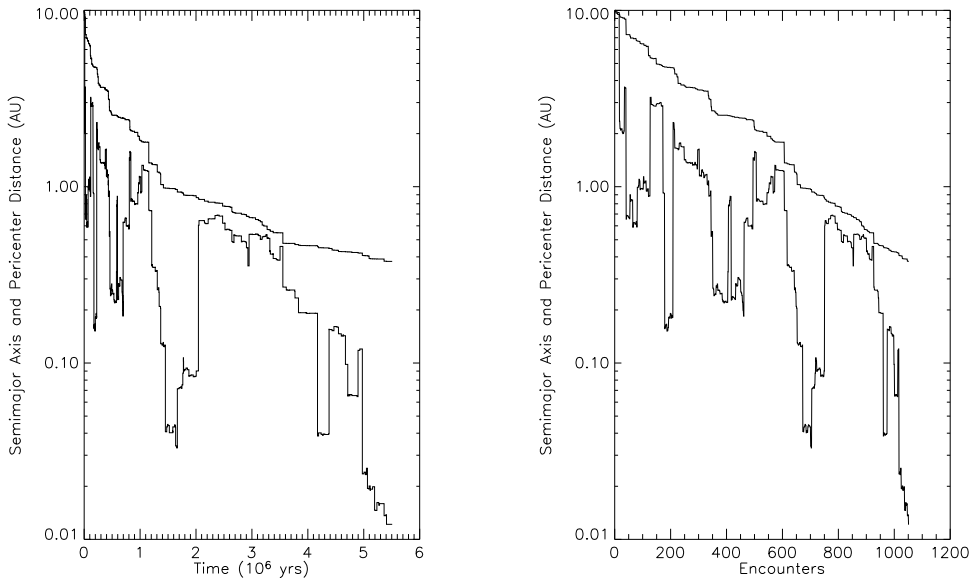

Figure 2.1: Newtonian 1000:10:10 sequence. These panels show the semimajor axes (upper curves) and pericenter distances (lower curves) as functions of time (left panel) and number of encounters (right panel) for one sequence of encounters with no gravitational wave emission. Each change in a and r_p is the result of a three-body encounter. Since the binary is hard, the semimajor axis gradually tightens by a roughly constant fractional amount per encounter with most of the time spent hardening the final fraction when close encounters are rare. The pericenter distance, however, fluctuates greatly due to large changes in eccentricity during a single encounter. The sequence ends at a very high eccentricity when the binary would merge due to gravitational radiation before the next encounter.

ative velocity between the binary and the single black hole. If the velocity of the single black hole relative to the barycenter, and thus the globular cluster, is greater than the escape velocity of the cluster core (typically $v_{\rm esc} = 50$ km s^{-1} for a dense cluster; see Webbink 1985), then the single mass will be ejected from the cluster. The average number of ejected masses per sequence, $\langle n_{\rm ej} \rangle$, also increases with increasing mass ratio because the higher mass ratio sequences have a larger number of encounters and because the larger mass at a given semimajor axis has more energy for the interloper to tap. Conservation of momentum guarantees that if a mass is ejected from the cluster at high enough velocity, the binary will also be ejected. Table 2.2 lists $\langle f_{\rm binej} \rangle$, the fraction of sequences that result in the ejection of the binary

Table 2.2. Sequence Statistics.

m_0	Case	$\langle n_{\rm enc}\rangle$	$\langle n_{\rm ej}\rangle$	$\langle f_{\rm binej}\rangle$	$\langle t_{\rm seq}\rangle /10^6$ yr	$\langle a_f\rangle$ /AU	$\langle e_f\rangle$
10	Newt.	51.6	3.9	0.880	82.72	0.164	0.929
	GR Evol.	48.7	3.7	0.839	59.89	0.190	0.901
20	Newt.	51.3	6.5	0.835	65.94	0.178	0.924
	GR Evol.	47.1	6.1	0.776	43.46	0.230	0.898
30	Newt.	58.9	9.3	0.753	49.11	0.198	0.926
	GR Evol.	55.1	8.6	0.676	31.89	0.222	0.892
50	Newt.	73.2	14.6	0.581	33.75	0.230	0.919
	GR Evol.	66.7	13.0	0.455	22.73	0.285	0.892
100	Newt.	102.0	24.0	0.229	21.35	0.327	0.936
	GR Evol.	93.4	20.1	0.161	14.97	0.357	0.873
200	Newt.	158.4	38.2	0.043	15.13	0.387	0.938
	GR Evol.	140.3	31.5	0.026	9.998	0.444	0.872
300	Newt.	208.5	49.1	0.013	11.89	0.468	0.943
	GR Evol.	184.0	39.4	0.006	7.822	0.445	0.874
500	Newt.	308.7	71.1	0.001	9.920	0.528	0.944
	GR Evol.	269.1	54.9	0	6.225	0.488	0.860
1000	Newt.	562.4	117.3	0	7.363	0.641	0.953
	GR Evol.	483.0	88.9	0	4.427	0.556	0.851

Note. — Table 2.2 summarizes the main results of our simulations of sequences of three-body encounters. For each dominant mass, m_0, we ran 1000 sequences of pure Newtonian encounters (Newt.) and 1000 sequences of the more realistic Newtonian encounters with gravitational radiation between encounters (GR Evol.). The columns list the average number of encounters per sequence $\langle n_{\rm enc}\rangle$, the average number of black holes ejected from the cluster in each sequence $\langle n_{\rm ej}\rangle$, the fraction of sequences in which the binary is ejected from the cluster, $\langle f_{\rm binej}\rangle$, the average total time for the sequence $\langle t_{\rm seq}\rangle$, the average final semimajor axis $\langle a_f\rangle$, and the average final eccentricity $\langle e_f\rangle$.

from the cluster. As expected, the fraction decreases sharply with increasing mass such that virtually none of the binaries with mass greater than 300 $M_\odot$ escapes the cluster.

The shape and size of the orbit after its last encounter determine the dominant gravitational wave emission during the inspiral and are of particular interest to us. The distribution of pre-merger semimajor axes for all mass ratios is shown in Figure 2.2. The distributions all have a similar shape that drops off at low a because the binary tends to merge before another encounter can harden it. For large orbits

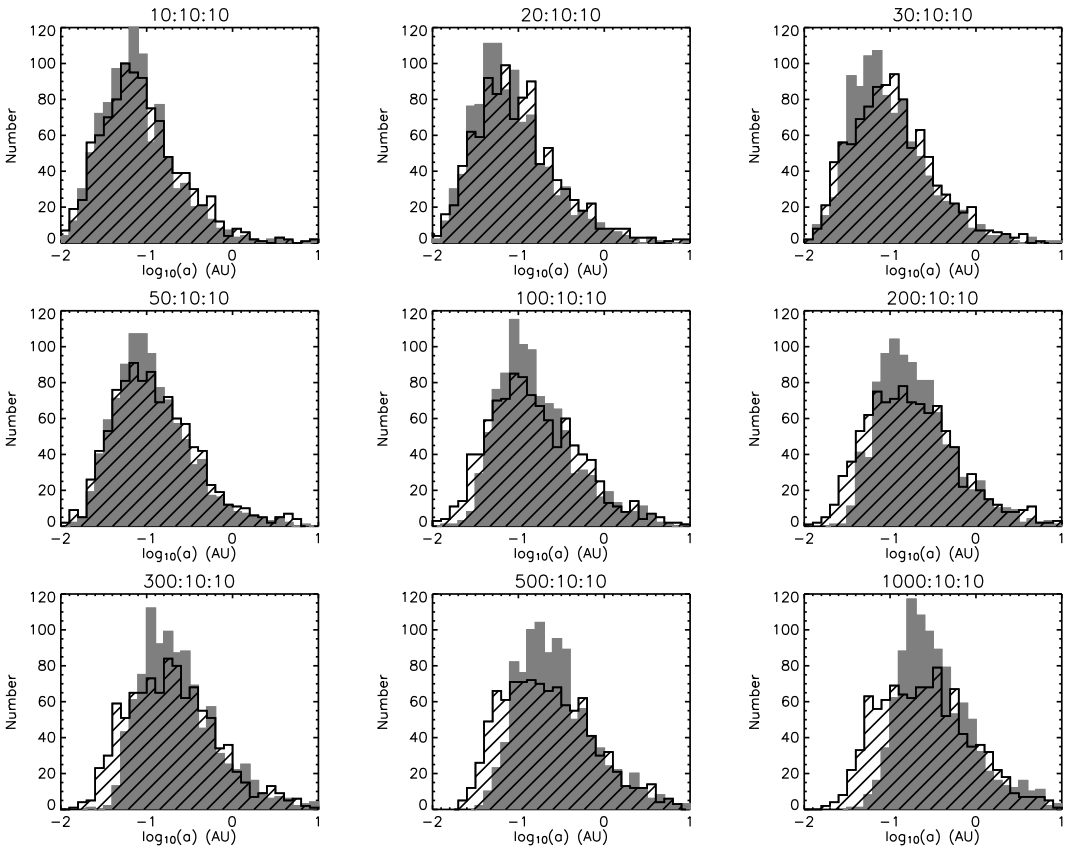

Figure 2.2: Histograms of final semimajor axes for all mass ratios. The solid histograms are pure Newtonian sequences, and the hatched histograms are sequences with gravitational radiation between encounters. The histograms all have similar shapes with a sharp drop at low a since the binary tends to merge before another encounter can harden it, and they have long tails at high a where the binary will only merge with high eccentricity. The sequences with gravitational radiation have falloffs at smaller a than those without due to both the circularization and the extra source of hardening.

the binary will only merge for a high eccentricity, and thus there are long tails in the histograms towards high a from encounters that resulted in an extremely high eccentricity. The distributions for lower mass ratios are shifted to smaller a because for a given orbit, a less massive binary will take longer to merge. This can also be seen in the mean final semimajor axis, $\langle a_f \rangle$, in Table 2.2.

Figure 2.3 shows the distribution of binary eccentricities after the final encounter for one mass ratio. The plot is strongly peaked near $e = 1$, a property shared by

all other mass ratios. This distribution is definitely not thermal, a distribution in which the probability scales as $P(e) = 2e$ and the mean eccentricity of which is $\langle e \rangle_{\rm th} \approx 0.7$. The high eccentricity before merger results from both the strong dependence of merger time on eccentricity and the fact that the eccentricity can change drastically in a single encounter (see Figure 2.1). As the semimajor axis decreases by roughly the same fractional amount in each encounter, the eccentricity increases and decreases by potentially large amounts with each strong encounter. When the eccentricity happens to reach a large value, the binary will merge before the next encounter. Figure 2.4 shows the eccentricity distribution for all encounters after the first 10 for all 1000 sequences with a mass ratio of 1000:10:10. The first ten encounters are excluded so that the binary has faced sufficient encounters to thermalize. The distribution is roughly thermal up to high eccentricity where the binaries merge. Thus merger selectively removes high eccentricity binaries from a thermal distribution.

2.3.2 General Relativistic Binary Evolution

The addition of gravitational radiation between Newtonian encounters is expected to alter a sequence since it is an extra source of hardening and since it circularizes the binary. Figure 2.5 shows a typical sequence for the 1000:10:10 mass ratio including gravitational radiation. Three-body interactions drive the binary's eccentricity up to $e = 0.959$ and its semimajor axis down to $a = 0.713$ AU. Then starting at $t = 2.2 \times 10^6$ yr over the course of about ten interactions that only weakly affect the eccentricity and semimajor axis, gravitational radiation causes the orbit to decay to $a = 0.550$ AU and $e = 0.946$ while the pericenter distance remains roughly constant. The corresponding semimajor axis change in the Newtonian-only sequences in Figure 2.1 takes 45 encounters and more than twice as long although one must

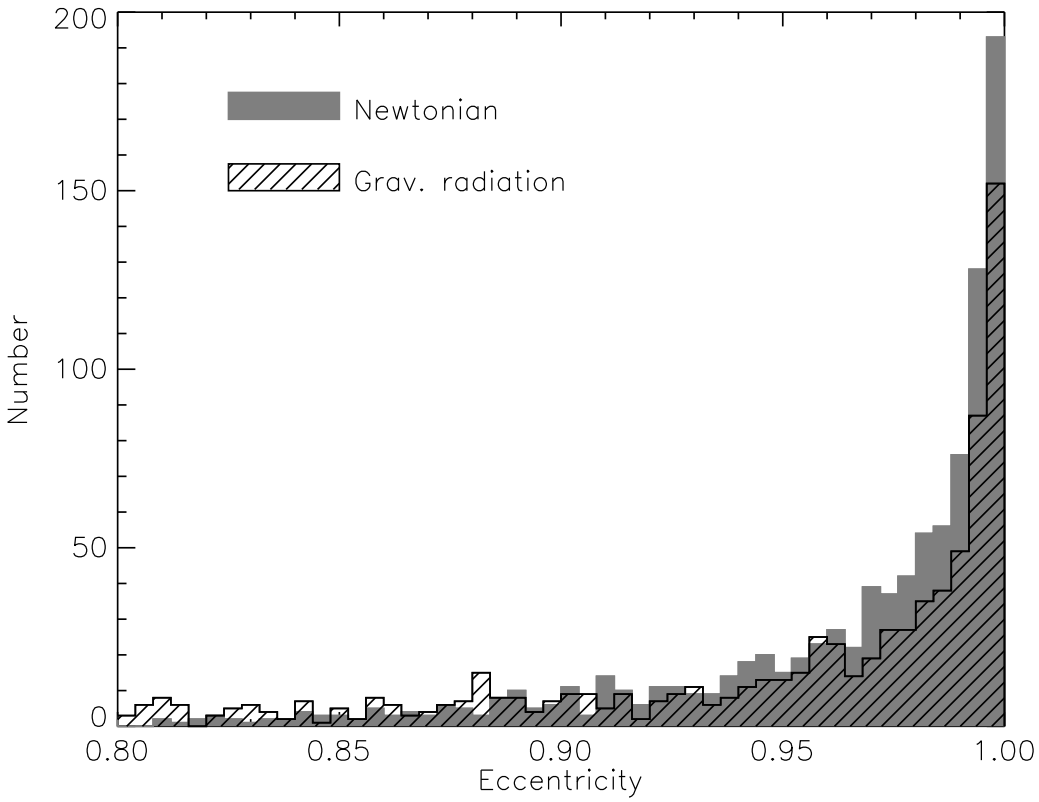

Figure 2.3: Histogram of final eccentricities for 1000:10:10 mass ratio. The solid histogram is from pure Newtonian sequences, and the hatched histogram is from sequences with gravitational radiation between encounters. The histogram is cut at $e = 0.8$ because $e_f < 0.8$ is rare. The histograms have roughly the same shape for both cases and for all mass ratios although the gravitational wave sequences have a consistently lower mean at higher mass ratios because gravitational wave emission damps eccentricities. The histograms show a decidedly non-thermal distribution and are strongly peaked near $e = 1$. Because the timescale to merge due to gravitational radiation is so strongly dependent on e, the binary will merge when it happens to reach a high eccentricity.

be careful when comparing two individual sequences. Gravitational waves make the most difference when the pericenter distance is small, which is guaranteed at the end of a sequence, but can also happen in the middle as Figure 2.5 shows.

Table 2.2 summarizes the effect of adding gravitational radiation. In general the effect is greater at higher masses because gravitational radiation is stronger for a given orbit. Because of the extra energy sink, the binaries merge with fewer encoun-

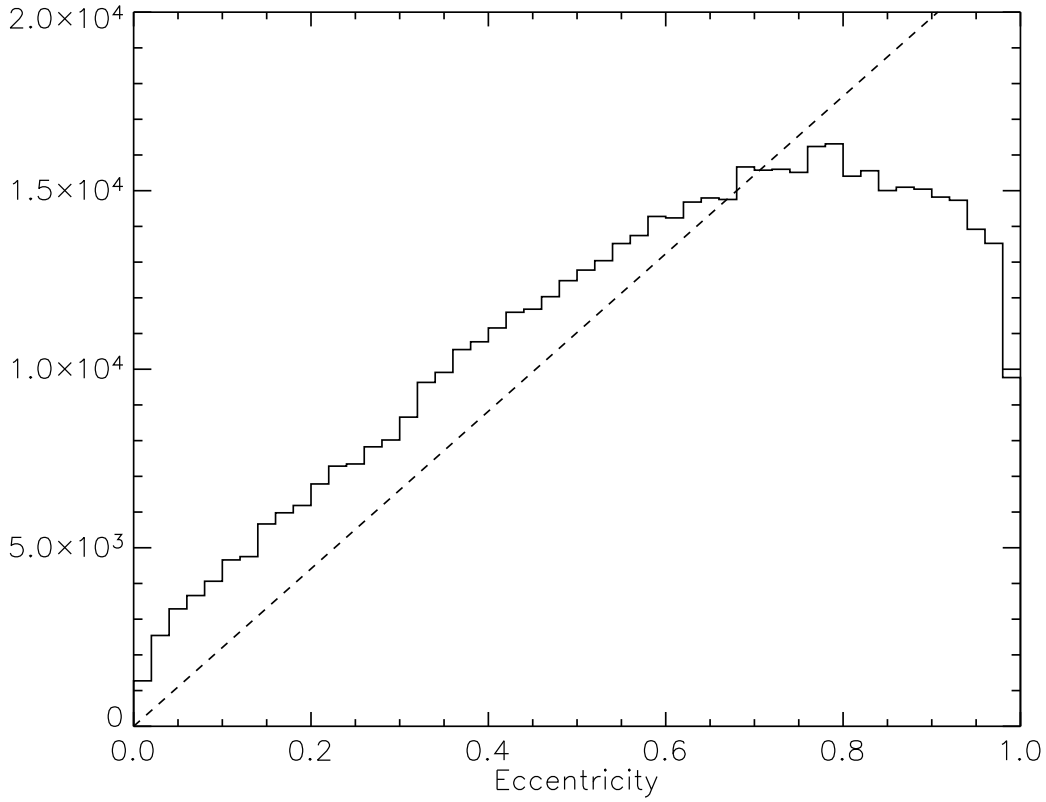

Figure 2.4: Solid line is a histogram of all eccentricities after each encounter except for the first ten for all pure Newtonian sequences of 1000:10:10. The dashed line is a thermal distribution of eccentricities. The distribution is roughly thermal for low eccentricity but deviates for $e \gtrsim 0.6$. The expected thermal distribution of eccentricities is altered by losses of high eccentricity orbits to merger.

ters, fewer black holes are ejected, and the fraction of sequences in which a binary is ejected is smaller. The most dramatic change is in the duration of the sequence, which gravitational radiation reduces by 27% to 40%. The distributions of final semimajor axes (Figure 2.2) and final eccentricities (Figure 2.3) have similar shapes to the Newtonian-only distributions. Due to the circularizing effect of gravitational radiation, binaries of all mass ratios merge with a smaller $\langle e_f \rangle$ than Newtonian-only sequences with the largest difference at high mass ratios. Gravitational radiation also produces a smaller $\langle a_f \rangle$ for $m_0 \gtrsim 300\ M_\odot$. This can be seen in Figure 2.2 where the gravitational radiation simulations display an excess number of sequences with

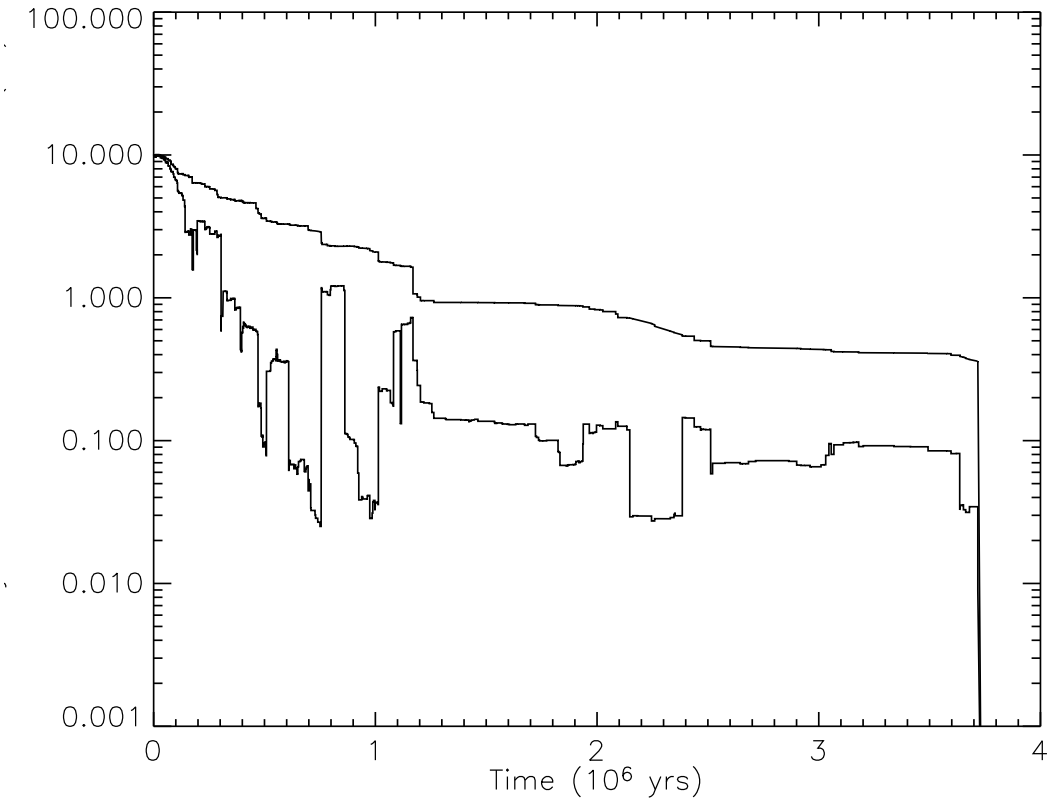

Figure 2.5: 1000:10:10 gravitational radiation sequence. Same as Figure 2.1a but for a sequence with gravitational radiation between encounters. The effects of gravitational radiation can be seen between 2.2 and 2.4×10^6 years. Over this period, the binary undergoes about ten interactions that do not significantly affect its orbit. During this time, the semimajor axis decays from $a = 0.713$ AU to 0.550 AU while the pericenter distance remains small and roughly constant. When an encounter reduces the eccentricity at 2.4×10^6 years, gravitational radiation is strongly reduced. Gravitational radiation becomes important again at the end of the sequence. The sequence ends with the binary's merger from gravitational waves.

low a_f, which is a consequence of the binaries' lower e_f.

2.4 Implications for IMBH Formation and Growth

We can use these simulations to test the Miller & Hamilton (2002b) model of IMBH formation. We assume that a 50 $M_\odot$ seed black hole with a 10 $M_\odot$ companion will undergo repeated three-body encounters with 10 $M_\odot$ interloping black holes in a globular cluster with $v_{\rm esc} = 50$ km s^{-1} and $n = 10^5$ pc^{-3}. We also assume that the density of the cluster core remains constant as the IMBH grows. We then test whether the model of Miller & Hamilton (2002b) can build up to IMBH masses, which we take to be 10^3 $M_\odot$, (1) without ejecting too many black holes from the cluster, (2) without ejecting the IMBH from the cluster, and (3) within the lifetime of the globular cluster. We also test how answers to these questions depend on escape velocity and seed mass. It should be noted that the 1000 $M_\odot$ canonical IMBH is not required to explain the observations of ULXs and is taken as a round number, and if the kinematical evidence of black holes in G1 and M15 with mass $M > 10^3$ $M_\odot$ to 10^4 $M_\odot$ is flawed as has been suggested, then IMBHs with masses $M \lesssim 500$ $M_\odot$ are sufficient to explain the ULXs. We return to this point in Chapter 4.

If the number of black holes ejected is greater than the total number of black holes in the cluster core, then the IMBH cannot build up to the required mass by accreting black holes alone. To calculate the total number of black holes ejected while building up to large masses, we sum the average number of ejections using a linear interpolation of the values in Table 2.2. Assuming a cluster escape velocity of $v_{\rm esc} = 50$ km s^{-1}, we find that the total number of black holes ejected when building up to 1000 $M_\odot$ is approximately 6800 for our Newtonian-only and 5300 for gravitational radiation simulations. This is far greater than the estimated 10^2 to 10^3 black holes available (Portegies Zwart & McMillan 2000). If there were initially one thousand 10 $M_\odot$ black holes in the cluster, mergers of the massive black hole with a

series of 10 $M_\odot$ black holes would exhaust half of the black holes in $\sim 2.6\times10^8$ yr and would ultimately produce a 240 $M_\odot$ black hole. Increasing the seed mass increases the final mass of the IMBH when half of the field black holes run out. If the seed mass were 100, 200, or 300 $M_\odot$, then the model would produce a 270, 330, or 410 $M_\odot$ black hole after exhausting half of the cluster black hole population in 1.9, 1.1, or 0.8×10^8 yr, respectively. Figure 2.6 shows the number of black holes ejected as a function of initial black hole mass for a range of escape velocities. Gravitational radiation recoil velocity, which we did not simulate, however, would increase the number of ejections at small masses. These growth times are much shorter than the $\sim 0.4 - 1.0 \times 10^9$ yr necessary for stellar-mass black holes to eject each other from the cluster (O'Leary et al. 2006; Portegies Zwart & McMillan 2000; Sigurdsson & Hernquist 1993). Therefore, self-depletion of stellar-mass black holes is not a limiting factor.

Of particular concern is whether the three-body scattering events will eject the binary from the cluster. The black hole can only merge with other black holes while it is in a dense stellar environment. The probability of remaining in the cluster after one sequence is $P = 1 - \langle f_{\rm binej} \rangle$. As can be seen in Table 2.2, once the black hole has built up to ~ 300 $M_\odot$, it is virtually guaranteed to remain in the cluster. When starting with 50 $M_\odot$, we calculate the total probability of building up to 300 $M_\odot$ to be 0.0356. Figure 2.7 shows the probability of building up to 300 $M_\odot$ as a function of starting mass for different escape velocities for the gravitational radiation case. Table 2.3 lists probabilities for selected seed masses and escape velocities for the gravitational radiation case.

In a similar manner, we calculate the total time to build up to 1000 $M_\odot$, assuming that the supply of stellar-mass black holes and density remain constant, an assumption which leads to an underestimation of the time. While the time per

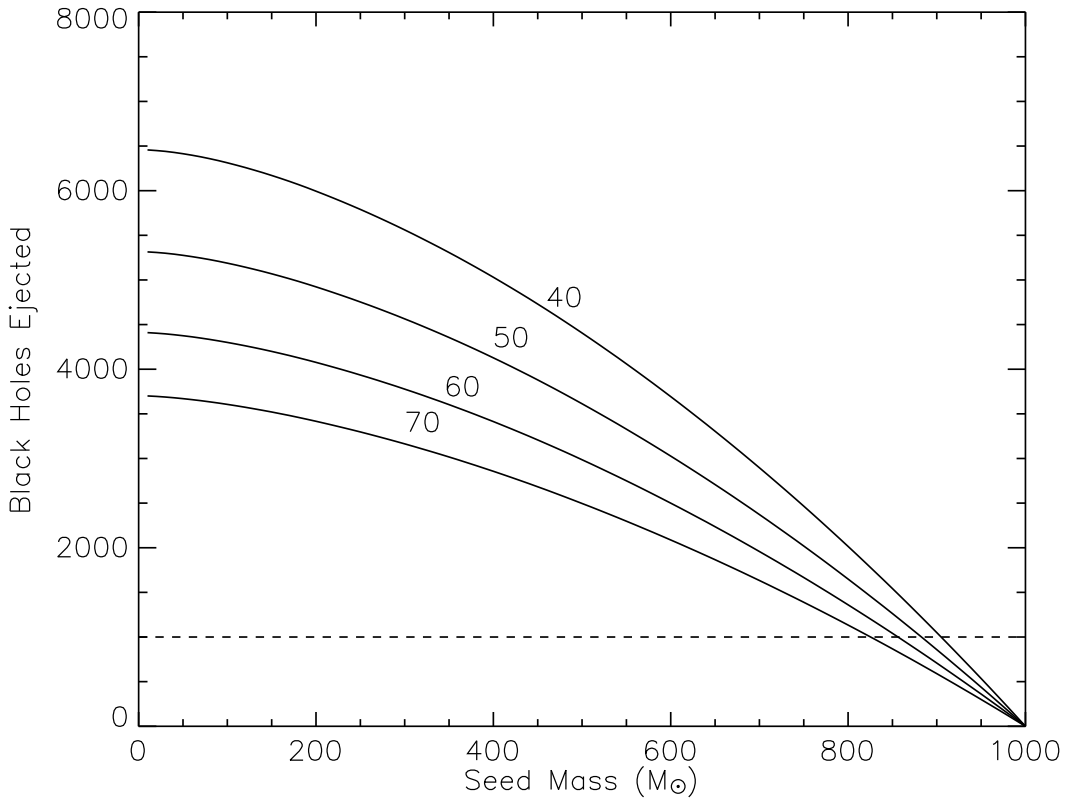

Figure 2.6: Plot of total number of black holes ejected in building up to 1000 $M_{\odot}$ as a function of seed mass for the gravitational radiation case assuming different escape velocities. The four curves show different assumed cluster escape velocities in km s^{-1}. For all but the largest seed masses, the number of black holes ejected is greater than the estimated $\sim 10^3$ (indicated by the dashed line) present in a young globular cluster.

merger is larger for the smaller masses, the total time is dominated at the higher masses since more mergers are needed for the same fractional increase in mass. For Newtonian-only simulations the total time is 1.1×10^9 yr, and for simulations with gravitational radiation the total time is 7.1×10^8 yr. These are much less than the age of the host globular clusters. Figure 2.8 shows the time to reach a specified mass for both the Newtonian and gravitational radiation cases. If the interactions of stellar-mass black holes with IMBHs or interactions among themselves eject the black holes from the cluster core but not from the cluster, however, the number

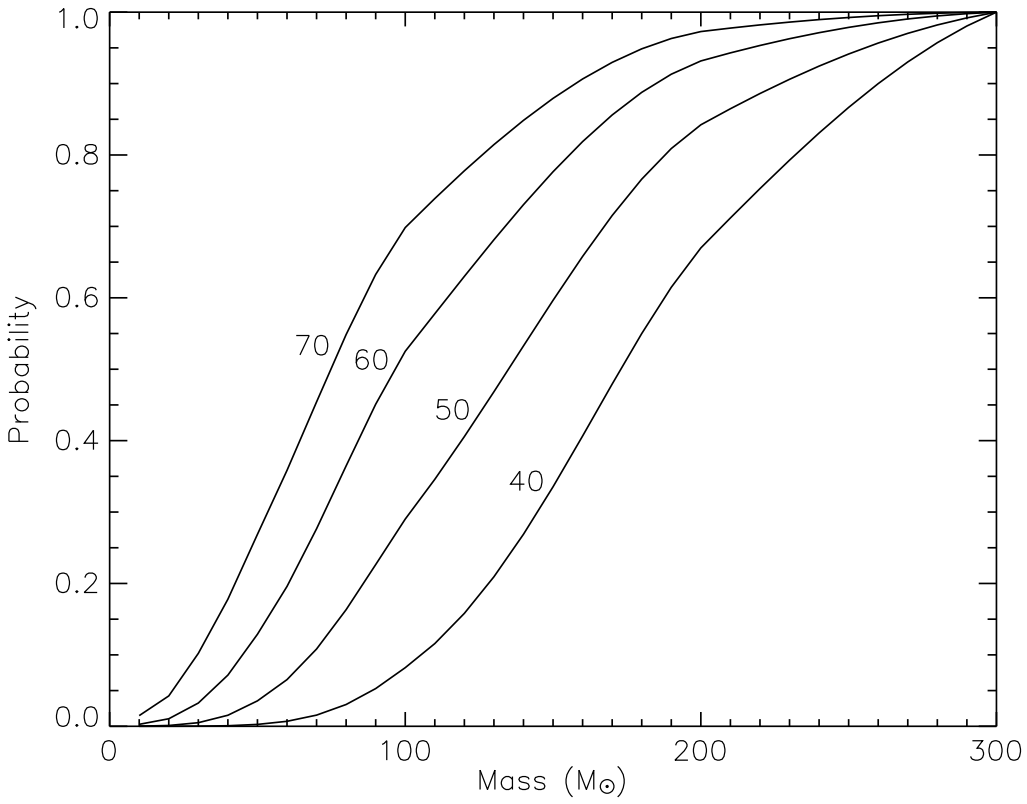

Figure 2.7: Plot of an IMBH's probability of remaining in the cluster and building up to 300 $M_\odot$ as a function of starting mass of the dominant black hole for the gravitational radiation case assuming different escape velocities labeled in km s^{-1}. Once the black hole has built up to 300 $M_\odot$ it is very unlikely that it will be ejected from the cluster. The lowest mass binaries are much more readily ejected and thus are very unlikely to survive a sequence of encounters. Miller & Hamilton (2002b) suggest that IMBHs can be built in this manner with a starting mass $\approx 50\ M_\odot$. We find that such small initial masses are likely to be ejected from the cluster core for reasonable escape velocities of dense clusters.

density and therefore the rate of growth decrease. This analysis of the growth time ignores the time it takes the IMBH progenitor to acquire a companion, but this is unlikely to cause a large increase in the total time. See Appendix A for an estimate of the extra time required.

Although there is clearly enough time to build IMBHs as Miller & Hamilton (2002b) propose, the issues of whether there are enough stellar-mass black holes and whether the cluster will hold onto the IMBH remain. The combination of an initial

Table 2.3. IMBH Formation.

Seed Mass ($M_\odot$)	$v_{\rm esc}$ (km s^{-1})	Probability to remain in cluster	Number of BH ejections	Time (10^8 yr)
50.0	40.0	0.00264	6414	7.06
	50.0	0.0356	5276	
	60.0	0.129	4038	
	70.0	0.269	3573	
100.0	40.0	0.0821	6312	6.15
	50.0	0.290	5188	
	60.0	0.525	3963	
	70.0	0.698	3606	
200.0	40.0	0.670	5995	4.93
	50.0	0.842	4922	
	60.0	0.932	4077	
	70.0	0.978	3417	
300.0	40.0	1.000	5561	4.05
	50.0	1.000	4564	
	60.0	1.000	3777	
	70.0	1.000	3164	

Note. — This table lists values for selected seed masses and cluster escape velocities for the gravitational radiation case. Column 3 lists the probability for the IMBH to remain in the cluster until it reaches a mass of 300 $M_\odot$. The fourth column lists the total number of black holes ejected in building up to 1000 $M_\odot$. Column 5 lists the total time to build up to 1000 $M_\odot$. The total time is not affected by the escape velocity because the density of black holes in the cluster core is taken to be constant.

mass of 50 $M_\odot$ and an escape velocity of 50 km s^{-1} is not likely to produce an IMBH in a globular cluster through three-body interactions with 10 $M_\odot$ black holes, but the general process could still produce IMBHs. Miller & Hamilton (2002b) argued that a seed mass of 50 $M_\odot$ would be retained, but for analytical simplicity they assumed that every encounter changed the semimajor axis by the same fractional amount $\langle \Delta a/a \rangle$. Some encounters, however, can decrease the semimajor axis by several times the average value and thus impart much larger kicks. The authors therefore underestimated the minimum initial mass necessary to remain in the cluster. A hierarchical merging of stellar-mass black holes could, however, still produce an

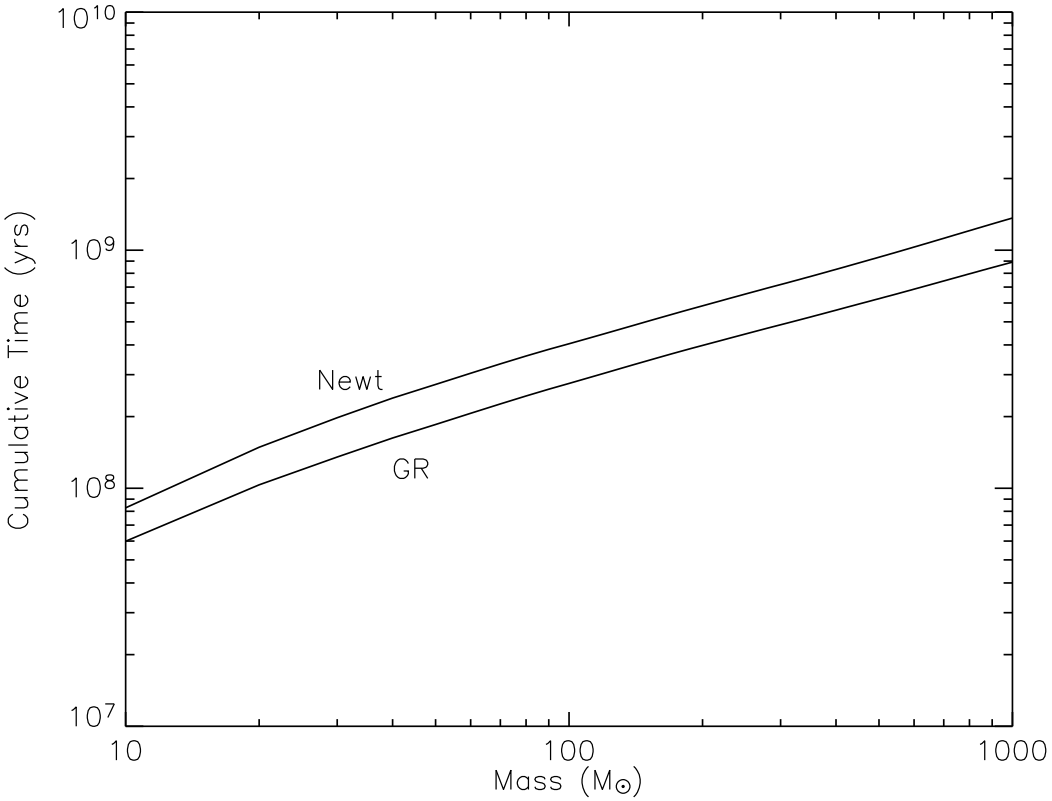

Figure 2.8: Plot of total time to build up to a certain mass when built by mergers with 10 $M_\odot$ black holes for Newtonian only results and for runs with gravitational radiation between encounters. The Newtonian only simulations are slower to build up, but both cases reach 1000 $M_\odot$ within about 10^9 years. The time plotted assumes a constant density of black holes for the duration of IMBH formation.

IMBH if (1) the initial mass of the black hole were greater than 50 $M_\odot$, (2) the escape velocity of the cluster were greater than 50 km s^{-1}, or (3) additional dynamics were involved. We consider each of these in turn.

If the mass of the initial black hole were, e.g., 250 $M_\odot$ before the onset of compact object dynamics, dynamical kicks would not be likely to eject the IMBH, and it would require fewer mergers to reach 1000 $M_\odot$ and thus a smaller population of stellar mass black holes. The initial black hole could start with such a mass if it evolved from a massive Population III star or from a runaway collision of main sequence stars (Gürkan et al. 2004; Portegies Zwart & McMillan 2002), or it could

reach such a mass by accretion of young massive stars, which would be torn apart by tidal forces and impart little dynamical kick.

Retention rates could also be increased by the higher escape velocities found in some globular clusters. NGC 6388, e.g., has an escape velocity of $v_{\rm esc} = 78$ km s^{-1} (Webbink 1985). If the escape velocity were $v_{\rm esc} = 70$ km s^{-1}, the interactions result in a smaller fraction of ejected binaries and the probability of building from 50 $M_\odot$ to 1000 $M_\odot$ then increases by almost an order of magnitude.

In addition, processes with lower dynamical kicks could prevent ejection. One promising mechanism is the Kozai resonance (Kozai 1962; Miller & Hamilton 2002a; Wen 2003). If a stable hierarchical triple is formed, then resonant processes can pump up the inner binary's eccentricity high enough so that it would quickly merge due to gravitational radiation and without any dynamical kick to eject the IMBH from the cluster. O'Leary et al. (2006) include Kozai-resonance-induced mergers in their simulations and find that it reduces the number of stellar-mass black holes ejected, but only by about 10%. Two-body captures (captures in which an interloper passes close enough to the isolated IMBH that it becomes bound and merges due to gravitational radiation) would also result in mergers without dynamical kicks. These kinds of two-body captures that occur during a larger three-body encounter are included in Chapter 3. Both Kozai-resonance-induced mergers and two-body captures are devoid of dynamical kicks, but they would suffer a gravitational radiation recoil. A system in which a 10 $M_\odot$ black hole merges into a 130 $M_\odot$ non-rotating black hole would have a recoil velocity 20 km s^{-1} $\leq v_r \leq$ 200 km s^{-1} (Baker et al. 2006; Blanchet et al. 2005; Damour & Gopakumar 2006; Favata et al. 2004). Since $v_r \sim (m_1/m_0)^2$, a merger between a 10 $M_\odot$ black hole and a seed black hole of mass of 250 $M_\odot$, as discussed above, would experience a recoil velocity $\lesssim$ 50 km s^{-1}. Mergers with lower mass objects that are torn apart by tidal forces, such as white

dwarfs, would impart no gravitational radiation recoil. Finally, a range of interloper masses instead of the simplified single mass population that we used here may also affect retention statistics since a smaller interloper would impart smaller kicks while still contributing to hardening.

Increasing the seed mass and the escape velocity will reduce the number of field black holes ejected but not by enough. As seen in Figure 2.6, using a seed mass $m_0 = 250\ M_\odot$ and an escape velocity $v_{\rm esc} = 70$ km s^{-1} reduces the number of black holes ejected by 40%, but this is still several times more than are available. The Kozai-resonance-induced mergers and two-body captures, however, are methods of merging without possibility of ejecting stellar-mass black holes. In order to reach our canonical 1000 $M_\odot$ intermediate mass while ejecting fewer than 10^3 black holes, either 70-80% of the mergers must come from these ejectionless methods, or else there must exist an extra method of hardening.

2.5 Implications for Gravitational Wave Detection

Our simulations make predictions interesting for gravitational wave detection. After the last encounter of a sequence, the binary will merge due to gravitational radiation. As mentioned in § 1.3.2, as the binary shrinks and circularizes, the frequency of the gravitational radiation emitted passes through the *LISA* band and then through the bands of ground-based detectors. By the time the binaries are detectable by ground-based instruments, they will have completely circularized, but while in the *LISA* band, some will have measurable eccentricities. We calculate the distribution of eccentricities detectable by *LISA* by integrating Equation 2.1 and Equation 2.2 until the orbital frequency reaches $\nu_{\rm orb} = 10^{-3}$ Hz at which point the gravitational

wave frequency is in *LISA*'s most sensitive range and is above the expected white dwarf background. Figure 2.9 shows the distribution of eccentricities for binaries with gravitational radiation in the *LISA* band. There are more low eccentricities at higher mass ratios. This is because at low mass ratios each encounter takes a fractionally larger amount of energy away from the binary than at high mass ratios. Thus at low mass ratios, the last encounter will tend to harden the binary such that it is closer to merger. At high mass ratios, however, encounters take a smaller fractional amount of energy from the binary, and, thus, the high mass ratio binaries have more time to circularize during their orbital decay. For the 1000:10:10 mass ratio, a large fraction of the eccentricities are in the range $0.1 \lesssim e \lesssim 0.2$ where the binary is eccentric enough to display general relativistic effects such as pericenter precession, but circular templates may be sufficient for initial detection of the gravitational wave.

2.6 Conclusions

We present results of numerical simulations of sequences of binary-single black hole scattering events in a dense stellar environment. We simulate three-body encounters until the binary will merge due to gravitational radiation before the next encounter. In half of our simulations, we include the effect of gravitational radiation between encounters.

1. Sequences of high mass ratio encounters. Our simulations cover a range of mass ratios including those corresponding to IMBHs interacting with stellar-mass black holes in stellar clusters. Because the binaries simulated are tightly bound, the encounters steadily shrink the binary's semimajor axis until it merges. The eccentricity, however, jumps chaotically between high and low values over the

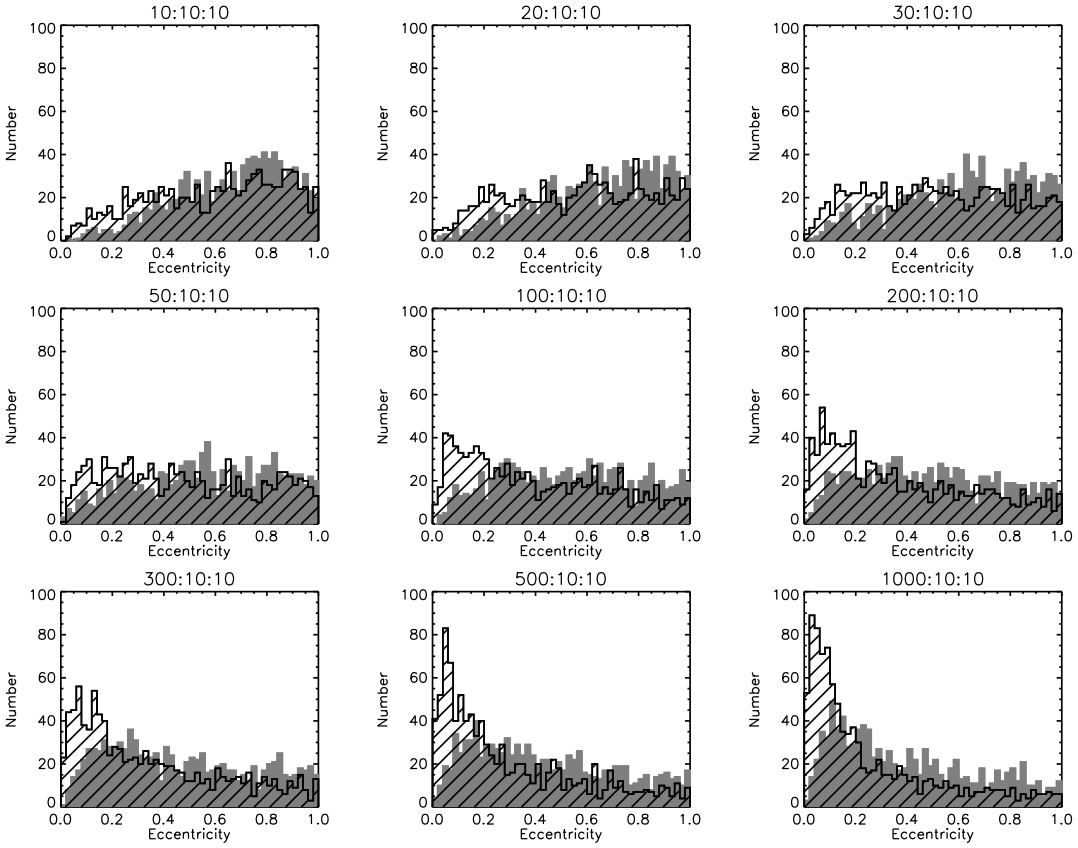

Figure 2.9: Distribution of eccentricities after integrating the Peters (1964) equations until in *LISA* band when the orbital frequency $\nu_{\rm orb} = 10^{-3}$ Hz. The solid histograms are the Newtonian only sequences, and the hatched histograms are sequences with gravitational radiation. The sequences with gravitational radiation tend towards lower eccentricity since they have already started to circularize during the sequence. There is more difference between the two cases at higher mass ratios since gravitational radiation is stronger. Higher mass ratio binaries have lower eccentricities than lower mass ratio binaries since the latter start closer to merger after the final encounter. The 1000:10:10 mass ratio shows that a large number of detectable binaries would have $0.1 \lesssim e \lesssim 0.2$ such that they would likely be detectable by *LISA* with circular templates yet display measurable pericenter precession.

course of a sequence. Merger usually occurs at high eccentricity since gravitational radiation is much stronger then.

2. Gravitational wave emission between encounters. The inclusion of gravitational radiation between encounters affects the simulations in several ways. The extra source of shrinking caused by gravitational wave emission has the effect of shortening the sequence in terms of both the number of encounters and the total time, and the circularization from gravitational waves has the effect of decreasing the final eccentricity of the binary before it merges.

3. IMBH formation. Our simulations directly test the IMBH formation model of Miller & Hamilton (2002b). We find that there is sufficient time to build up to 1000 $M_\odot$ when starting from 50 $M_\odot$, but our simulations also show that if there are a thousand 10 $M_\odot$ black holes in the globular cluster, the seed black hole would only be able to grow to 240 $M_\odot$ before exhausting half of the black holes in the cluster. In addition, the probability of the binary's remaining in the cluster during a growth from 50 to 240 $M_\odot$ is small. In order to avoid ejection from the cluster with a reasonable probability, either the black hole must have a larger mass at the onset of dynamical encounters, the cluster's escape velocity must be larger, or the black hole must grow by some additional mechanisms such as by Kozai-resonance-induced mergers, two-body captures, from smaller interlopers, or from interlopers that are tidally disrupted. Thes results are modified by our inclusion of gravitational radiation reaction in Chapter 3.

4. Gravitational wave detection. The mergers of binary black hole systems are strong sources of detectable gravitational waves. We find that the merging binary will typically start with very high eccentricity. By the time the binary is detectable by the Advanced LIGO detector, it will have completely circularized, but when detectable by *LISA*, it may have moderate eccentricity ($0.1 \lesssim e \lesssim 0.2$) such that it

will display general relativistic effects such as pericenter precession and still possibly be detectable with circular templates. We find a high rate of mergers in the first few hundred million years of a globular cluster's life. This suggests that recently formed, nearby super star clusters may be promising sources for gravitational radiation from IMBH coalescence.

Chapter 3

Three-Body Dynamics with Gravitational Wave Emission

3.1 Overview

In this chapter we present a study of the dynamics of black holes in a stellar cluster using numerical simulations that include the effects of gravitational radiation. We include gravitational radiation reaction by adding a drag force to the Newtonian gravitational calculation. Our treatment is similar to that of Lee (1993), but we focus on individual encounters and sequences of encounters and the resulting mergers instead of ensemble properties of the host cluster. Chapter 2 incorporated gravitational radiation by integrating the Peters (1964) orbit-averaged equations for orbital evolution of a binary that is emitting gravitational waves, but in this chapter we include the energy loss from gravitational radiation for arbitrary motion of the masses. Although the vast majority of three-body interactions do not differ greatly from a purely Newtonian simulation, an important few involve close approaches in which gravitational waves carry away a dynamically significant amount of energy

such that it may cause the black holes to merge quickly in the middle of the encounter. This is qualitatively different from the mergers in Chapter 2 which were caused by gravitational waves emitted by isolated binaries between encounters, and this new effect is important in considering detectable gravitational waves as well as IMBH growth.

In § 3.2 we describe our method of including gravitational waves as a drag force as well as numerical tests of its accuracy. We present our simulations and major results in § 3.3 and discuss the implications for IMBH formation and gravitational wave detection in § 3.4.

3.2 Numerical Method

The numerical method we use here is much the same as is described in § 2.2. In order to study the dynamics of a massive binary in a dense stellar environment, we simulate the encounters between the binary and single objects. We include both individual encounters and sequences of encounters, all of which include gravitational radiation emission. When simulating sequences, we allow the properties of the binary to evolve from interactions with singles, and we follow the binary until a merger occurs. A merger is determined to occur when the separation between the two masses is less than $G(m_0 + m_1)/c^2$. The simulations are run using the same code as in Chapter 2 with a few modifications. The integration engine is now HNDrag, which is an extension of HNBody (K. Rauch & D. Hamilton, in preparation). Both HNBody and HNDrag can include the first-order post-Newtonian corrections responsible for pericenter precession based on the method of Newhall et al. (1983). HNDrag also has the ability to include pluggable modules that can add extra forces or perform separate calculations such as finding the minimum separation between

all pairs of objects. In this paper we ignore the second-order post-Newtonian terms, which contribute higher-order corrections to the pericenter precession, but we include the effects of gravitational radiation on the dynamics of the particles through the addition of a force that arises from the 2.5-order post-Newtonian equation of motion for two point masses. We discuss the implications of ignoring lower-order post-Newtonian corrections in § 3.3.1. The acceleration on a mass m_0 from gravitational waves emitted in orbit around a mass m_1 can be written as

$$\frac{d\boldsymbol{v_0}}{dt} = \frac{4G^2}{5c^5}\frac{m_0 m_1}{r^3}\left(\frac{m_1}{m_0+m_1}\right)\left[\hat{r}\left(\hat{r}\cdot\boldsymbol{v}\right)\left(\frac{34}{3}\frac{G\left(m_0+m_1\right)}{r}+6v^2\right)\right.$$
$$\left.+\boldsymbol{v}\left(-6\frac{G\left(m_0+m_1\right)}{r}-2v^2\right)\right] \qquad (3.1)$$

where $\boldsymbol{r} = \boldsymbol{r_1} - \boldsymbol{r_0}$ and $\boldsymbol{v} = \boldsymbol{v_1} - \boldsymbol{v_0}$ are the relative position and velocity vectors between the two masses and $\hat{r}$ and $\hat{v}$ are their unit vectors (Iyer & Will 1993; Lee 1993). When orbit-averaged, Equation 3.1 gives the Peters (1964) equations for semimajor axis and eccentricity evolution (Equation 2.1 and Equation 2.2. See Appendix B for a derivation of Equation 2.1 for the circular case.). We tested the inclusion of this force in the integrator by comparison with direct, numerical integration of Equation 2.1 and Equation 2.2 for two different binaries with masses $m_0 = m_1 = 10\ M_\odot$ and initial semimajor axis $a_0 = 1$ AU: one with initial eccentricity $e_0 = 0$ and one with initial eccentricity $e_0 = 0.9$ (Figure 3.1). The N-body integration of these binaries made use of HNDrag's enhancement factor, which artificially augments the magnitude of the drag forces for the purposes of testing or simulating long-term effects. For this test and all numerical integrations with HNDrag, we used the fourth-order Runge-Kutta integrator. For both the circular and the high eccentricity cases, the N-body integrations agree very well with the Peters (1964) equations. Examination of Equation 3.1 reveals that even though physically the emission of gravitational radiation can only remove energy from the system, the

equation implies $\dot{E} > 0$ for $\hat{r} \cdot \hat{v} > 0$ in hyperbolic orbits, becoming worse as the eccentricity increases (Lee 1993). Integration of Equation 3.1 over an entire orbit, however, does lead to the expected energy loss. This is because there is an excess of energy loss at pericenter, which cancels the energy added to the system (Lee 1993). Thus this formulation does not introduce significant error as long as the integration is calculated accurately at pericenter, which we achieve by setting HNDrag's relative accuracy parameter to 10^{-13}, and the two objects are relatively isolated, which we discuss below.

We also tested the N-body integration with gravitational radiation for unbound orbits against the maximum periastron separation for two objects in an initially unbound orbit to become bound to each other (Quinlan & Shapiro 1989):

$$r_{p,\max} = \left(\frac{85\pi\sqrt{2}G^{7/2}m_0 m_1 \left(m_0 + m_1\right)^{3/2}}{12c^5 v_\infty^2} \right)^{2/7}, \tag{3.2}$$

where v_∞ is the relative velocity at infinity of the two masses. In Figure 3.2 we plot the orbits integrated both with and without gravitational radiation for two different sets of initial conditions that straddle the $r_{p,\max}$ threshold. For both sets of initial conditions, the integrations with gravitational radiation differ from the Newtonian orbits, and the inner orbit loses enough energy to become bound and ultimately merge. We used a bisection method of multiple integrations to calculate $r_{p,\max}$, and our value agrees with that of Quinlan & Shapiro (1989) to a fractional accuracy of better than 10^{-5}.

For systems of three or more masses, we compute gravitational radiation forces for each pair of objects and add them linearly. Although this method differs from the full relativistic treatment, which is nonlinear, the force from the closest pair almost always dominates. We may estimate the probability of a third object coming within the same distance by examining the timescales for an example system. A binary black hole system with $m_0 = 1000\ M_\odot$ and $m_1 = 10\ M_\odot$ with a separation

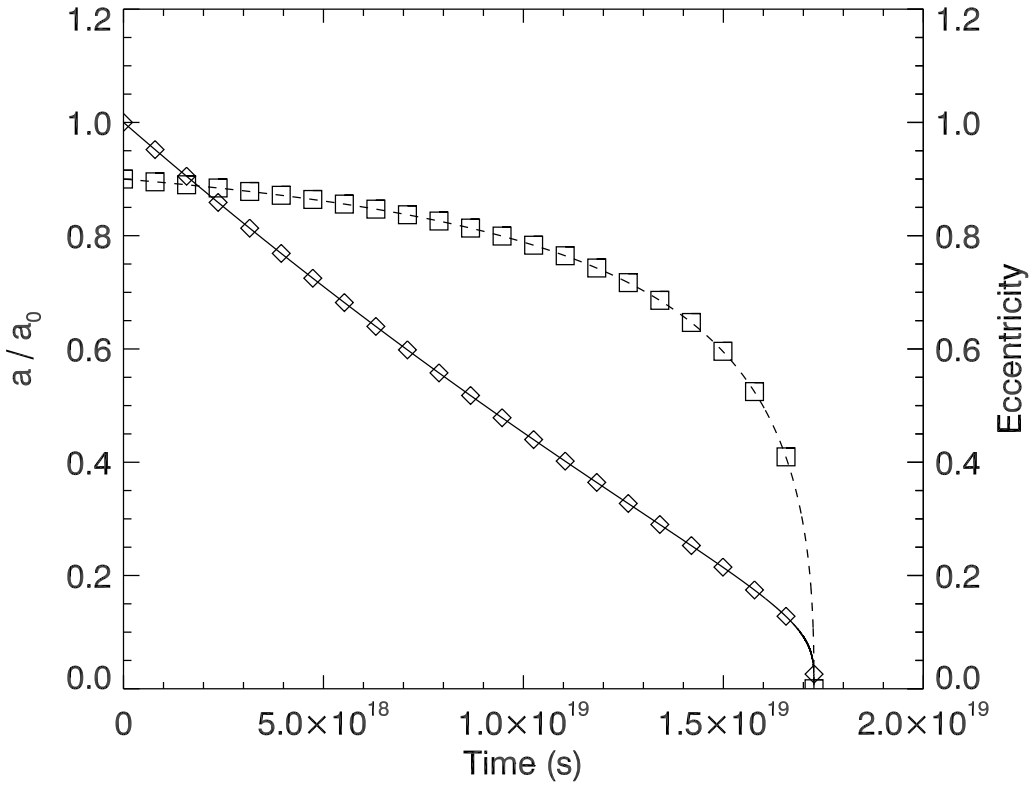

Figure 3.1: Comparison of HNDrag integration with numerical integration of Peters (1964) equations for an eccentric binary. Lines are numerical integration of Equation 2.1 for semimajor axis (solid line) and of Equation 2.2 for eccentricity (dashed line). The symbols are results from HNDrag integration with gravitational radiation for semimajor axis (diamonds) and eccentricity (squares). The binary shown has $m_0 = m_1 = 10\ M_\odot$ with an initial orbit of $a_0 = 1$ AU and $e_0 = 0.9$. The evolution of the binary's orbital elements is in very close agreement for the entire life of the binary.

$a = 10^{-2}$ AU ($\sim 1000GM/c^2$) will merge within (Peters 1964)

$$\tau_{\rm merge} \approx 6 \times 10^9 \frac{(1\ M_\odot)^3}{m_0 m_1\,(m_0+m_1)} \left(\frac{a}{10^{-2}\ {\rm AU}}\right)^4 \left(1-e^2\right)^{7/2} {\rm yr} \approx 600\ {\rm yr}. \qquad (3.3)$$

Though the expression for merger time in Equation 3.3 is valid only for high eccentricities ($e \to 1$), we calculate the time with $e = 0$, which serves as an upper limit. Including a more realistic eccentricity would only decrease the time and help this argument further. The rate of gravitationally focused encounters with a third mass

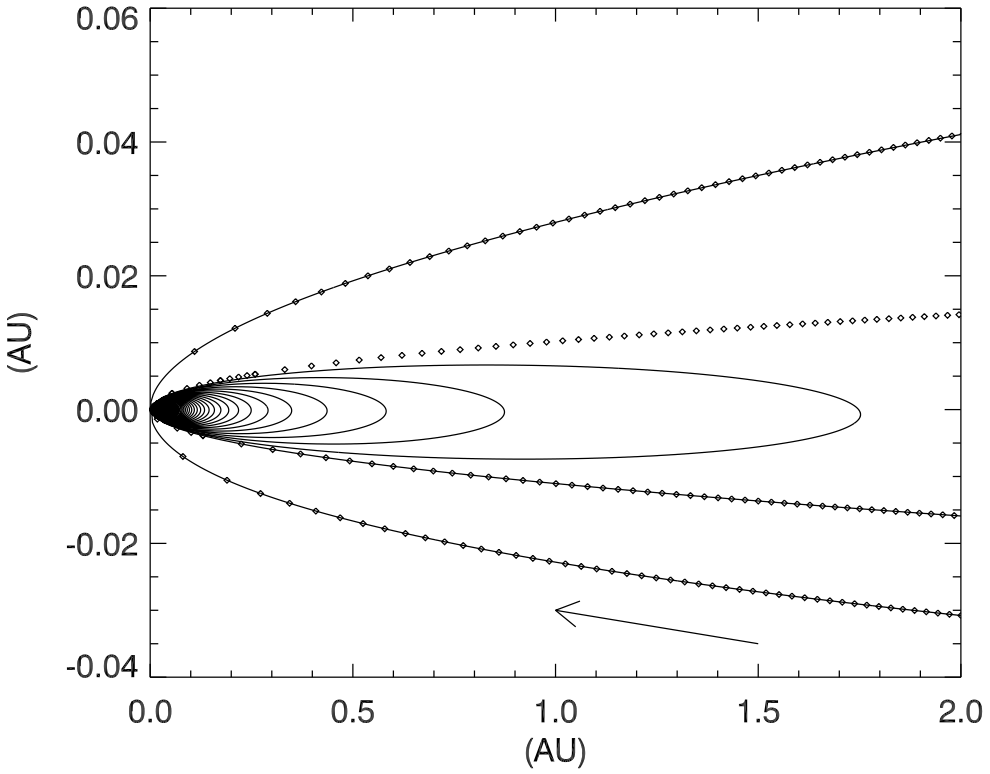

Figure 3.2: HNDrag-integrated orbits with and without gravitational radiation inside and outside of two-body capture pericenter. This plot shows orbits of two 10 $M_\odot$ black holes with relative velocity of 10 km s^{-1} and pericenter distances of $r_p = 0.2 r_{p,\max}$ and $r_p = 1.2 r_{p,\max}$. The lines show the orbits with gravitational radiation included in the integration, and the diamonds show the Newtonian orbits for the same initial conditions. The direction of the orbits is indicated by the arrow. Although it is not apparent for the outer orbit in this plot, both trajectories differ from their Newtonian counterparts. For the inner orbit, enough energy is radiated away for the black holes to become bound to each other and eventually merge.

m_2 within a distance r from an isotropic distribution is (Chapter 2)

$$\nu_{\rm enc} = 5{\times}10^{-10} \left(\frac{10 \text{ km s}^{-1}}{v_\infty}\right) \left(\frac{n}{10^6 \text{ pc}^{-3}}\right) \left(\frac{r}{10^{-2} \text{ AU}}\right) \left(\frac{m_0 + m_1}{1\ M_\odot}\right) \left(\frac{m_2}{1\ M_\odot}\right)^{1/2} \text{yr}^{-1}. \tag{3.4}$$

For a number density $n = 10^6$ pc^{-3}, a relative velocity $v_\infty = 10$ km s^{-1}, and an interloper mass $m_2 = 10\ M_\odot$, the rate of encounters within the same distance $r = a = 10^{-2}$ AU is $\nu_{\rm enc} \sim 2{\times}10^{-6}$ yr^{-1}. Thus the probability of an encounter within

the same distance is $P \sim \tau_{\rm merge}\nu_{\rm enc} \approx 10^{-3}$ for this mildly relativistic case. For a separation of 10^{-3} AU, the probability drops to 10^{-8}. Thus for most astrophysical scenarios and for all simulations in this chapter, the error incurred from adding the gravitational radiation force terms linearly is negligible.

3.3 Simulations and Results

3.3.1 Individual Binary-Single Encounters

Close Approach

We begin our study of three-body encounters including gravitational radiation by calculating the minimum distance between any two objects during a binary-single scattering event. This quantity has been well studied for the Newtonian case, but it is still not completely understood (Hut & Inagaki 1985; Sigurdsson & Phinney 1993). Following the initial condition choices of Hut & Inagaki (1985) and Sigurdsson & Phinney (1993), we present 10^5 simulations of a circular binary with masses $m_0 = m_1 = 1\ M_\odot$ and an initial semimajor axis $a_0 = 1$ AU interacting with an interloper of mass $m_2 = 1\ M_\odot$ in a hyperbolic orbit with respect to the center of mass of the binary. As in Chapter 2, we refer to the mass ratios of three-body encounters as m_0:m_1:m_2, where m_2 is the interloper and the binary consists of m_0 and m_1 with $m_{\rm bin} = m_0 + m_1$ and $m_0 \geq m_1$. The relative velocity of the binary and the interloper at infinity is $v_\infty = 0.5$ km s^{-1} with an impact parameter randomly drawn from a distribution such that the probability of an impact parameter between b and $b + db$ is $P(b) \propto b$ and a maximum value $b_{\rm max} = 6.621$ AU, which corresponds to a two-body pericenter distance of $r_p = 5a_0$. The encounters are integrated until finished as determined in Chapter 2 while tracking the minimum distances between

all pairs of objects. We follow Hut & Inagaki (1985) and Sigurdsson & Phinney (1993) in calculating a cumulative, normalized cross-section for close approach less than r

$$\sigma\left(r\right) = \frac{f\left(r\right) b_{\max}^2}{a_0^2} \left(\frac{v_\infty}{v_c}\right)^2, \tag{3.5}$$

where

$$v_c \equiv \sqrt{G \frac{m_0 m_1}{a m_2} \frac{\left(m_0 + m_1 + m_2\right)}{\left(m_0 + m_1\right)}} \tag{3.6}$$

is the minimum relative velocity required to ionize the system and $f(r)$ is the fraction of encounters that contain a close approach less than r. We plot $\sigma\left(r/a_0\right)$ for the Newtonian case at several different time intervals within the encounter in Figure 3.3. Our results for the total cross-section are in almost exact agreement with Sigurdsson & Phinney (1993) over the domain of overlap, but with the advantage of ten years of computing advances, we were able to probe down to values of r/a_0 that are 10^2 times smaller. In addition we examine how the total cross-section evolves from the initial close approach of the binary until the end of the interaction through subsequent near passes during long-lived resonant encounters. At the time of the interloper's initial close approach with the binary, the cross-section is dominated by gravitational focusing, and thus the bottom two curves in Figure 3.3 are well fit by power laws with slope of 1. As the interactions continue, resonant encounters with multiple close approaches are possible, and the cross-section for small values of r/a_0 increases. Each successive, intermediate curve approaches the final cross-section by a smaller amount because there are fewer encounters that last into the next time bin. A fit of two contiguous power laws to the final curve yields a break at $r/a_0 = 0.0102$ with slopes of 0.85 and 0.35 for the lower and upper portions, respectively. These values are very close to those obtained by earlier studies (Hut & Inagaki 1985; Sigurdsson & Phinney 1993). There is, however, no reason for a preferred scale for a Newtonian system, and simple models that assume close approaches

are dominated by pericenter passage after an eccentricity kick cannot explain the lower slope. We numerically calculate $d(\log\sigma)/d(\log r)$ by fitting multiple lines to $\sigma(r)$ in logarithmic space and plot the results in Figure 3.4. The derivative $d(\log\sigma)/d(\log r)$ appears to approach unity for very small values of r/a_0 where the close approach can be thought of as a gravitationally focused two-body encounter within the entire system (Hut & Inagaki 1985). It is surprising that this does not happen until $r/a_0 < 10^{-5}$.

In order to test the effects of gravitational radiation on the close approach as well as to test the sensitivity of the results to the phase of the binary, we ran the same simulations (1) with gravitational radiation, (2) with gravitational radiation and first-order post-Newtonian corrections, and (3) with just first-order post-Newtonian corrections. The three new cross-sections are plotted with the Newtonian results in Figure 3.5. A Kolmogorov-Smirnov test shows the differences between the three curves to be statistically insignificant ($P \geq 0.4$). Although not statistically significant, the curves with gravitational radiation appear to drop below the Newtonian curve for small r/a_0 and then climb above for very small r/a_0. This is as expected because gravitational radiation causes this effect by driving objects that become very close to each other closer still and, in some cases, causing them to merge. A larger number of simulations could indicate whether the drop is indeed physical or merely statistical fluctuation. For larger masses, the gravitational radiation is stronger, and the gravitational radiation curve will differ from the Newtonian curve at larger r/a_0 for a fixed value of a_0.

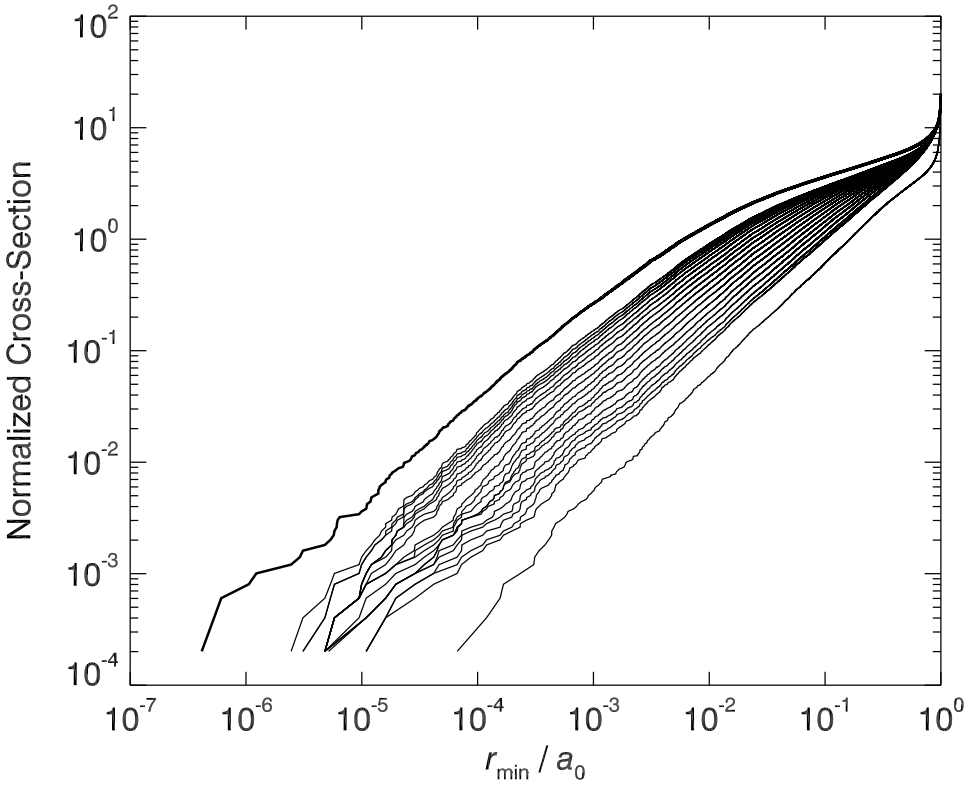

Figure 3.3: Cross-section for close approach during binary-single encounters as a function of $r_{\min}/a_0$. The thick, upper curve is the cross-section for the entire encounter. The remaining curves are the cross-section at intermediate, equally-spaced times during the encounter starting from the bottom near the time of initial close approach. Because we only include 20 intermediate curves, there is a gap between the last intermediate curve and the final curve. The bottom two curves have a slope close to 1, consistent with close approach dominated by gravitational focusing. As the encounters progress, resonant encounters with multiple passes are more likely to have a close approach at smaller $r_{\min}/a_0$, and the curves gradually evolve to the total cross-section for the entire encounter.

Merger Cross-Section

The most interesting new consequence from adding the effects of gravitational radiation to the three-body problem is the possibility of a merger between two objects. Though the two-body cross-section for merger can be calculated from Equation 3.2, the dynamics of three-body systems increases this cross-section in a nontrivial man-

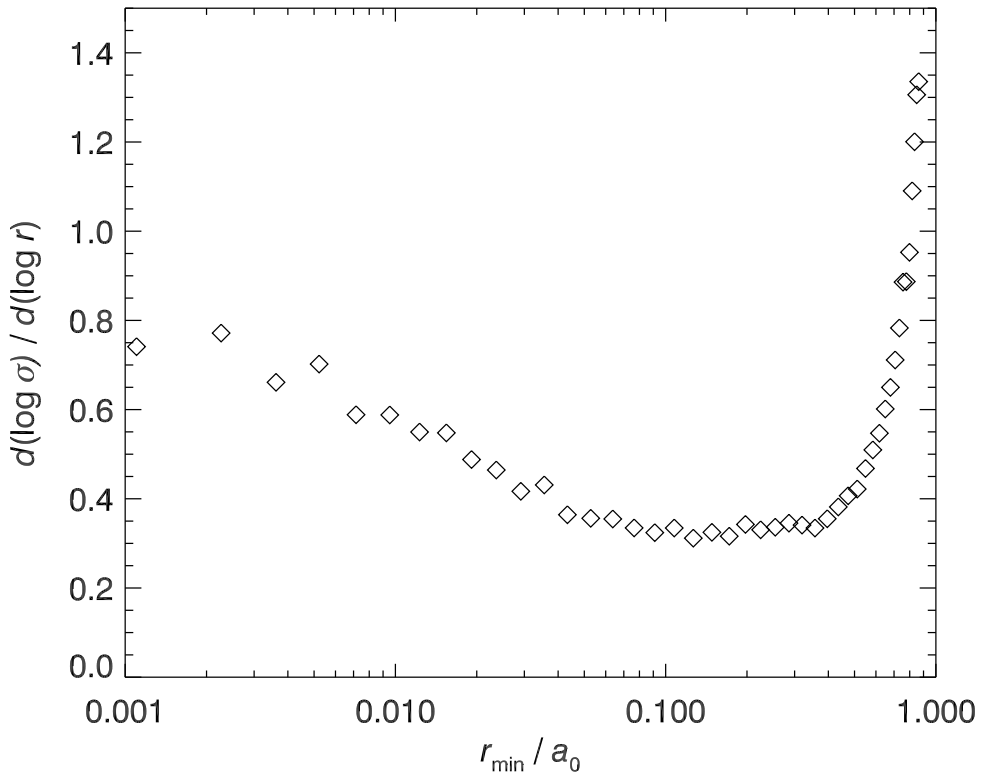

Figure 3.4: Derivative of close approach cross-section curve for the entire encounter. Each symbol is the slope for a line segment fit to the top curve from Figure 3.3 plotted as a function of the midpoint of the range. Because of the small number of encounters that result in very small close approaches, the multiple line segments used in the fits cover different ranges in $\log(r/a_0)$. They were selected so that each of the 100 line segments covers an additional 1000 encounters that make up the cumulative cross-section curve. The scatter in the points is indicative of the statistical uncertainty. For smaller close approaches, $d(\log\sigma)/d(\log r)$ appears to approach unity. The rise at the right occurs because the cross-section is formally infinite at $r_{\rm min}/a_0 = 1$.

ner. We present simulations of individual binary-single encounters for a variety of masses. As in Chapter 2, the interactions were set up in hyperbolic encounters with a relative velocity at infinity of $v_\infty = 10$ km s^{-1} with an impact parameter distribution such that the probability of an impact parameter between b and $b + db$ is $P(b) \propto b$ with $b_{\rm min} = 0$ and $b_{\rm max}$ such that the maximum pericenter separation would be $r_p = 5a_0$. The binaries were initially circular with semimajor axes ranging

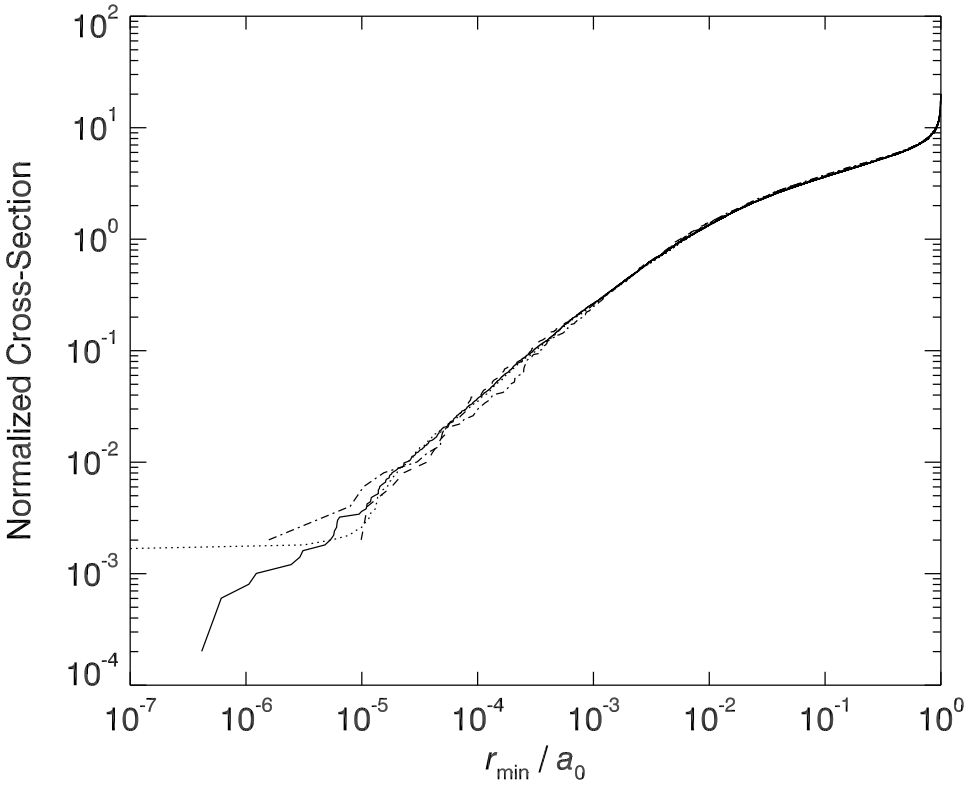

Figure 3.5: Cross-section for close approach like Figure 3.3 including different orders of Post-Newtonian corrections. The curves are purely Newtonian (solid), Newtonian plus 2.5-order PN (dotted), Newtonian plus 1-order PN (dashed), and Newtonian plus 1-order and 2.5-order PN (dash-dotted). The purely Newtonian and the Newtonian plus 2.5-order PN curves come from 10^5 encounters each. The other two curves come from 10^4 encounters each and show more statistical fluctuations. The differences among the curves are not statistically significant.

from 10^{-6} AU to 10^2 AU, depending on the mass. The masses were picked such that one of the three mass ratios was unity with all masses ranging from 10 $M_\odot$ to $10^3 M_\odot$ with roughly half-logarithmic steps. For each mass and semimajor axis combination, we run 10^4 encounters. We calculate the merger cross-section as $\sigma_m = f_m \pi b_{\max}^2$ where f_m is the fraction of encounters that resulted in a merger while all three objects were interacting. In Figure 3.6 through Figure 3.9 we plot, as a function of the semimajor axis scaled to the gravitational radius of the binary $\xi \equiv a/(Gm_{\rm bin}/c^2)$, the cross-section normalized to the physical cross-section of the Schwarzschild radius

of the mass of the entire system taking gravitational focusing into account:

$$\bar{\sigma}_m = \sigma_m \left[4\pi \frac{GM_{\rm tot}}{v_\infty^2} \frac{GM_{\rm tot}}{c^2} \right]^{-1}. \tag{3.7}$$

For all mass ratios $\bar{\sigma}_m$ increases with ξ because hard binaries with wide separations sweep out larger targets where the interloper can interact with and merge with the binary components. As ξ increases to the point that the binary is no longer hard, $\bar{\sigma}_m$ will approach the value expected from Equation 3.2. The curves flatten out for $\xi \lesssim 100$ as the cross-section is dominated by the mergers of binary members with each other because of hardening interactions and eccentricity kicks that bring the two masses together. For sufficiently small ξ, the merger cross-section would be formally infinite since all binaries would merge quickly. Thus the interesting regime is where ξ is neither too small nor too large; otherwise, the problem is effectively a two-body problem where one may ignore the interloper ($\xi \sim 1$) or where one may ignore one of the binary members ($\xi > 10^6$). For all mass series, as the mass ratios approach unity, the cross-section increases because complicated resonant encounters, which produce more numerous and smaller close approaches, are more likely when all three objects are equally important dynamically.

We note some interesting trends that can be seen in the plots. Note that for the scalings given, it is only the mass ratios that matter and not the absolute mass so that the 10:10:10 and 1000:1000:1000 cases only differ because of statistical fluctuations (Figure 3.6 and Figure 3.7). Thus our results can be scaled to others, e.g., 1000:100:100 would be the same as 100:10:10. For the 10:10:X mass series (Figure 3.6), the normalized cross-section decreases with increasing interloper mass, roughly as $\bar{\sigma}_m \sim (m_2/m_{\rm bin})^{-1}$. This happens because as the interloper dominates the total mass of the system, complicated resonant interactions with more chances for close approach are less likely. Thus for the 10:10:1000 case, there are far fewer chances for a close approach that results in merger. The 1000:1000:X series (Fig-

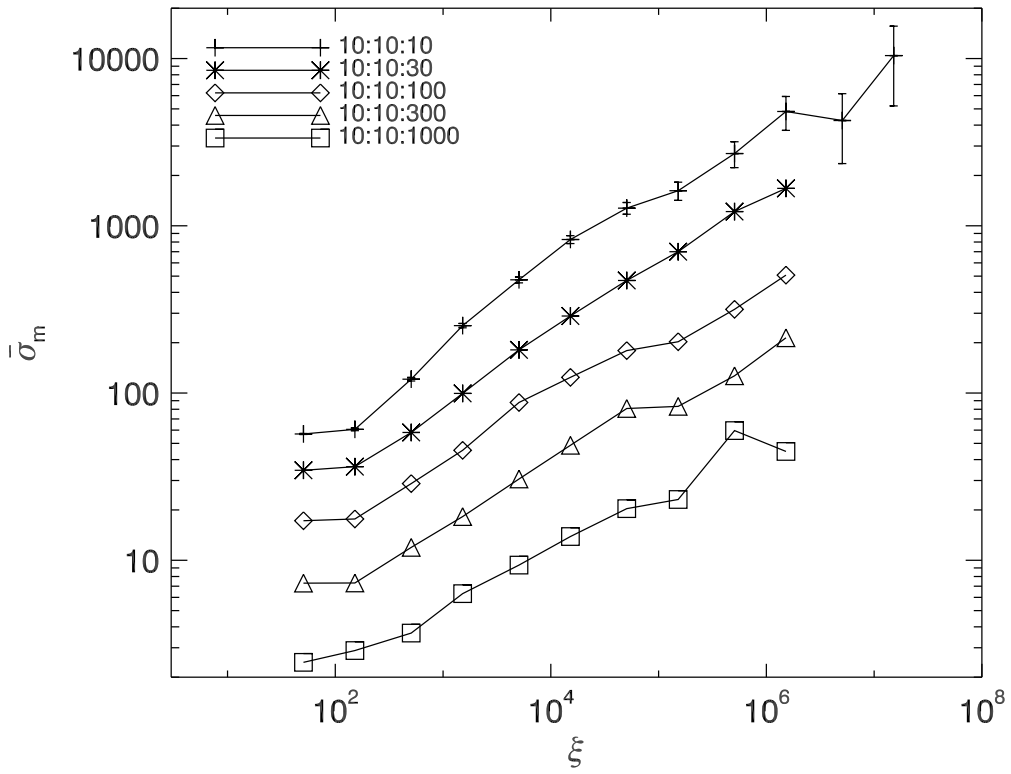

Figure 3.6: Normalized merger cross-sections (Equation 3.7) for individual binary-single encounters as a function of ξ for the 10:10:X mass series. The normalization is explained in the text. Each symbol represents 10^4 binary-single encounters. Error bars given for the top curve are representative for all merger cross-section curves in Figure 3.6 through Figure 3.9.

ure 3.7) shows a distinct break around $\xi \sim 100$. Since the binary mass is the same for all curves, they all approach the same value for $\xi \lesssim 100$ where the binary members merge with each other because of their small separation. For $\xi \gtrsim 100$, the higher mass interlopers are dynamically more important and cause more mergers. The X:10:10 series curves (Figure 3.8) all approach the 10:10:10 curve for $\xi \gtrsim 10^5$ where the dominant object in the binary has less influence over its companion.

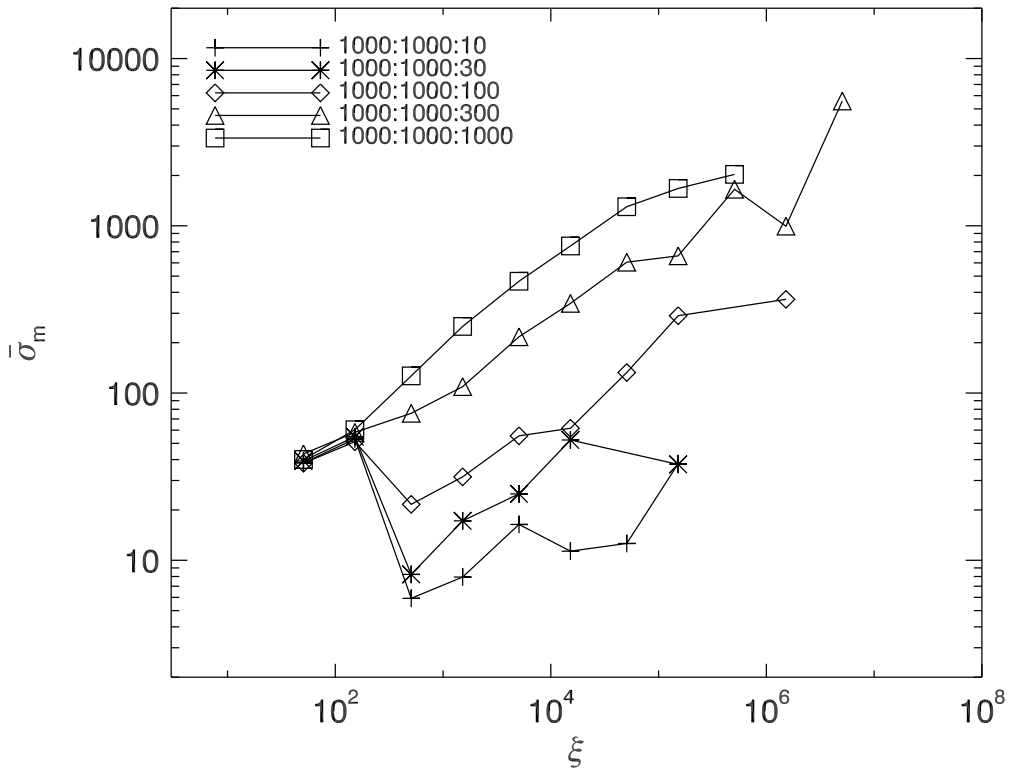

Figure 3.7: Normalized merger cross-sections like Figure 3.6 for 1000:1000:X series. The error bars from Figure 3.6 are representative for the curves in this figure.

3.3.2 Sequences of Encounters

Because a tight binary in a dense stellar environment will suffer repeated encounters until it merges from gravitational radiation, we simulate a binary undergoing repeated interactions through sequences of encounters including gravitational radiation reaction. As in Chapter 2, we start with a circular binary with initial semimajor axis $a_0 = 10$ AU and a primary of mass $m_0 = 10$, 20, 30, 50, 100, 200, 300, 500, or 1000 $M_\odot$ and a secondary of mass $m_1 = 10\ M_\odot$. We simulate encounters with interloping black holes with mass $m_2 = 10\ M_\odot$. After each encounter, we integrate Equation 2.1 Equation 2.2 to get the initial semimajor axis and eccentricity for the

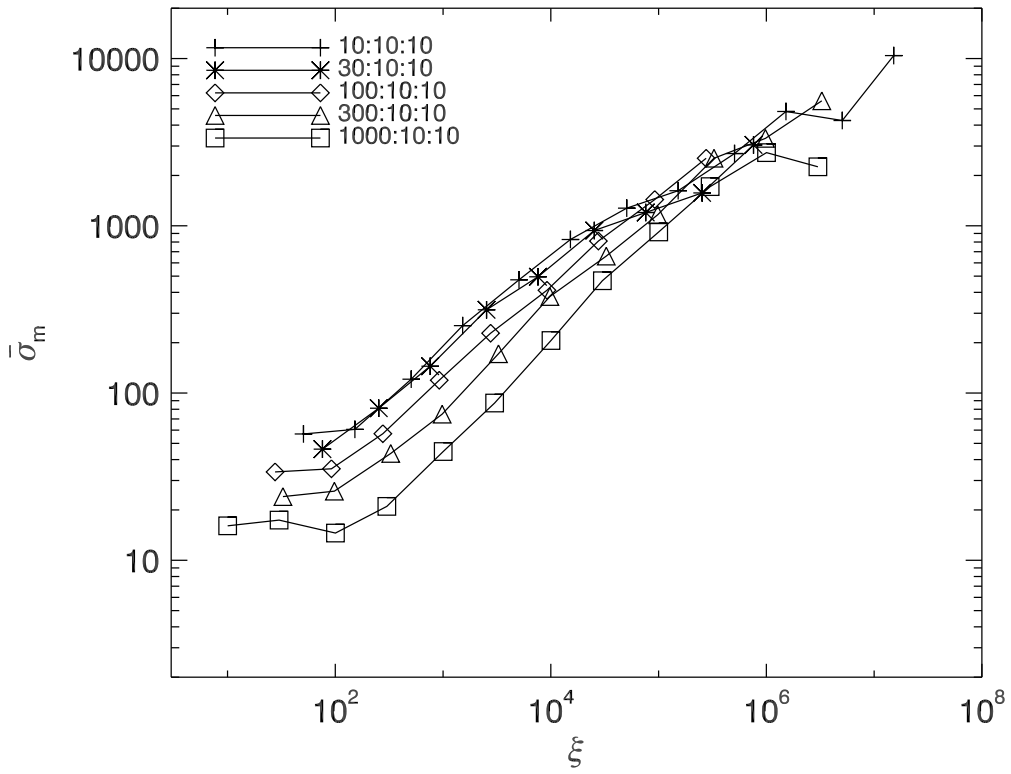

Figure 3.8: Normalized merger cross-section like Figure 3.6 for X:10:10 series. The error bars from Figure 3.6 are representative for the curves in this figure.

next encounter. This procedure continues until the binary merges from gravitational radiation or there is a merger during the encounter. Throughout our simulations we use an encounter speed of $v_\infty = 10$ km s^{-1}, an isotropic impact parameter such that the hyperbolic pericenter would range from $r_p = 0$ to $5a_0$, and a black hole number density in the core $n = 10^5$ pc^{-3} (See Chapter 2 for an explanation of these choices.). For each mass ratio we simulate 1000 sequences of encounters with gravitational radiation reaction.

Our results are summarized in Table 3.1. The inclusion of gravitational waves during the encounter makes a significant difference from the results reported in Chapter 2. The fraction of sequences that result in a merger during an encounter f_m is a good indicator of the importance of gravitational waves. Even for $m_0 = 10\ M_\odot$, a

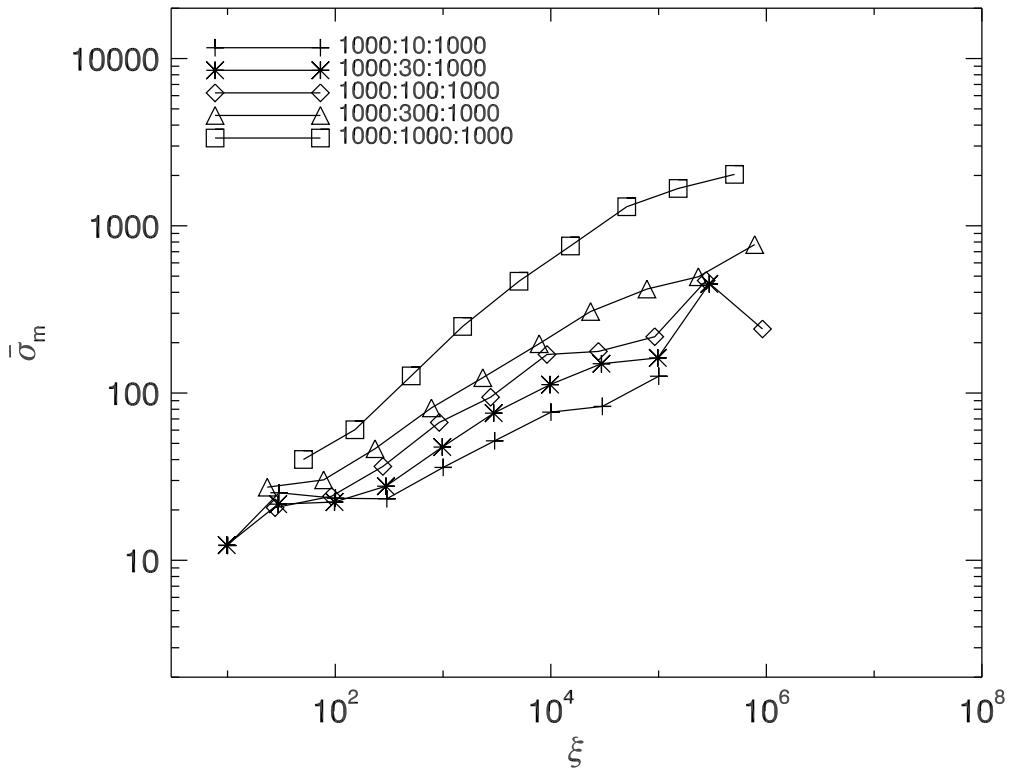

Figure 3.9: Normalized merger cross-section like Figure 3.6 for 1000:X:1000 series. The error bars from Figure 3.6 are representative for the curves in this figure.

significant fraction ($f_m > 0.1$) of the sequences merge this way, and for $m_0 > 300\ M_\odot$ this type of merger is more likely to occur than mergers between encounters, and thus this effect shortens the sequence significantly. In particular, for $m_0 = 1000\ M_\odot$ compared to the values from Chapter 2, the average number of encounters per sequence $\langle n_{\rm enc} \rangle$ is decreased by 42%; the average number of black holes ejected from the cluster $\langle n_{\rm ej} \rangle$ is reduced by 56%; and the average sequence length $\langle t_{\rm seq} \rangle$ is 67% shorter. One caveat for the study of sequences of encounters is that an IMBH in a cluster of much lower mass objects will gather a large number of companions in elongated orbits through binary disruptions, and thus the picture of an isolated binary encountering individual black holes may not hold when the IMBH becomes very massive (Pfahl 2005a).

Table 3.1. Sequence Statistics.

$m_0/M_\odot$	$\langle n_{\rm enc}\rangle$	$\langle n_{\rm ej}\rangle$	$f_{\rm binej}$	$\langle t_{\rm seq}\rangle/10^6$ yr	$\langle a_f\rangle$/AU	$\langle e_f\rangle$	f_m
10	46.4	3.2	0.652	54.10	0.174	0.904	0.134
20	46.7	5.1	0.515	40.86	0.224	0.900	0.130
30	52.4	7.3	0.457	29.47	0.290	0.898	0.156
50	62.3	10.8	0.329	19.17	0.291	0.897	0.190
100	83.9	16.6	0.103	11.65	0.401	0.893	0.275
200	123.0	24.3	0.011	7.26	0.411	0.885	0.387
300	147.8	26.9	0.002	4.74	0.543	0.881	0.492
500	197.5	33.1	-	3.03	0.611	0.879	0.627
1000	284.2	38.8	-	1.47	0.878	0.914	0.754

Note. — Main results of simulations of sequences of encounters with gravitational radiation included during the encounter. The columns are: the mass of the dominant black hole m_0, the average number of encounters per sequence $\langle n_{\rm enc}\rangle$, the average number per sequence of stellar-mass black holes ejected from a stellar cluster with escape velocity 50 km s^{-1} $\langle n_{\rm ej}\rangle$, the fraction of sequences in which the binary is ejected $f_{\rm binej}$ from a stellar cluster with escape velocity 50 km s^{-1}, the average time per sequence $\langle t_{\rm seq}\rangle$, the average final semimajor axis of the binaries after the last encounter $\langle a_f\rangle$, the average final eccentricity of the binaries after the last encounter $\langle e_f\rangle$, and the fraction of sequences that end with a merger during the encounter f_m. Note that $\langle a_f\rangle$ and $\langle e_f\rangle$ only refer to the binaries that do not merge during the encounter; these comprise $1 - f_m$ of the sequences.

3.4 Discussion

3.4.1 Implications for IMBH Formation and Growth

Our simulations provide a useful look into the merger history of an IMBH or its progenitor in a dense stellar cluster. As an IMBH grows through mergers with stellar-mass black holes, it will progress through the different masses that we included in our simulations of sequences. We interpolate the results in Table 3.1 to calculate the time it takes to reach 1000 $M_\odot$, the number of cluster black holes ejected while building up to 1000 $M_\odot$, and the probability of retaining the IMBH progenitor in the cluster for different seed masses and escape velocities of the cluster.

The time to build up to 1000 $M_\odot$ is dominated by $\langle t_{\rm seq} \rangle$ at high masses. Although each individual sequence is short, far more mergers are required for the same fractional growth in mass. In Figure 3.10 we plot the mass of the IMBH as a function of time for an initial mass of $m_0 = 10$, 50, and 200 $M_\odot$, for which total times to reach 1000 $M_\odot$ are 600, 400, and 250 Myr, respectively. Because we assume a constant core density throughout the simulations, the times are unaffected by changing the cluster's escape velocity. Without gravitational radiation, the times are roughly twice as long (Chapter 2) because the length of each sequence is dominated by the time it spends between encounters at small a when encounters are rarer. With gravitational radiation included, mergers that occur during an encounter are more likely at small separations, and the length of the sequence is shortened. These times are much shorter than the age of the globular cluster and are smaller than or comparable to timescales for ejection of black holes from the cluster, which we discuss below (see also O'Leary et al. 2006; Portegies Zwart & McMillan 2000). Thus time is not a limiting factor in reaching 1000 $M_\odot$ for an IMBH progenitor that can remain in a dense cluster with a sufficiently large population of stellar mass black holes.

Each time that an encounter tightens the binary, energy is transfered to the interloper, which leaves with a higher velocity. If energetic enough, this interaction will kick the interloper out of the cluster. If the interactions kick all of the interacting black holes out of the cluster, the IMBH cannot continue to grow. In a massive, and therefore dense, cluster, there are roughly 10^3 black holes (Chapter 2). With gravitational radiation included during the encounters, the number of black holes ejected is roughly halved compared with the number when gravitational radiation in included only between encounters (Figure 3.11), but the total number ejected while building up to 1000 $M_\odot$ is still a few times the number of black holes available even for an escape velocity of $v_{\rm esc} = 70$ km s^{-1}. Thus a black hole smaller than

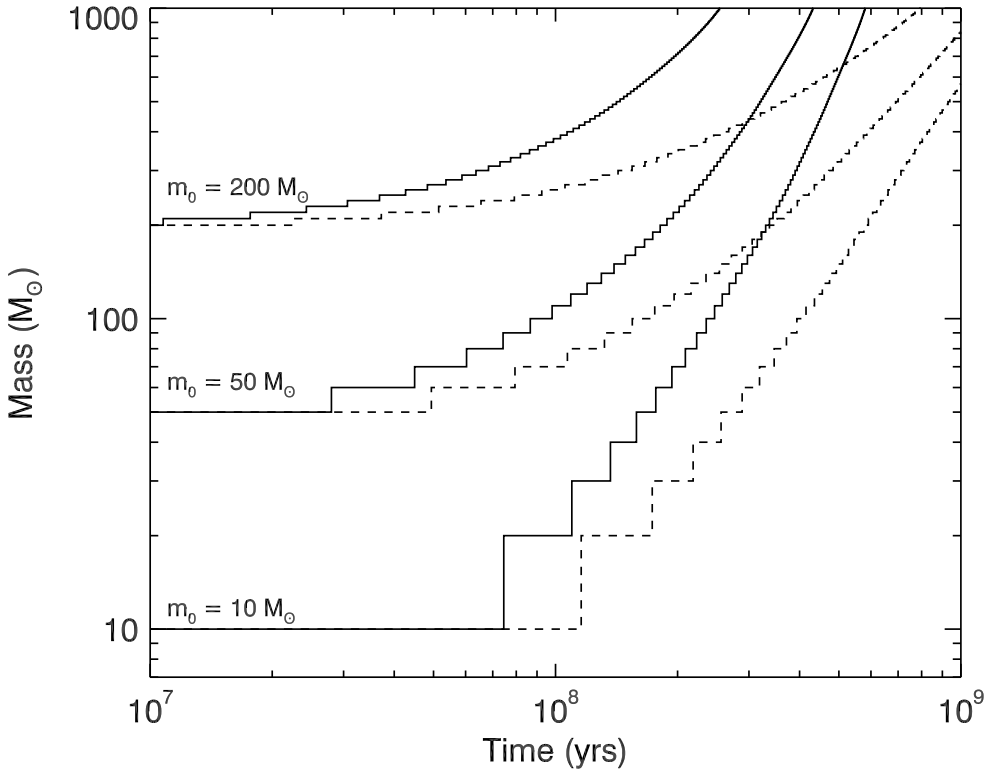

Figure 3.10: Mass of progenitor IMBH as a function of time as it grows through mergers with 10 $M_\odot$ black holes in a dense stellar cluster. Solid curves show results from this work in which gravitational radiation is included, and dashed curves show results from Chapter 2 in which this effect is only included between encounters. From bottom to top the curves show the growth of black holes with initial mass $m_0 = 10$, 50, and 200 $M_\odot$. The IMBH progenitors all reach 1000 $M_\odot$ in less than 600 Myr, and the inclusion of gravitational radiation significantly speeds up the growth of the black hole.

$m_0 \lesssim 600\ M_\odot$ cannot reach 1000 $M_\odot$ by this method without additional processes such as Kozai resonances (Gültekin et al. 2004; Miller & Hamilton 2002a; Wen 2003). However, O'Leary et al. 2006 find that Kozai-resonance induced mergers will only increase the total number of mergers by $\sim 10\%$. There is still the potential for significant growth in a short period of time. If we consider the point at which half of the black holes have been ejected from the cluster as the end of growth, then a black hole with initial mass of 50 $M_\odot$ will grow to 290 $M_\odot$ in 120 Myr, and a black

hole of 200 $M_\odot$ will grow to 390 $M_\odot$ in less than 100 Myr (compared to 240 $M_\odot$ and 330 $M_\odot$ without gravitational radiation during the encounter). In addition, this ejection of stellar-mass black holes by a binary with a large black hole is faster than by self-ejection from interactions among stellar-mass black holes calculated by Portegies Zwart & McMillan (2000), who find that $\sim 90\%$ of black holes are ejected in a few Gyr. O'Leary et al. (2006), however, find that the inclusion of a mass spectrum of black holes further speeds up the ejection of stellar-mass black holes by a small amount.

For every kick imparted on an interloper, conservation of momentum ensures a kick on the binary. Even with a large black hole, extremely large kicks can eject the binary from the cluster, at which point the IMBH progenitor can no longer grow. We can calculate the probability of IMBH retention for an individual sequence as $1 - f_{\rm binej}$, from which we interpolate the probability of remaining in the cluster while growing to 300 $M_\odot$ when the binary is essentially guaranteed to remain in the cluster. We plot this probability as a function of seed mass for several different escape velocities in Figure 3.12. The inclusion of gravitational waves during the encounter increases the retention probability for small masses. For $m_0 = 50\ M_\odot$ the cluster retains the binary more than 12% of the time, and 49% of the time for $m_0 = 100\ M_\odot$. Because the energy that an interloper can carry away from the system scales as

$$\Delta E \sim \frac{m_1}{m_0 + m_1} |E_B| = \frac{m_1}{m_0 + m_1} \frac{G m_0 m_1}{2a}, \tag{3.8}$$

the encounters at the end of the sequence, when a is smallest, are the most likely to impart a kick large enough to eject the binary from the cluster. This is also the point at which effects from gravitational radiation are strongest and at which close encounters are most likely to cause a merger. When the encounter ends in a merger, there can be no more ejections. The mergers from gravitational radiation

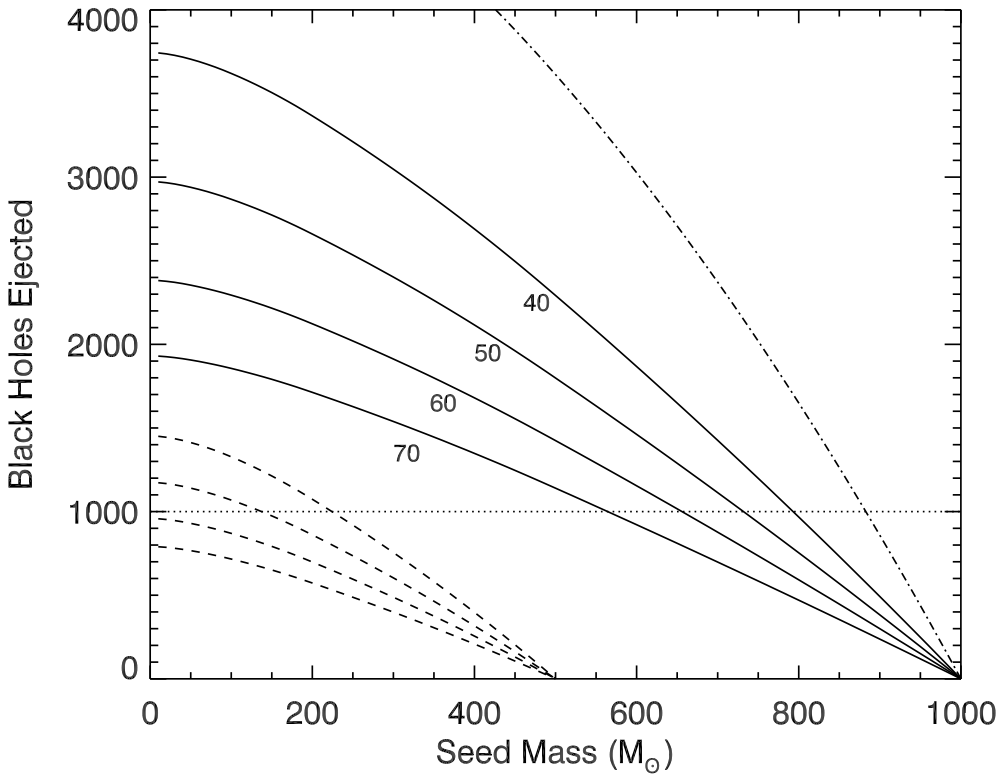

Figure 3.11: Number of black holes ejected in building up to 1000 $M_\odot$ (solid curves) and to 500 $M_\odot$ (dashed curves) as a function of seed mass for different cluster core escape velocities, given in units of km s^{-1}. The dotted line indicates the expected number of black holes in a large globular cluster. The dot-dashed curve from Chapter 2 shows the number of black holes ejected from the cluster in building up to 1000 $M_\odot$ for a cluster escape velocity of 50 km s^{-1} without the effects of gravitational waves during the encounter. For all but the largest seed masses, the globular cluster does not contain enough black holes for the IMBH to reach 1000 $M_\odot$. There are, however, a sufficient number of black holes to build up to 500 $M_\odot$ for a seed mass greater than 225 $M_\odot$ or an escape velocity of at least 60 km s^{-1}. The inclusion of gravitational radiation during the encounter roughly halves the number of ejections.

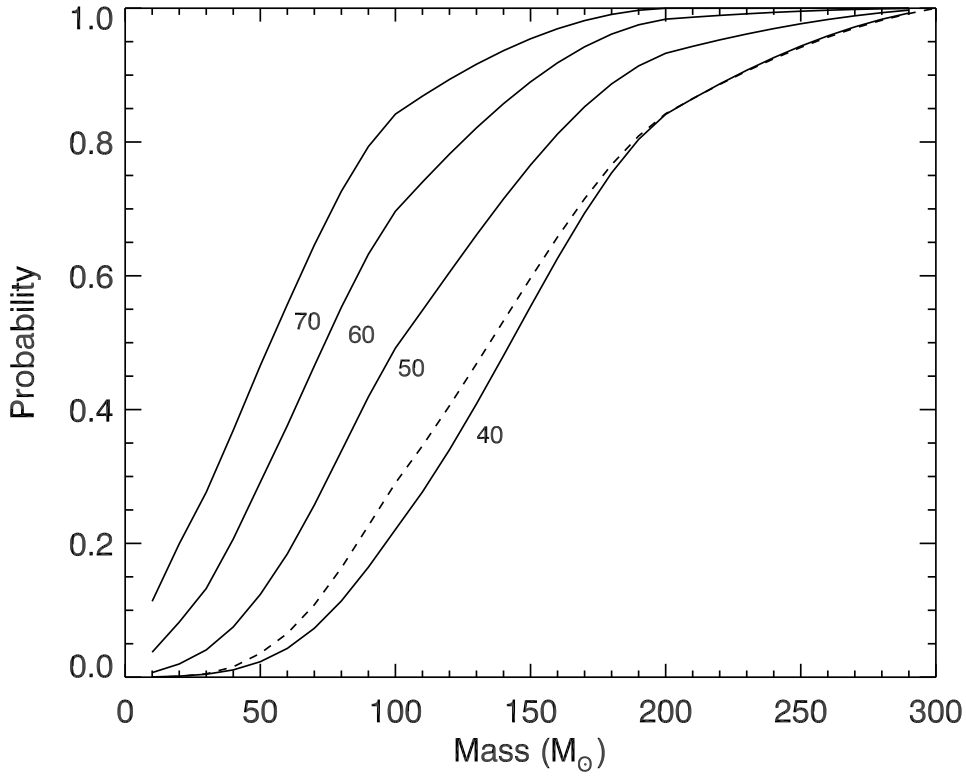

Figure 3.12: Probability for a binary with an IMBH to remain in the cluster until building up to 300 $M_\odot$ as a function of seed mass for different cluster core escape velocities given in units of km s^{-1}. Solid curves are results from this work, and the dashed curve is from Chapter 2 for an escape velocity of 50 km s^{-1}. The inclusion of gravitational radiation significantly increases the retention probability.

decrease the number of ejections by decreasing the number of encounters and thus the number of possible ejections as well as cutting off what would otherwise be the end of the sequence, in which ejections are more likely to occur.

As mentioned in § 2.2, our analysis of the ejection of stellar-mass black holes as well as of IMBH progenitors does not include the effects of gravitational radiation recoil. Based on the four most recent calculations (Baker et al. 2006; Blanchet et al. 2005; Damour & Gopakumar 2006; Favata et al. 2004), a seed mass of $m_0 = 150\ M_\odot$ merging with $m_1 = 10\ M_\odot$ companions will produce a recoil velocity $v_r \lesssim 50$ km s^{-1}, and if the numerical relativity simulations are the most accurate predictions, a seed

mass of $m_0 = 100\ M_\odot$ is sufficient. Therefore, a seed mass greater than 100 $M_\odot$is sure to avoid ejection from both dynamical interactions and gravitational radiation.

3.4.2 Implications for Gravitational Wave Detection

In addition to the likelihoods and rates of growth of black holes in dense stellar systems, our simulations shed light on the gravitational wave signals that come from the mergers of these black holes. Making optimistic assumptions, O'Leary et al. (2006) calculate upper limits for Advanced LIGO detection rates for black hole mergers in stellar clusters that formed at a redshift $z = 7.8$. For their wide range of cluster properties, they find detection rates ranging from $\nu_{\rm AdLIGO} \approx 0.6$ to 10 yr^{-1}. For cluster parameters that most closely resemble those used in Chapter 2 and in this work (GMH model series), they find $\nu_{\rm AdLIGO} \approx 2$ to 4 yr^{-1}. Our simulations show that when gravitational radiation is included in the integration the number of black holes ejected per merger decreases for all mass ratios. With fewer black holes ejected from the cluster, the overall rate of black hole mergers increases. For the 10:10:10 case, the number of ejections per merger decreases by $\sim 10\%$, and for the 1000:10:10 case the number decreases by more than a factor of 2, thus increasing the rates found by O'Leary et al. (2006). The exact increase in rate is difficult to estimate because the total number of mergers is dominated by mergers between stellar-mass black holes, yet the most easily detected mergers involve black holes with larger masses.

Because dynamical interactions strongly affect the eccentricity of a binary and because the timescale for merger is a such a strong function of eccentricity, binaries in a cluster tend to have very high eccentricities after their last encounter (Chapter 2, O'Leary et al. 2006). With the addition of gravitational radiation during the encounter, we find that the merging binaries become more eccentric because a sig-

nificant fraction of the mergers (f_m in Table 3.1) occur during the encounter. These mergers typically happen between two black holes that are not bound to each other until they come close to each other and emit a significant amount of gravitational radiation, after which the two black holes are in an extremely high eccentricity orbit ($1 - e \lesssim 10^{-3}$).

To see how these high eccentricities affect the detectability of the gravitational wave signal, we integrate Equation 2.1 and Equation 2.2 until the binaries are detectable by *LISA* and then Advanced LIGO. For circular orbits, the frequency of gravitational wave emission is twice the orbital frequency, but masses in eccentric orbits emit at all harmonics: $f_{\rm GW} = n\Omega/2\pi$, where n is the harmonic number and

$$\Omega = \left[\frac{G\left(m_0 + m_1\right)}{a^3}\right]^{1/2} \tag{3.9}$$

with peak harmonic for $e > 0.5$ at approximately $n = 2.16\left(1 - e\right)^{-3/2}$ (Farmer & Phinney 2003). We consider the binary to be detectable by *LISA* when the peak harmonic frequency is between 2 mHz and 10 mHz. We plot the distribution of eccentricities in Figure 3.13. The distributions are essentially a combination of those from Figure 2.9 and a sharp peak near $e = 1$, which comes from the mergers during the encounter. The number in the sharp peak increases with mass as f_m increases such that for 1000:10:10 more than 75% of the merging binaries detectable by LISA have an eccentricity greater than 0.9. Between 15% and 25% of all of the merging binaries have eccentricities so high that the peak harmonic frequency is above the most sensitive region of the LISA band, but they should still be emitting strongly enough at other harmonics to be detectable. Such high eccentricity presents challenges for the detection of these signals from the data of space-based gravitational wave detectors because (1) it requires a more computationally expensive template matching that includes non-circular binaries and (2) the binaries only emit a strong amount of gravitational radiation during the short time near periapse as they merge.

For a given semimajor axis, these extremely high eccentricities will also increase the gravitational wave flux emitted and thus increase the distance out to which *LISA* can detect them, but the detection rate may be compensated by the fact that more parameters are required (Will 2004). We also integrate the orbital elements of the binaries until they are in the Advanced LIGO band (40 Hz $< f_{\rm GW} < f_{\rm ISCO}$) or within a factor of 2 of their ISCO frequency for $m_0 > 100\ M_\odot$. We find that they have almost completely circularized (Figure 3.14). A tiny fraction ($< 0.5\%$) of the runs with $m_0 = 500$ and 1000 $M_\odot$ have merging binaries with eccentricities such that $1 - e \lesssim 10^{-6}$.

3.5 Conclusions

1. Gravitational radiation in N-body. We present results of numerical simulations of binary-single scattering events including the effects of gravitational radiation during the encounter. We include gravitational radiation by adding the 2.5-order post-Newtonian force term (Equation 3.1) to the equation of motion within the HNDrag framework. The code reproduces the expected semimajor axis and eccentricity evolution, and it gives the expected two-body capture radius.

2. Close approach and merger cross-sections. We use the new code to test the effects of gravitational radiation on a standard numerical experiment of binary-single encounters. We probe the close approach cross-section to smaller separations than has been simulated previously and find that the inclusion of gravitational radiation makes little difference except for extremely close encounters ($r_p < 10^{-5}a$), at which point gravitational radiation drives the objects closer together. We also present the cross-section for merger during binary-single scattering events for a variety of mass ratios and semimajor axes.

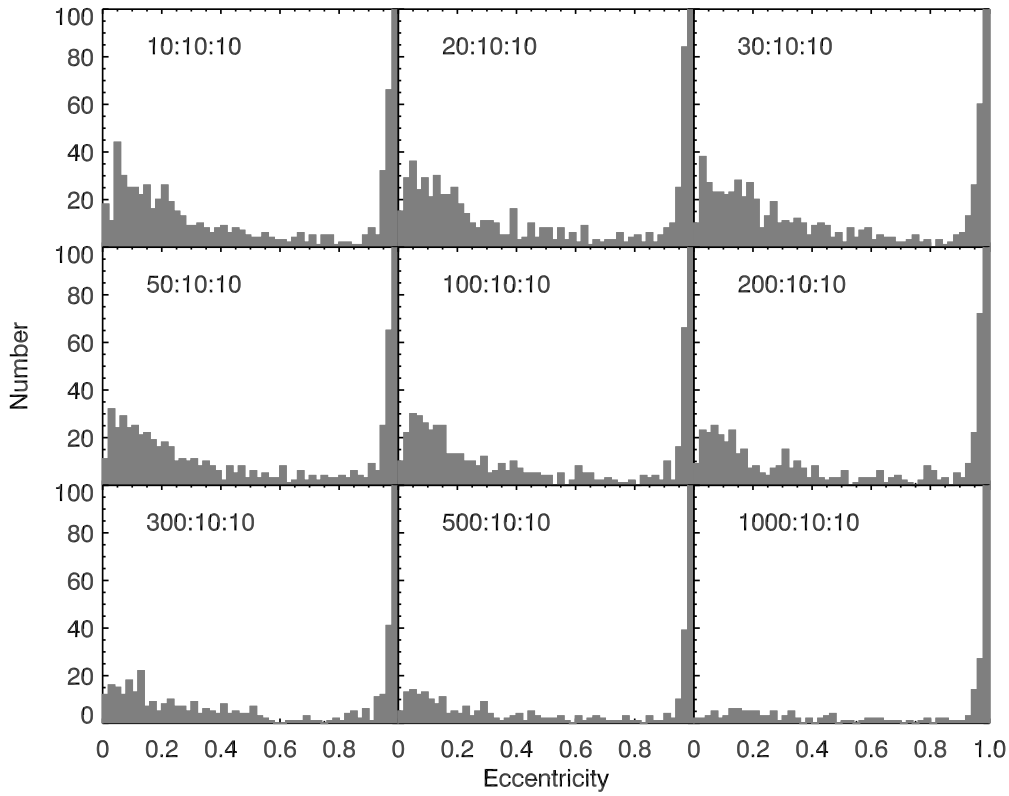

Figure 3.13: Histogram of eccentricities of merging binary while in the *LISA* band (f_{GW} = 2 mHz to 10 mHz) out of a total of 1000 sequences. The histograms show a combination of the binaries that merged after the last encounter with eccentricities concentrated around $0 < e \lesssim 0.3$ and the black holes that merged quickly during the encounter with eccentricities very close to unity. The peaks in the rightmost bin in all plots lie above the range of the plots.

3. IMBH growth in dense stellar clusters. We simulate sequences of binary-single black hole encounters to test for the effects of gravitational radiation and to test formation and growth models for intermediate-mass black holes in stellar clusters. We find that the inclusion of gravitational radiation speeds up the growth of black holes by a factor of 2, increases the retention of IMBH progenitors by a factor of 2, and decreases the ejection of stellar-mass black holes by a factor of 2. All of these effects act to enhance the prospects for IMBH growth.

4. Detectability of gravitational waves. We analyzed the merging binaries from

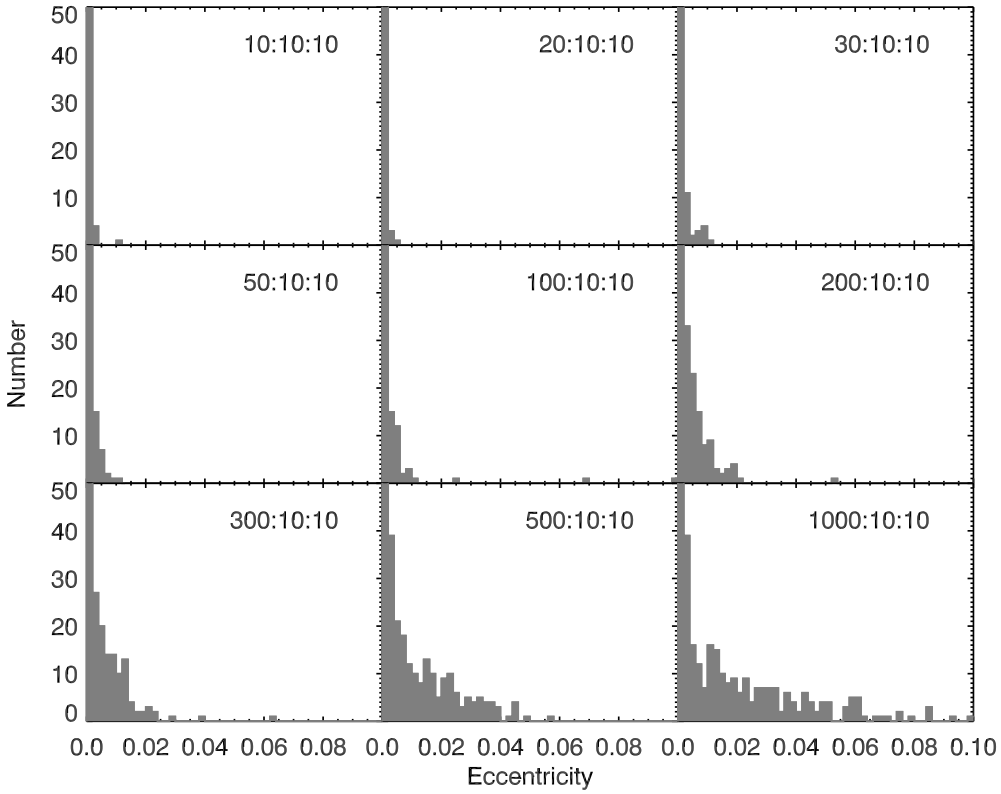

Figure 3.14: Histogram of eccentricities of merging binary while the gravitational wave frequency is detectable from current and future ground-based detectors. The upper limit of the frequency range is the ISCO frequency. We used a lower limit for frequency range of 100 Hz for $m_0 = 10$, and 20 $M_\odot$; 35 Hz for $m_0 = 30$, 50, and 100 $M_\odot$; and half the ISCO frequency for the higher mass binaries. The binaries are very close to circular once they are in the frequency range of ground-based detectors. The peaks in the leftmost bin in all plots lie above the range of the plots.

the simulations of black holes in dense stellar clusters to look at the detectability of the gravitational wave signals from these sources. We find that the mergers that occur rapidly during the encounter as opposed to those that occur after the final encounter are an important source of black hole mergers, becoming the dominant source of mergers at the higher mass ratios. The mergers that do occur during the encounter tend to have extremely high eccentricity ($e > 0.9$) while in the *LISA* band, presenting challenges for their detection. When the gravitational wave signal

from the merging black holes is in the Advanced LIGO band, the orbit will have completely circularized.

Chapter 4

Summary and Conclusions

4.1 Answers

Let us return to the questions raised in § 1.4, which may be simplistically paraphrased as, "Does the Miller & Hamilton (2002b) model of IMBH formation work; can we see any unique gravitational waves from this model; and what else have you learned?" These may be equally simplistically answered as, "Yes, with slight modifications; yes and no; and quite a bit." More specifically, the first question was:

1. Is the Miller & Hamilton (2002b) model of IMBH formation fast enough to make an IMBH before the globular cluster's supply of stellar-mass black holes eject themselves from the cluster through dynamical interactions ($\sim$ 0.4 to 1 Gyr)?

The simulations show that the process of repeatedly merging stellar-mass black holes with a seed mass can happen quickly enough. The simulations in this dissertation can be seen as building on each other with an additional layer of gravitational physics that the previous layer did not include. The first set of simulations in Chapter 2 used Newtonian integrations with a relativistic endpoint. The second

set of simulations in Chapter 2 added orbital decay between Newtonian encounters in a sequence with a relativistic endpoint, and the simulations in Chapter 3 added gravitational wave emission to the encounters. Each additional layer decreased the amount of time needed to reach 1000 $M_\odot$: from 1.1 Gyr to 0.71 Gyr to 0.41 Gyr, assuming a seed mass of 50 $M_\odot$. This is comparable to the $0.4-1.0$ Gyr that it takes for the stellar-mass black holes to eject themselves (O'Leary et al. 2006; Portegies Zwart & McMillan 2000; Sigurdsson & Hernquist 1993). This process happens more quickly than originally anticipated by Miller & Hamilton (2002b) because the authors assumed that the binaries would merge with eccentricity $e \approx 0.7$. Instead, the binaries merge with a high eccentricity, which allows the binaries to merge with a much larger semimajor axis and, therefore, in a much shorter time. The times listed above assume that the density of stellar-mass black holes remains constant throughout the process. In reality, the density will be decreasing as the stellar-mass black holes eject themselves and as the IMBH progenitor ejects them from the cluster core. This leads to the next question.

2. Can repeated mergers of stellar-mass black holes in a globular cluster produce an IMBH without ejecting too many stellar-mass black holes via the encounters that harden the IMBH-progenitor binary?

There are roughly 10^3 stellar-mass black holes in a typical large globular cluster, and the process of binary-hardening and merging will eject more than this when growing to 1000 $M_\odot$. As before, when each additional layer of gravitational physics is added, the number decreases: from 6800 to 5300 to 2900. This assumes that the interactions continue regardless of the number of black holes in the cluster. Another way of looking at this is that an IMBH (or its progenitor) in a binary in a stellar cluster is the dominant source of stellar-mass black hole ejections. Before all of the black holes are ejected, however, all scenarios allow 15 to 25 mergers before exhausting

roughly half of the black holes, and thus all scenarios allow for significant growth. These numbers also assume an escape velocity from the cluster of $v_{\rm esc} = 50$ km s^{-1}, which is a typical value. The escape velocity, however, has been found to be much higher for some Galactic globular clusters. For escape velocities of $v_{\rm esc} = 60$ and 70 km s^{-1}, the most realistic simulations find 2300 and 1900 black holes ejected, respectively. The total number of black holes in a very massive globular cluster could reach ~ 2000, and such a cluster would have a higher-than-average escape velocity. Thus it is entirely plausible that the Miller & Hamilton (2002b) model could reach 1000 $M_\odot$ in such a cluster. Finally, as seen in Figure 3.11, an escape velocity of $v_{\rm esc} \geq 60$ km s^{-1} will eject fewer than 1000 black holes when building up to 500 $M_\odot$. Such a black hole is certainly an IMBH and is massive enough to explain all but the brightest ULXs. Even the brightest ULX, M82 X-1, can be explained if its brightest fluxes come from short periods of accreting at ~ 2 times the Eddington rate.

3. Will a globular cluster retain an IMBH progenitor over the course of its merger history, or will the binary-single scattering events eject the IMBH progenitor with great regularity?

The answer to this question depends on the seed mass of the IMBH progenitor. The classical Miller & Hamilton (2002b) model calls for a 50 $M_\odot$ black hole as the seed mass. For the three layers of gravitational physics the probability of a seed mass's retention is 0.00766, 0.0356, and 0.124, respectively. The retention probability is the biggest quantitative change among the three classes of simulations: from negligible to respectable. If roughly 10^{-1} of all globular clusters can hold on to their IMBH progenitor, then only 10^{-2} of the IMBHs produced need to be currently accreting in order to explain the $\sim 10\%$ of nearby galaxies with ULXs, assuming 100 globular clusters per galaxy. So the classical model can withstand ejection by dynamical

kicks from three-body encounters. Withstanding ejection by gravitational radiation recoil is a different matter. As discussed in § 2.2, gravitational radiation carries momentum with it, and the asymmetric radiation from unequal masses causes the center of mass of the binary to spiral outwards from its original position as seen by an observer far from the binary. Using the fitting formula of Fitchett (1983) and the numerical relativity simulations of Baker et al. (2006), the recoil velocity is

$$v_{\rm recoil} = 9 \times 10^3 \frac{q^2 (1-q)}{(1+q)^5} \text{ km s}^{-1} \tag{4.1}$$

for $q \equiv m_1/m_0 \leq 1$, where the factor in front comes from setting $v_{\rm recoil} = 105$ km s^{-1} for $q = 0.67$. For a 50 $M_\odot$ black hole that only merges with 10 $M_\odot$ black holes, $q = 0.2$, and Equation 4.1 implies $v_{\rm recoil} \approx 115$ km s^{-1}. Thus the classical Miller & Hamilton (2002b) model cannot keep the seed mass in the cluster after the first merger. If, however, the seed mass were $m_0 = 100$ $M_\odot$, then the recoil velocity when merging with $m_1 = 10$ $M_\odot$ black holes would be $v_{\rm recoil} \approx 50$ km s^{-1}, or just at the escape velocity of a typical globular cluster. It is reasonable, however, for black holes to have mass $m_1 = 20$ $M_\odot$. To avoid ejection from mergers with such black holes, the seed mass would need to be $m_0 > 200$ $M_\odot$. If we only consider clusters with escape velocity $v_{\rm esc} > 60$ km s^{-1}, then a seed mass with $m_0 > 170$ $M_\odot$ would avoid ejection. Such 100 $M_\odot$ to 200 $M_\odot$ black holes are already exotic objects (IMBHs by our own definition!), and they require their own formation mechanism. One possibility is if two 50 $M_\odot$ black holes exist in a single cluster. They would likely find each other through interactions and end up in a binary. As equal-mass objects, they would suffer no gravitational radiation recoil when they merged, and then the resulting 100 $M_\odot$ black hole might grow to ~ 170 $M_\odot$ by merging with 10 $M_\odot$ black holes. Similarly, a 200 $M_\odot$ black hole could be created by hierarchical merging of four 50 $M_\odot$ black holes (or eight 25 $M_\odot$ black holes, etc.). While such scenarios are possible, they require finesse to prevent the wrong black holes from

meeting up at the wrong time. In addition, slightly unequal masses can still lead to recoil velocities greater than the escape velocity of the cluster, and misaligned spins would contribute as well. The most obvious method of providing a massive seed is from the core collapse phase of a stellar cluster. If the runaway collisions of stars during this phase produce a merger remnant that loses 80% to 90% of its mass in its evolution to a black hole, then it will produce a black hole with mass 200 to 300 $M_{\odot}$. If the merger remnant always retains its mass, a 200 to 300 $M_{\odot}$ seed can be formed if the collisions do not become a true runaway process. If the core collapse phase only results in 1 or 2 collisions of ~ 100 $M_{\odot}$ stars, the resulting 200 to 300 $M_{\odot}$ black hole could act as a seed in the host cluster.

It has been said that the Miller & Hamilton (2002b) model is an inefficient process for making IMBHs (e.g., O'Leary et al. 2006), but the most conservative conclusion one can draw from the simulations presented in this dissertation is that a 200 $M_{\odot}$ seed mass will grow to 500 $M_{\odot}$ in less than 200 Myr, within the available supply of black holes with a retention probability greater than 0.9. Put differently, it is unclear how such a seed mass could *avoid* such growth with any regularity. The model requires another mechanism to create the seed mass, but the core-collapse collisions appear to be a promising source. Finally, the Miller & Hamilton (2002b) model can "save" the runaway collisions method of forming IMBHs if the merger remnants cannot turn much of their mass into a black hole.

4. What is the observable gravitational-wave signature of these merging and inspiraling systems?

Though the expected detection rate of these events with *LISA* is low, detectable inspirals are likely to be from highly eccentric binaries. Again, the inclusion of gravitational radiation makes a difference for the expected eccentricity. From Figure 2.9, one can see the difference between the histograms for high masses, and in

Figure 3.13 one can see that gravitational radiation included during dynamical encounters completely changes the histogram. For LIGO events, the binaries will have almost completely circularized, but the increased rate of mergers for simulations that include gravitational radiation reaction forces indicates that detection rates may be higher than previously estimated.

5. What is the reason for the apparent broken power-law in the cross-section for closest approach in a three-body encounter?

The curves in Figure 3.3 show that as time progresses within a three-body encounter the cross-section for closest approach evolves from that expected for a single pass in a gravitationally focused encounter into the apparent broken power-law curve. This suggests that the reason is that multiple passes by resonant encounters with additional close approaches increase the number of encounters with small $r_{\rm min}/a_0$. The slope of the curve approaches unity, as expected, but it does not happen until very small values of $r_{\rm min}/a_0$. This is surprising because one would expect that as two objects get within a distance much smaller than the semimajor axis of the binary (the next smallest scale distance), one could approximate the encounter as a two-body encounter. These selected two-body encounters, however, probably do not come from the isotropic parameter space that would produce a curve with slope unity.

6. How does the cross-section for close approach change when gravitational waves are included?

The curves in Figure 3.5 show that gravitational radiation reaction forces do not significantly alter the cross-section except for extremely close encounters that are driven all the way to merger.

7. What is the likelihood of merger because of gravitational radiation during a binary-single encounter when the leading-order terms of energy loss from gravitational waves are included?

Figure 3.6 through Figure 3.9 show the shape of the merger cross-section curves. There appears to be no simple scaling that takes into account the different regimes of mass ratios possible.

4.2 Possible Future Work

Though it covers a lot, this dissertation does not represent all that could be done with this technique to answer these questions. The method of simulating an IMBH progenitor's evolution through dynamics and mergers with isolated encounters may be extended with additional considerations. One such consideration is to include simulations of the acquisition of the IMBH progenitor's binary companion. Although Appendix A shows that this will probably not siginificantly increase the time to grow an IMBH, it is possible that including the acquisition of the companion will decrease the time slightly if the typical initial orbit of the binary is much tighter or extremely eccentric. Including a mass spectrum instead of the single population of 10 $M_{\odot}$ black holes will also change the number of black hole ejections and retention probability. If the population contains a large number of black holes smaller than 10 $M_{\odot}$, the number of stellar-mass black holes ejected increases while the probability of the IMBH's ejection decreases, and vice versa for a large number of black holes more massive than 10 $M_{\odot}$. It is unclear what will happen if the population contains large numbers of both.

Binary-binary interactions are also important. Table 3.1 shows that $\sim 2 \times 10^4$ encounters are required to grow from 50 $M_{\odot}$ to 1000 $M_{\odot}$. This means that even

for a binary fraction $f_{\rm bin} \sim 10^{-2}$, there will be ~ 200 encounters with a binary. In binary-binary encounters of stars, collisions between stars are very frequent (Fregeau et al. 2004); so it is likely that mergers are important as well. Another intriguing aspect of binary-binary interactions is the possibility of long-lived triple systems as an outcome. Such triple systems may be subject to the Kozai (1962) mechanism that causes the inner binary's eccentricity to oscillate. Under the influence of gravitational radiation, the binary would merge when the eccentricity reached a very high value. The wide outer binary also increases the interaction cross-section, which may result in resonant single-triple encounters that result in mergers.

Finally, it would be possible to model the changing number density of the black hole population as it interacts with itself and an IMBH. This could be done with loss-cone theory (e.g., Yu & Tremaine 2003), and it may allow a more accurate calculation of the time and merger rate.

4.3 For Posterity

If one wishes to reduce this dissertation to a general, minimalist sound bite, it would be: *In order to understand the dynamics of compact objects in dense clusters or their gravitational waves, their influence on each other must be studied because Newtonian dynamics informs the generation of gravitational waves, and gravitational radiation alters the dynamics.*

Although the scientific motivation for this dissertation is sound science, it is possible that there is some fundamental assumption that is incorrect. There are, after all, dissertations concerning the ether (e.g., Gilbert 1901; Webster 1913). What is the relevance of this dissertation if the assumptions are wrong? If ULXs or cluster kinematics are shown not to be evidence of IMBHs, the process of repeated

mergers that increase the mass of black holes must still proceed to some extent if there is a seed mass. Even if runaway-collisions and the initial mass function of the cluster conspire to preclude massive black holes as seeds to this process, there are other possible channels to a seed, for example, binary black holes or non-runaway collisions such as blue stragglers. The overall efficiency of making big black holes will be reduced without a large seed, though. If very solid evidence that IMBHs definitely do not exist in clusters is found, then the question becomes what prevents repeated mergers of black holes in clusters? The merger cross-sections and close approach cross-sections should be relevant unless the solid underlying physics of general relativity or Newtonian dynamics does not hold. Even then, the mathematical aspects of the three-body problem or three-body plus drag problem exist.

Appendix A

Time for IMBH Progenitor to Acquire a Companion

Because the simulations of sequences of encounters do not include the interactions that result in the initial acquisition of a companion, the time needed to do so is not included in the analysis of IMBH growth. Here we estimate the time needed. Because of the exchange bias that leads to more-massive objects in binaries and less-massive objects ejected from the system, an IMBH progenitor is favored to pick up a companion in a strong encounter with a binary. In order to reach the starting point of the simulations in Chapter 2 and Chapter 3, the IMBH progenitor needs to acquire a black hole companion. Analogous to the derivation of Equation 2.4, the average time to interact with a black hole in a binary system is $\langle \tau_{\rm comp} \rangle = 1/\langle n_{\rm bin} v_\infty \sigma(r) \rangle$, where $n_{\rm bin}$ is the number density of black holes with a companion of any mass. If the black holes in binaries are distributed evenly throughout the entire population of black holes, then $n_{\rm bin} = n f_{\rm bin}$, where $f_{\rm bin}$ is the fraction of black holes with a companion. In reality, black holes with companions will be more massive than average and therefore have a smaller scale height and larger density, but we will

ignore the mass of the companion for now: $m_{\rm bin} = m_{\rm BH} + m_{\rm comp} \approx m_{\rm BH} = 10\ M_\odot$.

As in Equation 2.3, $\sigma(r)$ is the gravitationally focussed cross section for interaction

$$\sigma\left(r\right) \approx \pi r^2 + 2\pi r G m_{\rm IMBH}/v_\infty^2 \approx 2\pi r G m_{\rm IMBH}/v_\infty^2, \tag{A.1}$$

for gravitationally-focusing-dominated interactions for an IMBH progenitor of mass $m_{\rm IMBH}$. For a strong interaction to result in an exchange, the distance must be of order the resulting semimajor axis of the binary after the encounter a_f. If the binding energy of the binary does not change with the encounter, the distance of the encounter is $r \sim a_f \sim a_0 m_{\rm IMBH}/m_{\rm comp}$ for an initial semimajor axis a_0. The distribution of semimajor axes among black holes with companions in a dense stellar cluster is difficult to determine, but the largest binaries would be near the hard/soft boundary, which is

$$a_0 = \frac{G m_{\rm BH}}{v_\infty^2} \approx 100\ {\rm AU}, \tag{A.2}$$

where we have assumed an average $v_\infty = 10\ {\rm km\ s^{-1}}$. If semimajor axes are distributed with equal number per decade as they are with main sequence binaries, then a conservative average semimajor axis would be $\langle a_0 \rangle = 3$ AU. The average time is then

$$\left\langle \tau_{\rm comp}\left(m_{\rm IMBH}\right) \right\rangle = \left\langle \frac{v_\infty m_{\rm comp}}{2\pi n_{\rm BH} f_{\rm bin} G m_{\rm IMBH}^2 a_0} \right\rangle = \frac{0.04\ {\rm Myr}}{f_{\rm bin}\left(m_{\rm IMBH}/50\ M_\odot\right)^2 \left(\langle a_0 \rangle /3\ {\rm AU}\right)}, \tag{A.3}$$

where we have used $n_{\rm BH} = 10^5\ {\rm pc^{-3}}$, $m_{\rm comp} = 0.4\ M_\odot$. The total time spent acquiring binaries while building from 50 $M_\odot$ to 1000 $M_\odot$ is

$$T = \sum_{i=1}^{96} \left\langle \tau_{\rm comp}\left(m_{{\rm IMBH},i}\right) \right\rangle f_{\rm ex}^{-1}, \tag{A.4}$$

where $m_{{\rm IMBH},i} = 50\ M_\odot + (i-1) m_{\rm BH}$ is the mass of the growing IMBH progenitor and $f_{\rm ex}$ is the fraction of such encounters that results in the desired exchange. For the mass ratios considered here, $f_{\rm ex} \gtrsim 0.05$ (Heggie et al. 1996). Because of the strong

dependence on the mass of the IMBH progenitor, the total time is dominated at small masses. Even for $f_{\rm bin} = 0.05$ and $\langle a_0 \rangle = 3$ AU, $T \approx 80$ Myr, which is less than 25% of the smallest total growth time when starting at 50 $M_\odot$. In Figure 3.10, a seed mass of 200 $M_\odot$ grows to 1000 $M_\odot$ in 250 Myr, but because Equation A.4 is dominated by the time when the progenitor mass is small, the total time spent acquiring companions is less than 10 Myr.

If anything, these estimated times are over-estimates. For example, the IMBH progenitor has a $\sim 2 - 5\%$ probability of acquiring the lower-mass object as a companion, which may then be exchanged for a stellar-mass black hole during one of the many hardening encounters that will take energy out of the binary. A similar process may occur for a tight binary with two ~ 5 $M_\odot$ stars, which would also have sunk to the center of the stellar cluster with the other ~ 10 $M_\odot$ objects on the order of $\sim 10^6$ yr. Therefore, ignoring the time to acquire a companion introduces only a small systematic error to the total IMBH growth time calculated in § 2.4 and § 3.4.1.

For comparison, we may also calculate the time for the IMBH progenitor to acquire a black hole companion by two-body capture via gravitational radiation. This time is $\tau_{2-\rm body} = 1/\left\langle n v_\infty \sigma \left(r_{p,\rm max} \right) \right\rangle$, where $r_{\rm p,max}$ is the maximum periastron separation for two objects to become bound to each other, given by Equation 3.2. For $m_0 = m_{\rm IMBH} = 50$ $M_\odot$, $m_1 = m_{\rm BH} = 10$ $M_\odot$, and the values given above, the maximum periastron separation is $r_{p,\rm max} = 3.3 \times 10^{-4}$ AU, and the average time is $\tau_{2-\rm body} \approx 40$ Gyr. Thus, three-body encounters with exchanges are the dominant source of binary acquisition.

Appendix B

Demonstration that 2.5PN Drag Force Reproduces the Peters Equations for Circular Orbits

In this appendix we show that Equation 3.1 produces the Peters (1964) orbit-averaged equations for semimajor axis evolution (Equation 2.1) for circular orbits. Peters (1964) has the derivation for the general case, but the circular case is elegant.

In the barycentric frame, the velocity vectors of the two masses m_0 and m_1 are always anti-aligned, and $m_0\boldsymbol{v}_0 + m_1\boldsymbol{v}_1 = 0$, so that the relative velocity between the two masses is

$$\boldsymbol{v} \equiv \boldsymbol{v}_1 - \boldsymbol{v}_0 = -(1 + m_0/m_1)\boldsymbol{v}_0. \tag{B.1}$$

The semimajor axis of a binary may be expressed as a function of the relative velocity between the two masses:

$$a = \frac{GM}{v^2}, \tag{B.2}$$

where $M = m_0 + m_1$ is the total mass of the binary. Differentiating Equation B.2

with respect to time yields

$$\frac{da}{dt} = -\frac{2GM}{v^3}\frac{dv}{dt}. \tag{B.3}$$

Substituting Equation B.1 into Equation B.3, we get

$$\frac{da}{dt} = \frac{2GM}{v^3}\left(\frac{M}{m_1}\right)\frac{dv_0}{dt}. \tag{B.4}$$

Since $\hat{r} \cdot \boldsymbol{v} = 0$ for a circular orbit, Equation 3.1 becomes

$$\frac{d\boldsymbol{v_0}}{dt} = \frac{4G^2}{5c^5}\frac{m_0 m_1}{a^3}\left(\frac{m_1}{M}\right)\left[\boldsymbol{v}\left(-6\frac{GM}{a} - 2v^2\right)\right], \tag{B.5}$$

where we have taken $r = a$. Substituting Equation B.5 into Equation B.4 gives

$$\frac{da}{dt} = -\frac{2GM}{v^3}\left[\frac{4G^2}{5c^2}\left(\frac{m_0 m_1}{a^3}\right)v\left(6\frac{GM}{a} + 2v^2\right)\right]. \tag{B.6}$$

Using Equation B.2 and rewriting, this becomes

$$\frac{da}{dt} = -\frac{64}{5}\frac{G^3}{c^5}\frac{m_0 m_1 M}{a^3}, \tag{B.7}$$

which is equivalent to Equation 2.1 for $e = 0$.

Appendix C

Summary of Code

The code used in this dissertation is called *iabl*, which stands for "*It's a binary's life*." It was written to be as general purpose as possible though it is optimized for the simulations run for this dissertation. The source for *iabl* consists of 12 files, which total over 3800 lines of C code. The code uses HNBody or HNDrag (HNBody hereafter) for the actual integration of the orbits with its classical Runge-Kutta integrator, but the rest of the tasks are done by *iabl* itself. The code was developed to be modular and reusable in other contexts. Because the computation is dominated by the actual N-body integration, the rest of the routines could be designed for readability and simplicity as long as the integrations were efficient. The code can be broken down into four primary sections: an initial conditions generator, the interface between HNBody and *iabl*, examination of integration, and the two-body approximator. We now describe these primary sections.

C.1 Initial Conditions Generator

The initial conditions generator uses drand48, a standard random number generator to produce a Monte Carlo sampling of the multi-dimensional parameter space of the three-body problem. The initial conditions generator is supplied with the masses of the three objects, m_0, m_1, and m_2, the initial semimajor axis of the binary, a_0, the initial eccentricity of the binary, e_0, the relative speed of the encounter between the center of mass of the binary and the interloper at infinity, v_∞. These are either supplied as command-line arguments or derived from the final conditions of the previous encounter in the sequence. The parameters generated are the true anomaly of the binary, f, the impact parameter of the interloper with respect to the center of mass of the binary as measured from infinity, b_∞, the azimuth of the interloper's initial velocity vector with respect to the pericenter of the binary, ϕ, the zenith angle of the interloper's initial velocity vector with respect to the plane of the binary's orbit, θ, an angle to determine in which direction the impact parameter takes effect, ψ.[1] A limitation of the code is that the distribution of encounters is assumed to be either isotropic in three dimensions or isotropic and coplanar. This could in principle be changed to accommodate any distribution of encounters. The above parameters are converted to Cartesian coordinates in the barycentric frame. The above parameters are stored in a structure within the main function, and are output with other output dumps for analysis.

[1]Note that the use of some of the symbols in this Appendix is inconsistent with their use elsewhere in this dissertation.

C.2 HNBody-*iabl* Interface

Without full access to the HNBody's source code, there were two choices available for the interface: (1) write a new driver for HNBody using the documented API or (2) use system calls to HNBody with its mature, distributed driver. We chose the latter because it limited the initial work required to produce a functioning program despite the loss of efficiency. As mentioned above, because the integration of the N-body equations of motion dominates the computational load, the efficiency lost from using system calls instead of linked function calls does not significantly affect the overall efficiency.

Before calling HNBody, *iabl* writes to files the input data from the initial conditions generator as well as the amount of time for HNBody to integrate. The initial guess for how long the encounter will take is that of a simple hyperbolic encounter of the interloper about the center of mass of the binary from an initial distance $r_i = 30(a_0^2 + b^2)^{1/2}$ to a final distance $r_f = 30a_0$. The time is given by

$$t_0 = \sqrt{\frac{a^3}{GM}} \left[e \left(\sinh F_i + \sinh F_f \right) - \left(F_i + F_f \right) \right] \tag{C.1}$$

where a and e are the semimajor axis and eccentricity of the hyperbolic orbit and F is the hyperbolic analog of the eccentric anomaly given by

$$F = \cosh^{-1} \left[\frac{1}{e} \left(1 + \frac{r}{a} \right) \right] \tag{C.2}$$

(Goldstein et al. 2002; Richardson et al. 1998). If the encounter is determined not to have finished in this time, the integration time is doubled. This time doubling repeats 10 times after which the time for the next integration grows as $t_i = 1.2t_{i-1}$. After 25 time extensions, *iabl* resets the encounter with new initial conditions.

C.3 Examination of Integration

One of the most sophisticated parts of *iabl* is its series of routines used to determine whether the integration has completed. The first test that *iabl* runs is to check for merger by gravitational waves. Though *iabl* currently uses the HNBody module ExitCondition to determine merger status, the simulations in this dissertation looked for errors from HNBody either from the exit value or the output, which indicates that objects came too close to each other for HNBody to continue.

If a merger has not occurred, *iabl* checks for an ionization. In this check *iabl* (1) looks to see that the total energy of the system is positive; (2) checks to see that no pair of objects are bound to each other; (3) checks to see that no object is bound to the center of mass of the other two objects; (4) checks to see that each particle's velocity vector is pointed away from the center of mass of the system ($r \cdot v < 0$ in barycentric coordinates). If all four tests are passed, a static variable flag is set, and the integration is extended. If *iabl* finds that the systems passes all tests twice in a row, an ionization is determined to have occurred. The twice-in-a-row test is used because of pathological cases in which no ionization occurred but it appears to be so. It is very unlikely for such already unlikely cases to occur at the second point of integration.

If no merger and no ionization has occurred, *iabl* checks to see if the encounter has resolved itself. First *iabl* determines the closest pair of objects and hypothesizes that they are the binary. The encounter is determined not to have finished, and the integration is extended if (1) the third object is within a distance of $30a_0$, (2) the closest pair of objects is not bound to each other, (3) the third object is bound to the center of mass of the binary with semimajor axis $a_3 < 2000$ AU, or (4) the third object is unbound but approaching the center of mass of the system. If the

third object (1) is bound to the center of mass of the binary with a semimajor axis $30a_{\rm ib} < a_3 < 2000$ AU, where $a_{\rm ib}$ is the semimajor axis of the inner binary, (2) is separated from the center of mass of the binary by a distance $r > 30a_{\rm ib}$, and (3) has its velocity vector pointed away from the center of mass of the system, then the two-body approximation is run. If all of these tests fail, then the encounter is determined to have finished.

C.4 Two-Body Approximator

The two-body approximator in *iabl* is conceptually simple yet speeds up typical simulations by a factor between 7 and 15. Empirically, we have found that roughly 10% of the encounters in a simulation take 90% of the total time. These encounters are long, resonant encounters in which all three objects become temporarily bound to each other. When the result of a binary-single encounter, these systems are unstable and eventually disrupt themselves. The two body approximator speeds this process up by treating hierarchical triples as two sets of binaries: the inner and the outer. The outer binary approximates the inner binary as a single particle at the location of its center of mass. The approximator advances the outer binary until it is returning toward the center of mass at a distance $r = 30a_{\rm ib}$. The approximator calculates the time elapsed and advances the inner binary's orbit. Then *iabl* calls HNBody to integrate the orbit again.

Appendix D

Other Applications of the Code

Though the primary purpose of *iabl* was for the research in this dissertation, it has been used for several other studies, three of which we outline here.

D.1 Planet in Close Triple System

The recently found planet in the hierarchical triple-stellar system HD 188753 (Konacki 2005) motivated the study of dynamical interactions that can create observed planets in multiple systems. The planet has a minimum mass of 1.14 times that of Jupiter, 1.14 M_J, and is in an $a = 0.045$ AU orbit around a 1.06 $M_\odot$ star. This star, the optical primary of the system, is in an $a = 12.3$ AU eccentric orbit ($e = 0.5$) around a tight, single-line spectroscopic binary. The tight binary is composed of a 0.96 $M_\odot$ star with a 0.67 $M_\odot$ companion in an $a = 0.67$ AU orbit with an eccentricity $e = 0.1$. The ~ 6 AU minimum separation between the primary and the tight binary poses a problem for the *in situ* formation of the planet, which is expected to have formed at a distance of ~ 3 AU before it migrated close to the star. Because of its high eccentricity, the tight binary will truncate the protoplanetary disk at a distance of 1.3 AU, preventing it from forming giant planets (Jang-Condell 2005;

Pichardo et al. 2005).

If the system could not have formed as we currently observe it, then it must have evolved to this state. Since most stars, especially stars in multiple systems, form in clusters, dynamical interactions are likely to play an important role in the evolution of this system. In addition, while far from definitive, the eccentricity of the primary with respect to the spectroscopic binary ($e = 0.5$) is suggestive of a dynamical interaction. Binaries that have undergone a significant interaction have their eccentricities distributed such that after a single encounter the probability of having an eccentricity e is $P(e) = 2e$. For a binary with an initially low eccentricity, dynamical interactions are the most likely method to boost the eccentricity. Jang-Condell (2005) suggests that the tight binary may have captured the planet-bearing star after the planet had formed, but purely dynamical captures involving three stars cannot lead to a stable triple-system. A dynamical interaction that ends in a stable triple system must use a fourth star that does not end up in the system. The three most likely interactions involving four stars are outlined in Figure D.1. In all cases the planet forms before the dynamical interaction and, due to its small mass and small separation, plays only a minor role in the essential dynamics of creating a triple system.

In method E, "Formation by Exchange," the star with the planet (A) encounters a close, hierarchical triple system composed of a tight binary (B) and another star (X), with masses M_A, M_B, and M_X, respectively. Star A interacts with the triple and exchanges into the binary thus ejecting star X. Although triple-single exchange interactions are not well studied, we may approximate the tight binary as a single object with its combined mass. In binary-single interactions, the most massive objects tend to end up in the binary (e.g., Heggie et al. 1996). Thus if $M_X < M_A, M_B$, the exchange reaction is more likely to happen.

In method H, "Formation by Hardening," star A is in a hierarchical triple system with binary B with a separation wide enough for a planet to form ($> 50 - 100$ AU). The triple system then faces repeated encounters with several different stars X. The interactions extract energy from the wide binary and carry it away from the system. This hardens the binary in a method analogous to that of Miller & Hamilton (2002b). The circular speed of A about B in HD 188753 is $v_{\rm circ} = (GM/a)^{1/2} = 13.8$ km s^{-1}, and the typical velocity dispersion of an open cluster is $v_{\rm clust} \sim 0.3$ to 3 km s^{-1} (e.g., Binney & Tremaine 1987). For the less-studied triple-single interactions, it is not clear whether the wide or tight binary is more likely to harden.

Method EH, "Formation by Exchange and Hardening," involves both an exchange and a hardening in a single interaction. Star A starts in a wide binary system with star X and interacts with binary B. Binary B exchanges into the system and ejects star X. Although binary-binary interactions are more likely to occur in a cluster than triple-single interactions, this process is the least likely to occur. The reason is that in order for the exchange to be favored, M_X must be the smallest mass, but for an equal-energy orbit that increases in mass, the semimajor axis will increase. Each of the above three methods may be complicated further by replacing any star with a binary with the same total mass and with separation much smaller than the next closest object.

As a proof of concept, *iabl* was used to integrate a triple-single-plus-planet encounter that displays the desired exchange and the observed configuration (Figure D.2). This is done by starting with the observed triple system and integrating the encounter backwards. The final results become the initial conditions for the desired reaction. For simplicity, the ejected star is assumed to have the same mass as star A $M_X = M_A$ and a final velocity at infinity $v_f = v_{\rm clust} = 1$ km s^{-1}. The initial configuration that leads to the triple system has a wide binary semimajor axis

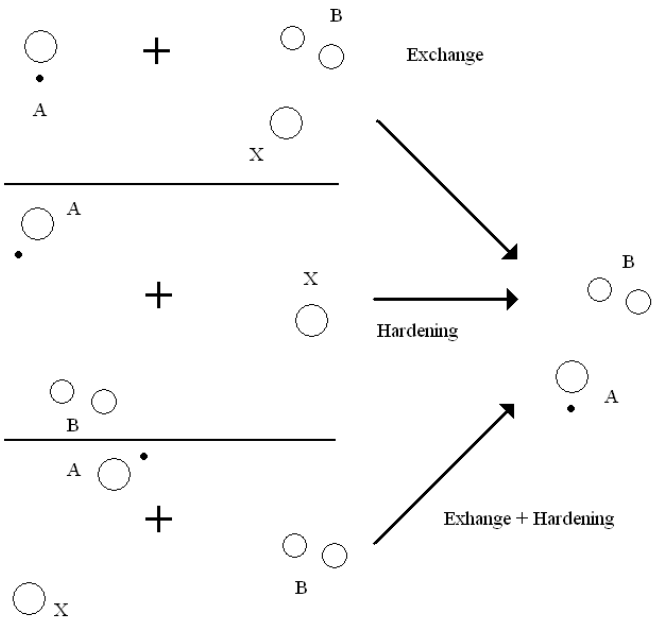

Figure D.1: Three methods of forming a stellar triple system with a planet. The methods are labeled, from top to bottom, E, H, and EH.

of 10.1 AU, eccentricity $e = 0.61$ and a relative velocity of 9.8 km s^{-1} with respect to star A. Although integrating backwards from a known configuration is useful for testing the crude feasibility of such scenarios, it is not appropriate for determining the probability of these exchanges because the discovered initial conditions will not be representative of the environment in the host cluster, such as the high relative velocity in this example. A broad parameter search of likely initial conditions would be necessary. The conclusions found in this study were generally the same as those found by Portegies Zwart & McMillan (2005) and Pfahl (2005b)

D.2 Near-Earth Asteroid Binary Disruption

As part of a large project studying the tidal disruption of near-Earth asteroids (NEAs), *iabl* was used to compute the fraction of binaries disrupted on close approach to Earth for a variety of parameters, including impact parameter, semimajor

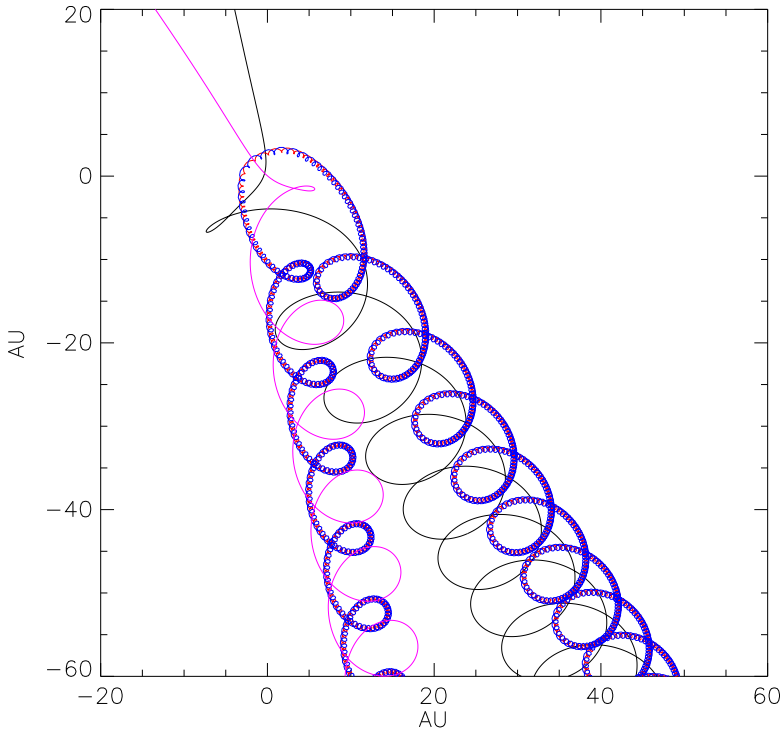

Figure D.2: Orbits of triple-single-plus planet encounter that results in an exchange into the configuration observed for HD 188753 by method E. The magenta curve is star A (and planet), which comes in from the upper-left. The initial triple system comes in from the bottom-right, and contains the close binary system (blue and red) and the star that is eventually ejected (black).

axis, relative velocity, and mass ratio of the binary. Figure D.3 shows an example curve compared to simulations by Bottke & Melosh (1996) for a relative velocity $v_\infty = 12$ km s^{-1}, binary asteroid mass ratio $q = 0.125$ with an $a = 3$ km circular orbit for asteroids of mass density $\rho = 2.6$ g cm^{-3}.

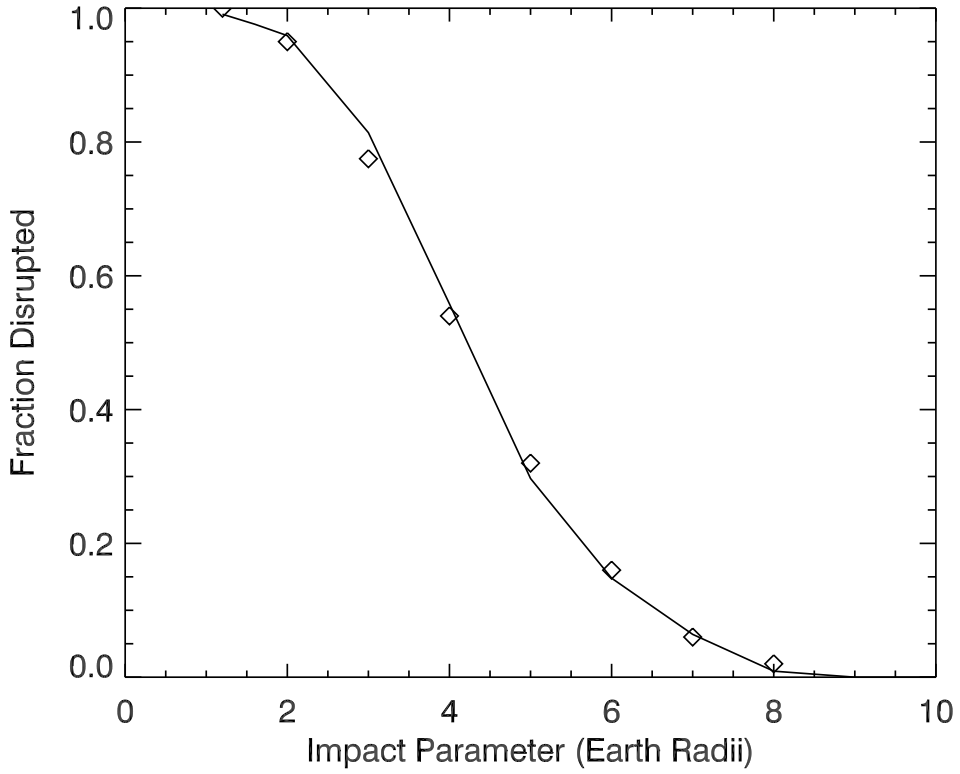

Figure D.3: Plot of fraction of binaries disrupted as a function of impact parameter in units of the Earth's radius. Symbols are from simulations by Bottke & Melosh (1996), and the line is from simulations run by *iabl*. See text for details. The agreement between the two sets of simulations is very good. Data provided by K. Walsh.

D.3 IMBH-IMBH Binaries

Recent simulations of young stellar clusters have shown that collisional runaways can lead to two or more IMBHs (Gürkan et al. 2006). These IMBHs would sink to the center and eventually form a binary with each other and, through subsequent interactions with stars in the cluster, harden and ultimately merge. During inspiral, these massive binaries are extremely loud *LISA* signals and may possibly be used as star-formation tracers to the young stellar clusters in which they formed. To test the lag time between the formation of an IMBH-IMBH binary and merger, we ran

simulations similar to those in this dissertation but with initial binary $m_0 = m_1 = 1000\ M_\odot$, $a = 20000$ AU with encounters with $m_2 = 10\ M_\odot$ stars that were assumed to be tidally disrupted if they got too close to either IMBH. We found that the time to merge was roughly 2 Myr and that the merging binaries were not likely to be very eccentric when detectable by *LISA*.

Bibliography

Aarseth, S. J. & Lecar, M. 1975, ARA&A, 13, 1

Ando, M. & the TAMA collaboration. 2002, Classical and Quantum Gravity, 19, 1409

Angelini, L., Loewenstein, M., & Mushotzky, R. F. 2001, ApJ, 557, L35

Arons, J. 1992, ApJ, 388, 561

Baker, J. G., Centrella, J., Choi, D.-I., Koppitz, M., van Meter, J. R., & Miller, M. C. 2006, ArXiv Astrophysics e-prints, arXiv:astro-ph/0603204

Baraffe, I., Heger, A., & Woosley, S. E. 2001, ApJ, 550, 890

Barish, B. C. 2000, Advances in Space Research, 25, 1165

Begelman, M. C. 2002, ApJ, 568, L97

—. 2006, ArXiv Astrophysics e-prints, arXiv:astro-ph/0602022

Binney, J. & Tremaine, S. 1987, Galactic dynamics (Princeton, NJ, Princeton University Press, 1987, 747 p.)

Blanchet, L., Qusailah, M. S. S., & Will, C. M. 2005, ApJ, 635, 508

Bottke, W. F. & Melosh, H. J. 1996, Icarus, 124, 372

Bruns, H. 1887, Acta Mathematica, 11, 25

Colbert, E. J. M. & Mushotzky, R. F. 1999, ApJ, 519, 89

Colbert, E. J. M. & Ptak, A. F. 2002, ApJS, 143, 25

Colpi, M., Mapelli, M., & Possenti, A. 2003, ApJ, 599, 1260

Colpi, M., Possenti, A., & Gualandris, A. 2002, ApJ, 570, L85

Cruz-González, C. & Poveda, A. 1971, Ap&SS, 13, 335

Cruz-González, C. & Poveda, A. 1972, in Gravitational N-Body Problem, Proceedings of IAU Colloq. 10, held in Cambridge, England, 12-15 August, 1970. Edited by Myron Lecar. D. Reidel Publishing Company, 1971., p.99, ed. M. Lecar, 99–

Cutler, C. & Thorne, K. S. 2002, ArXiv General Relativity and Quantum Cosmology e-prints, arXiv:gr-qc/0204090

Damour, T. & Gopakumar, A. 2006, ArXiv General Relativity and Quantum Cosmology e-prints, arXiv:gr-qc/0602117

Danzmann, K. 2000, Advances in Space Research, 25, 1129

Dewangan, G. C., Griffiths, R. E., & Rao, A. R. 2006, ArXiv Astrophysics e-prints, arXiv:astro-ph/0602472

Ebisuzaki, T., Makino, J., Tsuru, T. G., Funato, Y., Portegies Zwart, S., Hut, P., McMillan, S., Matsushita, S., Matsumoto, H., & Kawabe, R. 2001, ApJ, 562, L19

Einstein, A. 1905, Annalen der Physik, 17, 891

—. 1915, Sitzungsberichte der Königlich Preußischen Akademie der Wissenschaften, 844

—. 1916, Sitzungsberichte der Königlich Preußischen Akademie der Wissenschaften, 688

Fabbiano, G., Zezas, A., & Murray, S. S. 2001, ApJ, 554, 1035

Farmer, A. J. & Phinney, E. S. 2003, MNRAS, 346, 1197

Favata, M., Hughes, S. A., & Holz, D. E. 2004, ApJ, 607, L5

Ferraro, F. R., Possenti, A., Sabbi, E., Lagani, P., Rood, R. T., D'Amico, N., & Origlia, L. 2003, ApJ, 595, 179

Fidecaro, F. & VIRGO Collaboration. 1997, in General Relativity and Gravitational

Physics; Proceedings of the 12th Italian Conference, edited by M. Bassan, V. Ferrari, M. Francaviglia, F. Fucito, and I. Modena. World Scientific Press, 1997., p.163, 163

Fitchett, M. J. 1983, MNRAS, 203, 1049

Flanagan, É. É. & Hughes, S. A. 1998a, Phys. Rev. D, 57, 4535

—. 1998b, Phys. Rev. D, 57, 4566

Fregeau, J. M., Cheung, P., Portegies Zwart, S. F., & Rasio, F. A. 2004, MNRAS, 352, 1

Fregeau, J. M., Joshi, K. J., Portegies Zwart, S. F., & Rasio, F. A. 2002, ApJ, 570, 171

Freitag, M., Gürkan, M. A., & Rasio, F. A. 2006a, MNRAS, 335

Freitag, M., Rasio, F. A., & Baumgardt, H. 2006b, MNRAS, 324

Fryer, C. L. & Kalogera, V. 2001, ApJ, 554, 548

Fryer, C. L., Woosley, S. E., & Heger, A. 2001, ApJ, 550, 372

Fullerton, L. W. & Hills, J. G. 1982, AJ, 87, 175

Gaffney, N. I., Lester, D. F., & Telesco, C. M. 1993, ApJ, 407, L57

Gammie, C. F. 1998, MNRAS, 297, 929

Gebhardt, K., Kormendy, J., Ho, L. C., Bender, R., Bower, G., Dressler, A., Faber, S. M., Filippenko, A. V., Green, R., Grillmair, C., Lauer, T. R., Magorrian, J., Pinkney, J., Richstone, D., & Tremaine, S. 2000, ApJ, 543, L5

Gebhardt, K., Rich, R. M., & Ho, L. C. 2002, ApJ, 578, L41

—. 2005, ApJ, 999, L999

Gerssen, J., van der Marel, R. P., Gebhardt, K., Guhathakurta, P., Peterson, R. C., & Pryor, C. 2002, AJ, 124, 3270

Gilbert, N. E. 1901, Ph.D. Thesis

Goad, M. R., Roberts, T. P., Knigge, C., & Lira, P. 2002, MNRAS, 335, L67

Goldstein, H., Poole, C., & Safko, J. 2002, Classical Mechanics (San Francisco: Addison-Wesley, 3rd ed.)

Gültekin, K., Miller, M. C., & Hamilton, D. P. 2004, ApJ, 616, 221

—. 2006, ApJ, 640, 156

Gürkan, M. A., Fregeau, J. M., & Rasio, F. A. 2006, ApJ, 640, L39

Gürkan, M. A., Freitag, M., & Rasio, F. A. 2004, ApJ, 604, 632

Heggie, D. C. 1975, MNRAS, 173, 729

Heggie, D. C., Hut, P., & McMillan, S. L. W. 1996, ApJ, 467, 359

Heggie, D. C. & Rasio, F. A. 1996, MNRAS, 282, 1064

Holmberg, E. 1941, ApJ, 94, 385

Hopman, C. & Portegies Zwart, S. 2005, ArXiv Astrophysics e-prints, arXiv:astro-ph/0506181

Hornschemeier, A. E., Bauer, F. E., Alexander, D. M., Brandt, W. N., Sargent, W. L. W., Bautz, M. W., Conselice, C., Garmire, G. P., Schneider, D. P., & Wilson, G. 2003, AJ, 126, 575

Hulse, R. A. & Taylor, J. H. 1975, ApJ, 195, L51

Hut, P. & Bahcall, J. N. 1983, ApJ, 268, 319

Hut, P. & Inagaki, S. 1985, ApJ, 298, 502

Irwin, J. A., Athey, A. E., & Bregman, J. N. 2003, ApJ, 587, 356

Iyer, B. R. & Will, C. M. 1993, Physical Review Letters, 70, 113

Jackson, J. D. 1999, Classical Electrodynamics (New York: Wiley, 3rd ed.)

Jang-Condell, H. 2005, ArXiv Astrophysics e-prints, arXiv:astro-ph/0507356

Julliard-Tosel, E. 2000, Celestial Mechanics and Dynamical Astronomy, 76, 241

Kaaret, P., Prestwich, A. H., Zezas, A., Murray, S. S., Kim, D.-W., Kilgard, R. E., Schlegel, E. M., & Ward, M. J. 2001, MNRAS, 321, L29

Kaaret, P., Ward, M. J., & Zezas, A. 2004, MNRAS, 351, L83

King, A. R., Davies, M. B., Ward, M. J., Fabbiano, G., & Elvis, M. 2001, ApJ, 552, L109

Konacki, M. 2005, Nature, 436, 230

Kozai, Y. 1962, AJ, 67, 591

Kudritzki, R.-P. The First Stars. Proceedings of the MPA/ESO Workshop held at Garching, Germany, ed. , A. WeissT. G. Abel & V. Hill, 127

Kuntz, K. D., Gruendl, R. A., Chu, Y.-H., Chen, C.-H. R., Still, M., Mukai, K., & Mushotzky, R. F. 2005, ApJ, 620, L31

Lee, M. H. 1993, ApJ, 418, 147

Liu, J.-F., Bregman, J. N., Irwin, J., & Seitzer, P. 2002, ApJ, 581, L93

Madau, P. & Rees, M. J. 2001, ApJ, 551, L27

Maillard, J. P., Paumard, T., Stolovy, S. R., & Rigaut, F. 2004, A&A, 423, 155

Martel, K. & Poisson, E. 1999, Phys. Rev. D, 60, 124008

Matsubayashi, T., Shinkai, H., & Ebisuzaki, T. 2004, ApJ, 614, 864

Matsumoto, H., Tsuru, T. G., Koyama, K., Awaki, H., Canizares, C. R., Kawai, N., Matsushita, S., & Kawabe, R. 2001, ApJ, 547, L25

McCrady, N., Gilbert, A. M., & Graham, J. R. 2003, ApJ, 596, 240

Miller, J. M., Fabian, A. C., & Miller, M. C. 2004, ApJ, 614, L117

Miller, M. C. 1984, Gifted Children Newsletter, 10, 15

—. 2002, ApJ, 581, 438

Miller, M. C. & Colbert, E. J. M. 2004, International Journal of Modern Physics D, 13, 1

Miller, M. C. & Hamilton, D. P. 2002a, ApJ, 576, 894

—. 2002b, MNRAS, 330, 232

Misner, C. W., Thorne, K. S., & Wheeler, J. A. 1973, Gravitation (San Francisco: W.H. Freeman and Co., 1973)

Mukai, K., Still, M., Corbet, R. H. D., Kuntz, K. D., & Barnard, R. 2005, ApJ, 634, 1085

Newhall, X. X., Standish, E. M., & Williams, J. G. 1983, A&A, 125, 150

O'Leary, R. M., Rasio, F. A., Fregeau, J. M., Ivanova, N., & O'Shaughnessy, R. 2006, ApJ, 637, 937

Pakull, M. W. & Mirioni, L. 2002, ArXiv Astrophysics e-prints, arXiv:astro-ph/0202488

Peters, P. C. 1964, Physical Review, 136, 1224

Pfahl, E. 2005a, ApJ, 626, 849

—. 2005b, ApJ, 635, L89

Pichardo, B., Sparke, L. S., & Aguilar, L. A. 2005, MNRAS, 359, 521

Poincaré, H. 1892, Les methodes nouvelles de la mecanique celeste (Paris, Gauthier-Villars et fils, 1892-99.)

Portegies Zwart, S. F. & McMillan, S. L. W. 2000, ApJ, 528, L17

—. 2002, ApJ, 576, 899

—. 2005, ApJ, 633, L141

Ptak, A. & Colbert, E. 2004, ApJ, 606, 291

Quinlan, G. D. 1996, New Astronomy, 1, 35

Quinlan, G. D. & Shapiro, S. L. 1989, ApJ, 343, 725

Rauch, K. P. & Hamilton, D. P. in preparation, AJ

Reynolds, C. S., Loan, A. J., Fabian, A. C., Makishima, K., Brandt, W. N., & Mizuno, T. 1997, MNRAS, 286, 349

Richardson, D. C., Bottke, W. F., & Love, S. G. 1998, Icarus, 134, 47

Roberts, T. P., Goad, M. R., Ward, M. J., Warwick, R. S., O'Brien, P. T., Lira, P., & Hands, A. D. P. 2001, MNRAS, 325, L7

Schilling, R. 1998, in AIP Conf. Proc. 456: Laser Interferometer Space Antenna,

Second International LISA Symposium on the Detection and Observation of Gravitational Waves in Space, 217–221

Schneider, R., Ferrara, A., Natarajan, P., & Omukai, K. 2002, ApJ, 571, 30

Sigurdsson, S. & Hernquist, L. 1993, Nature, 364, 423

Sigurdsson, S. & Phinney, E. S. 1993, ApJ, 415, 631

—. 1995, ApJS, 99, 609

Strohmayer, T. E. & Mushotzky, R. F. 2003, ApJ, 586, L61

Swartz, D. A., Ghosh, K. K., Tennant, A. F., & Wu, K. 2004, ApJS, 154, 519

Taylor, J. H., Fowler, L. A., & McCulloch, P. M. 1979, Nature, 277, 437

von Hoerner, S. 1960, Zeitschrift fur Astrophysik, 50, 184

Webbink, R. F. 1985, in IAU Symp. 113: Dynamics of Star Clusters, 541–577

Webster, D. L. 1913, Ph.D. Thesis

Wen, L. 2003, ApJ, 598, 419

Whittaker, E. T. 1989, A Treatise on the Analytical Dynamics of Particles and Rigid Bodies (Cambridge, UK: Cambridge University Press)

Will, C. M. 2004, ApJ, 611, 1080

Winter, L. M., Mushotzky, R. F., & Reynolds, C. S. 2005, ArXiv Astrophysics e-prints, arXiv:astro-ph/0512480

Yu, Q. & Tremaine, S. 2003, ApJ, 599, 1129